THE EFFECT OF REACTIVE SINTERING ON THE DENSIFICATION OF BORON CARBIDE ZIRCONIUM DIBORIDE COMPOSITE

Ömer YÜCEL

Master of Science Thesis

Department of Institute of Graduate Programs

Programme in Nanotechnology

Supervisor: Prof. Dr. Servet TURAN

Eskişehir

Eskişehir Technical University

Institute of Graduate Programs

January 2022

ABSTRACT

THE EFFECT OF REACTIVE SINTERING ON THE DENSIFICATION OF BORON CARBIDE ZIRCONIUM DIBORIDE COMPOSITE

Ömer YÜCEL

Department of Institute of Graduate Programs

Programme in Nanotechnology

Eskişehir Technical University, Institute of Graduate Programs, January 2022

Supervisor: Prof. Dr. Servet TURAN

In this thesis, different additives (Zirconia, Zirconium Silicate, Carbon) are used to produce Boron Carbide/Zirconium Diboride (B_4C/ZrB_2) composite by Spark Plasma Sintering (SPS). Effects of different additives and sintering parameters (sintering temperature, sintering time, pressure, heating rate, etc.) on the densification of the composite are observed. Firstly, B_4C/ZrB_2 composite is produced using B**4**C and ZrB_2 powders via non-reactive sintering. Then, different additives (ZrO_2-$ZrSiO_4$) zirconium (Zr) sources are used to make the same composite by reactive sintering, and effects of reactive sintering are observed. The relative density of the sample, produced by B_4C and ZrB_2 powders at 2150 °C by 15.7 MPa pressure, is %99.4734. When reactive sintering (samples produced by B_4C and ZrO_2 powders) is considered, the highest relative density (%97.2111) is achieved by sintering 15 minutes at 2000 °C via 31.4 MPa pressure. For the samples in which $ZrSiO_4$ is the zirconium source, the highest relative density (%96.0524) is achieved by sintering 15 minutes at 2107 °C by 15.7 MPa pressure. Archimedes Method is used for relative density calculations, Scanning Electron Microscope (SEM) is used for microstructure observation, and X-ray Diffraction analysis is used to observe phases in produced parts. The positive effect of reactive sintering on the densification at lower temperatures is observed, besides the importance of the contribution of the control on the phases and gases produced during reactive sintering is observed.

Keywords: Reactive Spark Plasma Sintering, Boron Carbide, Zirconium Diboride

ÖZET

REAKTIF SINTERLEMENIN BOR KARBÜR ZIRKONYUM DIBORÜR KOMPOZITININ YOĞUNLAŞMASI ÜZERINDEKI ETKISI

Ömer YÜCEL

Lisansüstü Eğitim Enstitüsü Anabilim Dalı

Nanoteknoloji Bilim Dalı

Eskişehir Teknik Üniversitesi, Lisansüstü Eğitim Enstitüsü, Ocak 2022

Danışman: Prof. Dr. Servet TURAN

Bu tez çalışmasında Bor Karbür (B_4C) malzemesinin farklı katkı tozlarıyla (zirkonyum dioksit, zirkonyum diborür, zirkonyum silikat ve karbon) Bor Karbür/Zirkonyum diborür (B_4C/ZrB_2) kompozitinin üretimi spark plazma sinterleme (SPS) yöntemi ile yapılmıştır. B_4C/ZrB_2 kompozitinin üretiminde farklı katkıların ve sinterleme parametrelerinin (Sinterleme sıcaklığı, sinterleme süresi, basınç, ısıtma hızı vb.) üretilen örneklerin yoğunlaşması üzerindeki etkileri gözlemlenmiştir. Öncelikle B_4C/ZrB_2 kompoziti B_4C ve ZrB_2 tozlarıyla üretilmiştir daha sonra ZrO_2-$ZrSiO_4$ gibi farklı Zirkonyum (Zr) kaynakları kullanılarak reaktif sinterleme yönteminin yoğunlaşma üzerindeki etkileri gözlemlenmiştir. B_4C ve ZrB_2 tozlarıyla 2150 °C sıcaklıkta ve 15.7 MPa basınç altında üretilen örnek %99.4734 nispi yoğunluk göstermiştir. ZrO_2-B_4C tozlarıyla (reaktif sinterleme ile) üretilen örneklerde 2000 °C de 15 dakika ve 31.4 MPa basınç altında sinterlenen örnek ise (%97.2111) nispi yoğunluğu göstermiştir. Zirkonyum silikat katkılı malzemelerde en yüksek nispi yoğunluk, 2110 °C sıcaklıkta 15.7 MPa basınçla 15 dakika sinterlenen örnekle elde edilmiştir (%96.0524). Üretilen örneklerin nispi yoğunluğu Arşimet Metoduyla, iç yapısı tarayıcı elektron mikroskopu, faz analizleri X-ışını kırınım analizi ile karakterize edilmiştir. Reaktif sinterlemenin daha düşük sıcaklıklarda daha iyi sonuçlar verdiği gözlemlenmiş ve reaksiyonlar sonucu oluşan fazların ve gazların kontrolünün yoğunlaştırma üzerindeki etkisinin önemi saptanmıştır.

Anahtar Sözcükler: Reaktif Spark Plazma Sinterleme, Bor Karbür, Zirkonyum Diborür.

ACKNOWLEDGEMENTS

I would like to thank Prof. Dr. Servet TURAN for allowing me to pursue my Master of Science Dissertation on the Reactive Sintering subject. I also like to thank him for providing the resources, advice, and supervision on my thesis.

I would also like to thank A. Furkan BULUÇ for support, guidance, and conversations on technical matters.

I would also like to express my gratitude to the staff in the Department of Material Science and Engineering for providing technical support to enable a smooth running of the thesis.

Lastly, I would like to thank my family and Özgü ÇALIN for their support during my education.

Ömer YÜCEL

CONTENTS

Page

HEADER PAGE ..... **I**

ABSTRACT ..... **II**

ÖZET ..... **III**

ACKNOWLEDGEMENTS ..... **IV**

CONTENTS ..... **V**

LIST OF TABLES ..... **VII**

LIST OF FIGURES ..... **VIII**

LIST OF IMAGES ..... **XI**

1. INTRODUCTION **1**

1. BORON CARBIDE AND CERAMIC MATERIALS **2**

1.1. Carbides **2**

1.1.1. Boron carbide **2**

1.1.2. Silicon carbide **4**

1.2. Zirconium Diboride **5**

1.3. Production Of Ceramic Materials by Powder Methods **7**

1.4. Sintering **14**

2. SCOPE OF THE THESIS **30**

3. EXPERIMENTS **31**

4. RESULTS OF EXPERIMENTS **35**

4.1. Analysis Of X-ray Diffraction Results **35**

4.2. Analysis of Spark Plasma Sintering Results **42**

4.3. Analysis of Secondary Electron Microscope Analysis **45**

4.4. Analysis of Relative Density Results **53**

4.5. Analysis of Electrical and Mechanical Properties of Boron Carbide Zirconium Diboride Composite **61**

5. CONCLUSION AND FUTURE WORK **68**

REFERENCES..... 69

APPENDIX..... 76

CURRICULUM VITAE

LIST OF TABLES

Page

Table 1.1. Relative densities of pressureless sintered B**4**C with different additives 3
Table 1.1. Desired properties of powders for advanced ceramic production 7
Table 1.2. Additives in ceramics and their functions (G. Heinrich et all, 1977) 8
Table 1.3. Advantages and disadvantages of Additive Manufacturing 13
Table 3.1. Weight percentages of four different powder mixtures. 31
Table 3.2. Parameters of the mixing process of powders. 32
Table 4.1. Displacement data of the B-O samples: a) with the constant Heating rate (100 °C/min), pressure constant (15.7 MPa), b) Heating rate is lowered to 50 °C/min between 1600-2000 °C, pressure increased to 31.4 MPa at 39th minute. 44
Table 4.2. Header styles 45
Table 4.3. Comparison of B**4**C sintering with and without additives. 54
Table 4.4. Comparison of the effect of ZrO**2** and ZrSiO**4** additives on the mechanical properties of B**4**C. 65
Table 4.5. Effect of relative density and in-situ formed phases on the electrical conductivity of B**4**C/ZrB**2** composite 66

LIST OF FIGURES

Page

Figure 1.1. Classification of Materials 1
Figure 1.1. Uniaxial Dry Pressing 10
Figure 1.2. Wet Bag Isostatic Pressing 11
Figure 1.3. Dry Bag Isostatic Pressing 12
Figure 1.4. Process steps of Additive Manufacturing 13
Figure 1.5. Sintering steps: a) powder compact, b) initial step, c) intermediate step, d) final step 14
Figure 1.6. The chemical formula of paracetamol 15
Figure 1.7. Spark Plasma Sintering graph of B**4**C-ZrB**2** composite 16
Figure 1.8. Simplified views of; a) Pressureless Sintering, b) Hot Pressure Sintering, c) Self-propagating High-Temperature Sintering, d) Spark Plasma Sintering. 19
Figure 1.9. Schematic representation of HIP 21
Figure 1.10. Yearly analysis of publications have (Spark Plasma Sintering) in their title (adapted from www.webofscience.com) 22
Figure 1.11. Fields of publications that have SPS in their title. (adapted from www.webofscience.com) 23
Figure 1.12. Movement of pulsed current between powder particles. 25
Figure 1.13. The first and second stages of SPS, a) Initial step (spark discharging), b) generation of spark and ionization 26
Figure 1.14. Third and Fourth stages of SPS, a) Surface of particles start to melt and vaporize, b) Sputtering of vaporized-melted particles via generated spark impact pressure 27
Figure 1.15. V. stage of SPS (Neck formation). 28
Figure 3.1. Particle size distribution of ZrSiO**4** powder during three hours of ball milling. 32
Figure 4.1. XRD analysis of B-O: composites heated to 1200,1500 1600 °C and raw powder 36
Figure 4.2. XRD analysis of B-O samples: a) one step sintered sample at 2090 °C (15.7 MPa), b) Two-step sintered sample at 2090 °C (15.7 MPa), c)

Two-step sintered sample at 2000 °C (15.7 MPa), d) Two-step sintered sample at 2000 °C (31.4 MPa). 37
Figure 4.3. XRD analysis of B-Si-C: composites heated to 1200,1500 1600 °C and raw powder 38
Figure 4.4. XRD analysis of one-step sintered B-Si-C samples at a) 2093 °C, b) 2012 °C, c) 1930 °C 39
Figure 4.5. B-Si-C powder mixture sintered at 1930 °C and dwelled at 1500 °C for; a) 5 minutes, b) 10 minutes, c) 15 minutes 40
Figure 4.6. XRD analysis of the oxidized layer of B**4**C-ZrSiO**4** sample..... 41
Figure 4.7. *SPS graph of B-O samples; a) Heating rate constant (100 °/min), pressure constant (15.7 MPa), b) Heating rate is lowered to 50 °/min between 1600-2000 °C and 31.4 MPa pressure is applied after 39th minute to the end of the process.* 42
Figure 4.8. *SPS graph of B-O samples: a) Heating rate constant (100 °C/min), pressure constant (15.7 MPa), b) Heating rate is lowered to 50 °C/min between 1600-2000 °C, 31.4 MPa pressure is applied after 39th minute to the end of the process.* 43
Figure 4.9. SPS graphics of B-Si-C samples; a) 5 minutes held at 1500 °C, b) 15 minutes held at 1500 °C 44
Figure 4.10. *SPS samples: a) Sections created by cutting, b) Sections named to identify the locations of SEM images* 46
Figure 4.11. SEM images of the center of samples: a) B-Zr sample sintered at 2150 °C, b) B-O sample one step sintered at 2139 °C, c) Two-step sintered B-O sample at 2140 °C and dwelled at 1600 °C, d) B-O sample two-step sintered at 2000 °C and dwelled at 1600 °C 47
Figure 4.12. SEM images of B-O samples: a, b, and d images taken from sides of samples, c is taken from Surface-2 47
Figure 4.13. SEM images of B-O samples with 5,10,15 minutes of dwelling time and 15.7-31.4 MPa pressures 48
Figure 4.14. SEM images of Z-Si-C samples: a) Surface-1, b) Surface-2, c) Surface-2, d) Surface-2 49

Figure 4.15. SEM images of B-Si-C samples: a) Centre of the sample, b) Inner part of the Side region, c) Middle part of Side region, d) Middle part of Side region 50
Figure 4.16. SEM images of B-Si-C samples: a) Side region (dwelling time 5 minutes), b) Surface-2 of the sample (dwelling time 5 minute), c) Side region (dwelling time 15 minutes 51
Figure 4.17. SEM images of B-Si-C sample sintered at 2107 °C, by 15.7 MPa pressure, with 10 minutes of dwelling at 1500 °C: a) Side of the sample, b) Surface-2 of the sample, c) Smashed piece of the sample (Surface-2), d) Centre of sample 52
Figure 4.18. Effect of dwelling time and heating rate on the relative density of B-O samples 55
Figure 4.19. Effect of dwelling time and pressure on the relative density of B-O samples 56
Figure 4.20. Effect of dwelling time and pressure on the relative density of B-O samples 57
Figure 4.21. Effect of Sintering Time on the relative density of B-O samples 58
Figure 4.22. Effect of pressure and dwelling time on relative densities of B-Si-C samples 59
Figure 4.23. Effect of Temperature on the relative densities of B-Si-C samples, an applied pressure is 15.7 MPa, dwelling time is 10 minutes 60
Figure 4.24. Effect of temperature on relative densities of B-Si-C specimens, an applied pressure is 31.4 MPa, and dwelling time is 10 minutes. 61
Figure 4.25. Effect of relative density on the Hardness of B-O samples. 62
Figure 4.26. Crack propagation of B-O sample (97.2% relative density, 21.8 ±3.5 GPa Hardness) a) Propagation and blocking of crack, b) Toughening mechanisms 63
Figure 4.27. Crack propagation of a) B-O sample with 97.2% relative density, b) B-Zr sample with 99.5% relative density 63
Figure 4.28. Effect of relative density on the Hardness of B-Si-C samples. 64

LIST OF IMAGES

Page

Image 3.1. Carbon foils are used to cover powder samples inside carbon dies. 33
Image 4.1. Oxide layers on the surface of the B-Si-C samples..... 41

1. INTRODUCTION

Materials are either produced, by raw materials or collected from nature to use for a variety of purposes. To fulfill the desired properties, suitable kinds of materials should be used. Figure 0.1. shows a basic classification for materials (G. Heinrich et all, 1977). Besides using one material kind for meeting the requirements of an application, composite materials can be used when one kind does not meet desired properties. Natural materials and synthetic materials are classified by natural occurrence. Metals, semiconductors, and non-metallic materials are used for their conductivities. While metals are conductive materials and non-metallic materials are insulators, the conductivity of semiconductors stands between those two. Organic materials are carbon-based compounds. Ceramic materials are a sub-group of non-metallic, inorganic materials.

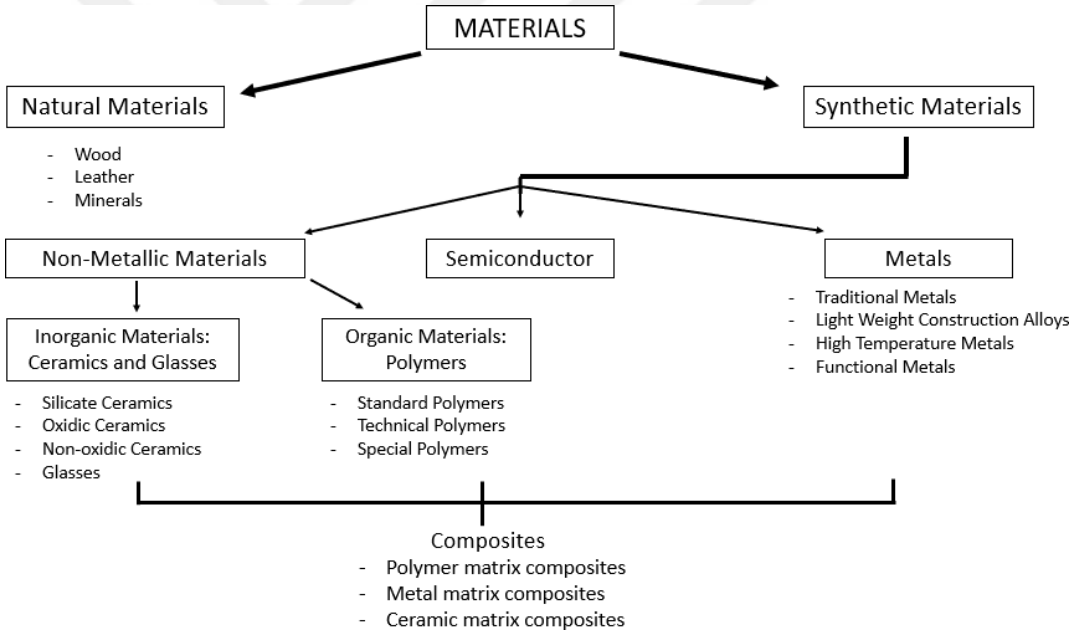

Figure 1.1. *Classification of Materials*

1. BORON CARBIDE AND CERAMIC MATERIALS

Ceramic materials are one of the main groups of solid materials, along with metals and polymers. This classification is based on chemical makeup and atomic structure (William D. Callister, 2007). Ceramics contain both metallic and non-metallic elements; oxides, nitrides, and carbides are the most common examples. SiO_2, Al_2O_3, SiC, B_4C, Si_3N_4 are some examples of ceramic materials. While the stiffness and strength of ceramics are comparable to those of metals, their brittle nature makes them susceptible to fracture (William D. Callister, 2007).

1.1. Carbides

Refractory carbides can be considered as a group of carbide ceramics that have high hardness, wear resistance, high melting point, and chemical inertness which is why they are used as a variety of industrial materials. Cutting and grinding tools, lightweight armors, high-temperature thermoelectric conversions are some of the examples of as mentioned industrial materials (Hugh O. Pierson, 1996).

There are two types of refractory carbides.

I. Interstitial Refractory Carbides: TiC, ZrC, HfC.
II. Covalent Refractory Carbides: SiC, B_4C.

There are two members in this group, namely SiC and B_4C. The difference in electronegativity and atomic radius difference between B-C or Si-C are small compared to interstitial refractory carbides. The strength of the short covalent bond between these atoms is the reason for the high melting temperature of B_4C and SiC (Hugh O. Pierson, 1996).

1.1.1. Boron carbide

Boron carbide is discovered in 1858, but the B_4C formula is identified in 1934 (Lafayette, 1991). Boron Carbide is a member of covalent refractory carbide ceramic materials. Low density (2.52 g/cm^3), high melting point, excellent hardness, great resistance to chemical agents, and high neutron absorption are significant properties of boron carbide (Thévenot, 1990). However low sinterability, caused by strong covalent bonding, requires high temperatures and/or sintering additives to achieve complete densification. As with other ceramic materials, low fracture toughness is a problem of boron carbide.

The molecular composition of boron carbide involves four boron and one carbon atom. A high boron percent of this substant makes it suitable for use as a boron source for powder production of some ceramic materials (e.g., reactive sintering of ZrB_2, HfB_2).

The useful mechanical properties of Boron Carbide are highly dependent on the densification of the product. Besides machining problems due to its brittle nature, pure boron carbide is hard to sinter completely which restricts the application of this material.

Table 1.1. *Relative densities of pressureless sintered B_4C with different additives.*

Additive Name	**Additive (wt%)**	**Sintering Temperature (C°)**	**Max Relative Density (%)**
Al	4	2050-2150	94
Carbon Black	-	2150	96
Phenolic Resin	-	2150	95
TiC	-	2150-2200	≥93
Si	5-10	2100	99.2-100
Ti	-	2190	87
Al_2O_3	3	2150	96
TiO_2	40	2190	95
$ZrO_2 + C$	30	1900-2000	97≤

Boron Carbide densification analysis is made in Table 2.1 (W. Zhang et al., 2019. Even though full relative densities are achieved, many other factors affect relative density(Oleg O. Vasylkiv et al, 2016).

1. Raw material properties; particle size, shape, boron to carbon ratio, etc.
2. Micro-Nano structure.
3. Processing types; Pressure assistance, liquid phase, or solid-state sintering.
4. Processing routes chosen for secondary phases.

To understand raw material-processing-properties connection, these factors should be considered. When one-factor changes, the whole process, and properties may be completely different.

In the early years after the discovery of boron carbide, processing routes were not able to produce stock with low impurity percent. There are eight routes for boron carbide production (Suri et al., 2010).

1. Carbothermic reaction
2. Magnesiothermic reaction
3. Synthesis from elements
4. Vapor phase reactions
5. Synthesis from polymer precursors
6. Liquid phase reactions
7. Ion beam synthesis
8. Vapor Liquid Solid (VLS) growth

Different raw materials as boron and carbon source are used in these methods. Some examples of reactions take place are (Suri et al., 2010):

$$4H_3BO_3(s) + 7C(s) \rightarrow B_4C(s) + 6CO(g) + 6H_2O(g) \quad (2.1)$$

$$2B_2O_{3\,(s)} + 6Mg\,(s) + C\,(s) \rightarrow B_4C\,(s) + 6MgO(s) \quad (2.2)$$

$$4BCl_3(s) + CCl_4\,(s) + 8H_2(g) \rightarrow B_4C(s) + 16HCl(l) \quad (2.3)$$

$$4BCl_3\,(g) + CH_4(g) + H_2(g) \rightarrow 4B_4C(s) + 12HCl\,(g) \quad (2.4)$$

Carbothermic synthesis has become the industrial route for boron carbide production. Sol-gel method and vapor phase synthesis are promising to produce fine powders which are important to reduce the sintering temperature of the final product (O. Oleg O. Vasylkiv et al, 2016).

1.1.2. Silicon carbide

Although silicon carbide was first reported by Berzelius in 1810 and 1821, Acheson was the person who found it by mistake and understood the potential of silicon carbide as an abrasive material. Besides the synthetic occurrence of silicon carbide, it also naturally exists in the world and space, which is observed in a sample of moon rock (Iethschmidt et al., 1974).

Silicon carbide, which is a non-oxide ceramic material, has been an industrial material for over a hundred years yet it does not lose attention (Aizat et al., 2017). As boron carbide, silicon carbide has been on the focus of attention due to being lightweight, resistant to chemically and thermally severe environments. Silicon carbide is the fourth hardest material known after diamond, cubic boron nitride, and boron carbide (Iii et al., 2015).

There are three main production methods for silicon carbide besides others (Iethschmidt et al., 1974).

a) The Acheson process.
b) The Elektroschmelzwerk Kempten (ESK) process.

There is a complex and stepwise formation of silicon carbide from silica, quartz, and carbon source (carbon black, charcoal, etc.).

$$SiO_2(l) + 3C(s) \rightarrow SiC(s) + 2CO(g) \quad (2.5)$$

Besides this overall reaction, there are many steps listed below (Biernacki et all, 1989).

$$SiO_2(l) + C(s) \rightarrow SiO(s) + CO(g) \quad (2.6)$$

$$SiO(s) + C(s) \rightarrow Si(l) + CO(g) \quad (2.7)$$

$$Si(l) + C(s) \rightarrow SiC(s) \quad (2.8)$$

Furthermore, formed SiC may cover carbon sources and prevent further SiC formation. In this case, SiC reacts with SiO_2 by reactions 2.9-2.10 (Suri et al., 2010).

$$SiC(s) + 2SiO_{2(l)} \rightarrow 3SiO(s) + CO(g) \quad (2.9)$$

$$SiC(s) + SiO(s) \leftrightarrow 2Si(l) + CO(g) \quad (2.10)$$

Reacties the equilibrium case.

1.2. Zirconium Diboride

Boride ceramic materials include many members: Aluminum Diboride, Tantalum Diboride, Cerium Hexaboride, Zirconium Diboride, etc. A special group of borides consists of Ultra High-Temperature Ceramics (UHTCs) which are Hafnium Diboride, Zirconium Diboride, Titanium Diboride, Niobium Diboride and Tantalum Diboride (Telle et al., 2000). This group is expected to preserve their functionality above 2000 °C. Compared to other ceramic materials, UHTCs consist of properties as high melting point (above 3000 °C), hardness, elastic modulus, good wear resistance, thermal conductivity, and chemical stability (Raju et al., 2020). The densities of Boride UHTCs vary between (4.5-12.5 g/cm^3) and fracture toughness between (4-5 $MPa.m^3$) (Raju et al., 2020).

Zirconium Diboride is a member of Ultra High-Temperature Ceramics which have the second-lowest density (6.1 g/cm^3) after Titanium Diboride. Besides having a high melting point, hardness, electrical and thermal conductivity, corrosion against molten iron makes it a candidate for many applications (Monteverde et al., 2002). The high price of Zirconium diboride-based ceramics results in usage in the aerospace industry as hypersonic re-entry vehicles, leading edges, nose craps, etc (Balak et al., 2017).

There are several routes for Zirconium Diboride powder production. Powder properties such as purity, morphology, defects, and particle size are strongly related to sinterability. Synthesis conditions are connected to the powder property. Desired properties may be accomplished by some methods (production of ZrB_2 powder from elements) yet economic issues do not let them become an industrial selection. Three methods below are most chosen, due to simplicity and cheap raw material, for ZrB_2 powder production.

Boron carbide reduction of zirconia is the most common production method of ZrB2 among others due to relatively cheap raw materials. The method involves boron carbide and carbon besides zirconia (ZrO_2).

$$2ZrO_2(s) + B_4C(s) + 3C(s) \rightarrow 2ZrB_2(s) + 4CO(g) \quad (2.11)$$

ZrB_2 powder is formed by reaction 2.11, which causes some boron loss as boron trioxide (B_2O_3), needs an excessive amount of boron source. An insufficient amount of boron source may yield the production of the Zirconium Carbide (ZrC) phase due to B_2O_3 evaporation. Production of pure ZrB_2 requires a temperature over 1800 °C, lower temperatures introduce both carbon and oxygen impurities into powder (Sonber & Suri, 2011).

Metallothermic reduction of ZrO_2 and B_2O_3 method is cheap due to relatively cheap raw materials. A reduction agent, mostly magnesium (Mg), is used to remove oxides from the system. The powder is produced by reaction 2.12. Besides the excess amount of B_2O_3, to affirm the complete formation of ZrB_2, an excess amount of Mg is required too (Sonber et all, 2011).

$$ZrO_2(s) + B_2O_3(s) + 5Mg(s) \rightarrow ZrB_2(s) + 5MgO(s) \quad (2.12)$$

1.3. Production Of Ceramic Materials by Powder Methods

Powder methods involve three steps: production of powders (mentioned some of them in earlier sections), consolidation of the powder into a shape, and elimination of voids between powders. After the densification process, additional methods can be used to get desired microstructure that affects the properties of materials.

The main disadvantages of the powder method are maintaining homogeneous products and the negative effect of agglomerates on densification (B.J. et all, 1990). Milling is accepted as a method to eliminate agglomerates, yet the introduction of impurities makes it unfavorable for some applications in which purity plays a vital role.

Modification of particle size of powders may be needed to improve the densification process by decreasing void sizes between particles. This step of ceramic material production depends on the wanted outcome of the properties of the product.

Powder properties such as particle size, particle shape, particle size distribution play a key role in the control of microstructure. Besides the effect on the densification of product, fine particle size is vital for chemical reactivity which is a very important issue in reactive sintering cases. Particle sizes below 1 μm are desirable for both chemical reactivity and densification (Rahaman, 2017).

As well as particle size, its distribution is a key factor in packing and densification. While broad particle size distribution improves packing and sintering, it has a negative effect (large grain size) on microstructure due to larger particles.

Desirable properties of powders for advanced ceramic production are listed in Table 2.2.

Table 1.1. Desired properties of powders for advanced ceramic production

Powder Characteristic	**Desired Property**
Particle size	Fine (< 1μm)
Particle size distribution	Narrow or monodisperse
Particle shape	Spherical or equiaxial
State of agglomeration	No agglomeration or soft agglomerates
Chemical composition	High purity
Phase composition	Single-phase

Forming techniques are used to create green bodies with a defined shape, size, density, and reproducible tolerances from deflocculated slurries, plasticized materials, or granules (G. Heinrich et all, 1977). Geometrical changes should be considered in this section to avoid unchangeable tolerances after firing. There are numerous additives used to control parameters of ceramic production shown in Table 2.3.

Table 1.2. *Additives in ceramics and their functions (G. Heinrich et all, 1977).*

Additive	**Function**
Ceramic powder	Matrix
Sintering additive	Densification aid
Solvent	Dispersion
Deflocculant	Control of surface charges and pH, Dispersion
Dispersing agent	Deagglomeration
Wetting agent	Reduce the surface tension of the solvent
Antifoaming agent	Avoidance of bubbles
Preservative	Avoidance of bacteria cultures
Binder	Green strength
Plasticizer	Flexibility
Softener	Flexibility
Lubricant	Reduce die and internal friction, mold release

Another important side of forming process is to produce near net shape stocks to prevent machining costs, especially for the harder structural materials that cause high-cost output.

There are three typical members of casting processes such as slip casting, pressure casting, and tape casting. Each process can be used for different advantages such as time and shape.

The slip casting process involves a porous mold that absorbs water, mostly made of gypsum, which is used to dry aqueous suspensions to create a solid green body. The cast thickness can be calculated by equation 2.1 which depends on the square root of material constant (c) and time (G. Heinrich et all, 1977).

$$x^2 = ct \tag{2.1}$$

Pressure casting has a more complex setup compared to slip casting which is more suitable for the industry that decreases time by using pressure. Another difference in this method is the use of plastic molds (G. Heinrich et all, 1977).

The last member of casting processes is the tape casting process which enhances the production of very thin ceramic substrates with a large area.

Important parameters for casting can be listed as solid loading which changes properties of the green body, the liquid choice may differ due to reaction between solid and water, also other additives listed in Table 2.3 should be used carefully to create suitable suspensions for each casting process (Rahaman, 2017).

Roller tool forming, extrusion, and injection molding are some plastic deformation forming techniques. Both conventional and structural ceramics can be shaped by these methods by producing suitable suspensions(Blackburn & Wilson, 2008).

Roller tool forming has two parts. The first one is the stationary plaster mold that holds the ceramic body and the second one is the mobile roller tool which enhances shaping (G. Heinrich et all, 1977).

Extrusion is a well-known technique in which a suspension prepared by ceramic powders and additives (plasticizer, solvent, dispersant, etc.) is forced to pass through a cross-section that decides the final form of the green body (J. P. Singh et all, 2012).

The injection molding method has similar steps to other shaping techniques such as selection of powder and additive, producing a homogeneous feeding material (Rahaman et all, 2017). The difference of this method is to inject feed to a mold which has more flexibility on three dimensions compared to slip casting or extrusion.

Pressing can be performed in either dry or wet conditions. Uniaxial pressing and isostatic pressing are examples of shaping by pressing.

Uniaxial dry pressing which is shown in Figure 1.1 is a method to compact powders into a relatively simple shape by pressure. This method is widely used for refractories, cutting tools, grinding disks, etc. The process involves three steps: the first one is to fill the mold, the second is to densification and the third one is to evacuate the as produced compact (G. Heinrich et all, 1977).

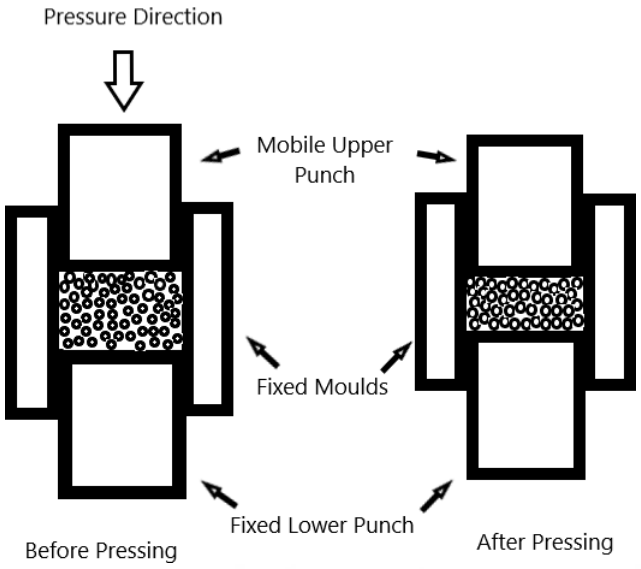

Figure 1.1. *Uniaxial Dry Pressing*

The densification step can be described by three steps on a pressure-density curve. The first step involves sliding and re-arrangement of particles by pressure and slight densification. The second region starts after the end of re-arrangement in which granules start to fracture and fill the voids between particles. Most of the densification percentage is obtained in the second step. In the third step, plastic deformation occurs slightly and densification reaches a peak which is mostly above 50% (Imran et al., 2009).

The relative density of the powder compact after densification is not homogeneously distributed. The upper mobile punch region shows higher densification yet densification negatively varies from up to bottom. This variation is the result of non-uniform friction of powders, powder, and mold as well (Zipse, 1997).

Another pressing method is isostatic pressing, also called cold isostatic pressing (CIP), which has sub-groups as, isostatic wet bag pressing and isostatic dry bag sintering. For samples that have complex shapes or bigger volumes can not be dry pressed. In isostatic processes, pressure is uniformly applied nearly from all directions that is why it is more suitable for complex shapes (Francis, 2016a).

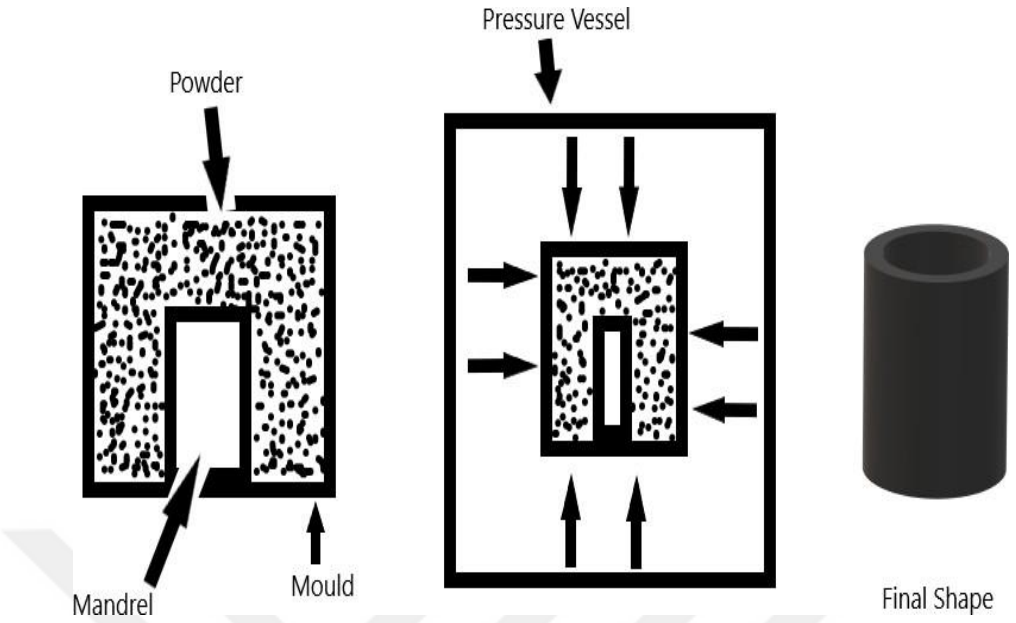

Figure 1.2. *Wet Bag Isostatic Pressing*

Isostatic wet bag pressing is the first sub-group of isostatic pressing that is shown in Figure 1.2. The process starts via loading elastomeric mold, which is separated from the system, and submerged into the system. After pressing is over, mold is taken from the vessel, the product is retrieved then the whole process can be repeated. An advantage of the system is multiple molds can be pressurized at the same time (Francis, 2016). Besides using a mold, uniaxial pressing is performed before isostatic wet bag pressing in some cases and mold usage becomes unnecessary.

The dry bag version is used for relatively small pieces with axisymmetric shapes. As illustrated in Figure 1.3, the process has three parts which are mandrel mold and pressure vessel. The method is used for high-quality ceramic parts for spark plugs yet, due to size and shapes limitations, they need to be green machining after production. Integration of rubber tooling into apparatus, performing of immersion and removal separately is not needed, enhances fast production (Rahaman, 2017).

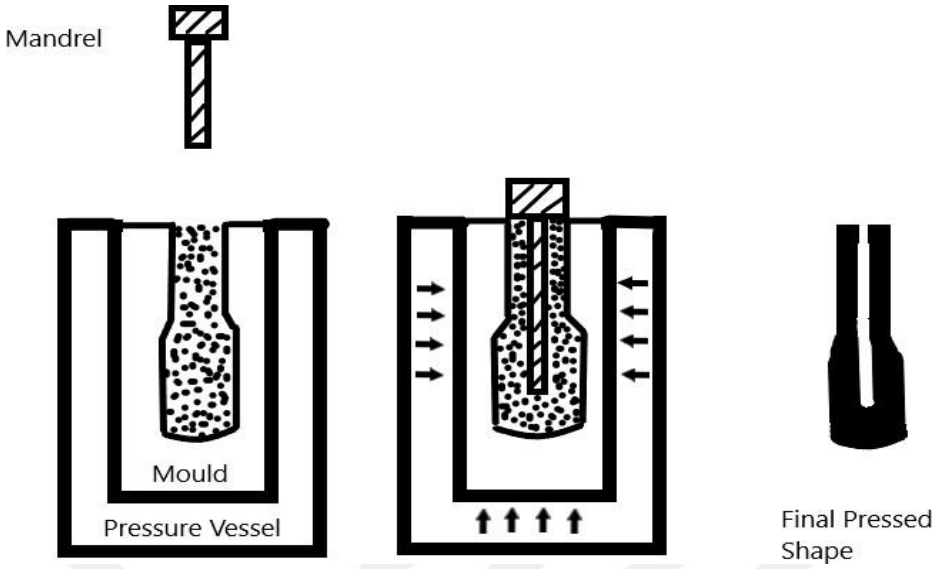

Figure 1.3. *Dry Bag Isostatic Pressing*

Additive manufacturing (AM) can be classified as both production and/or shaping techniques for ceramic materials. Direct production, which includes the densification step too, is used for some ceramic materials with relatively low melting temperatures. The utility of direct additive manufacturing depends on the melting temperature of the ceramic powder and the power limit of the system(Amit Bandyopadhyay, 2016).

A general approach for additive manufacturing is illustrated in Figure 1.4. In the first step a virtual shape is designed for production then this shape is sliced into pieces for additive manufacturing. In the third step, black parts show produced parts of the sample and blue ones are to be added on top of others. Finally, a three-dimensional (3D) product is produced via printing layers one by one.

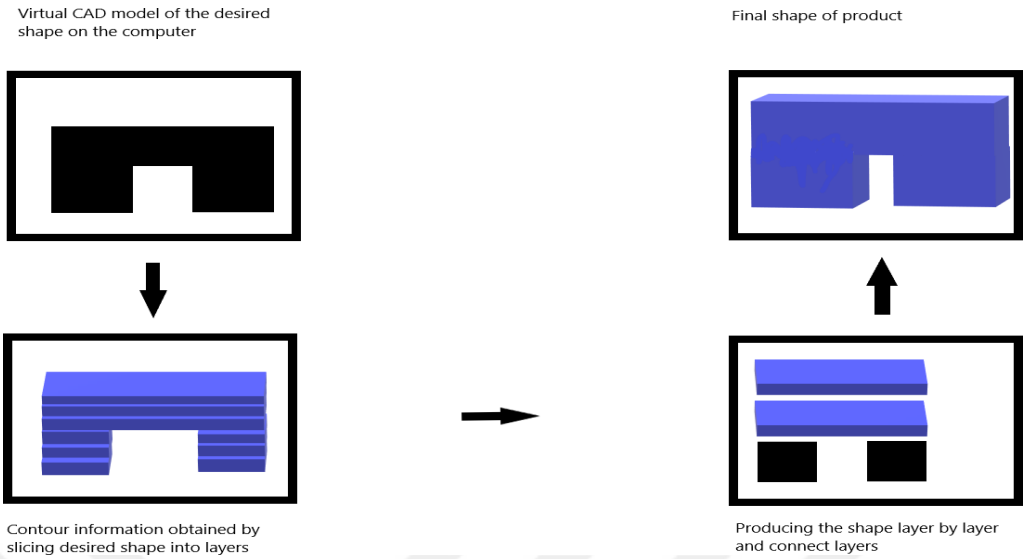

Figure 1.4. *Process steps of Additive Manufacturing*

The advantages and disadvantages of additive manufacturing are shown in table 2.4. Design freedom is the most important property of additive manufacturing. Manufacturing ceramic materials with complex shapes have been an issue and additive manufacturing enhances to overcome this problem. Furthermore, near-net-shape samples can be produced via additive manufacturing.

Table 1.3. *Advantages and disadvantages of Additive Manufacturing*

Advantages	**Disadvantages**
Design freedom: AM is suitable to produce any shape	Surface Finish: Optimal surface require post-processing
No tooling: Without any tooling, production can be done from start to finish	Susceptible for high-volume production due to slow production rate
Saving Material: Due to near-net-shape production, saves material	High printer cost: Large capital need for high-end printers
Versatility: Easy to change the design and its complexity	Production is 3D printer dependent (e.g., different volumes may require different tool formation)
Part optimization: Design freedom enhance to produce parts with higher strength and/or lower weight	

Besides the limitations of AM, it provides developments (e.g. complex shape production, design freedom) that are hard to achieve with conventional shaping methods.

While it is used broadly for polymer material production, its value will be noted better in the future for ceramic materials too.

1.4. Sintering

Ceramic materials are widely produced by sintering, especially medium and high-technology materials. Actual densification can only be maintained by bulk diffusion in pure systems. Other mechanisms contribute to sintering, providing bonding and neck formation such as evaporation-condensation and surface diffusion (R.Rice, 1999).

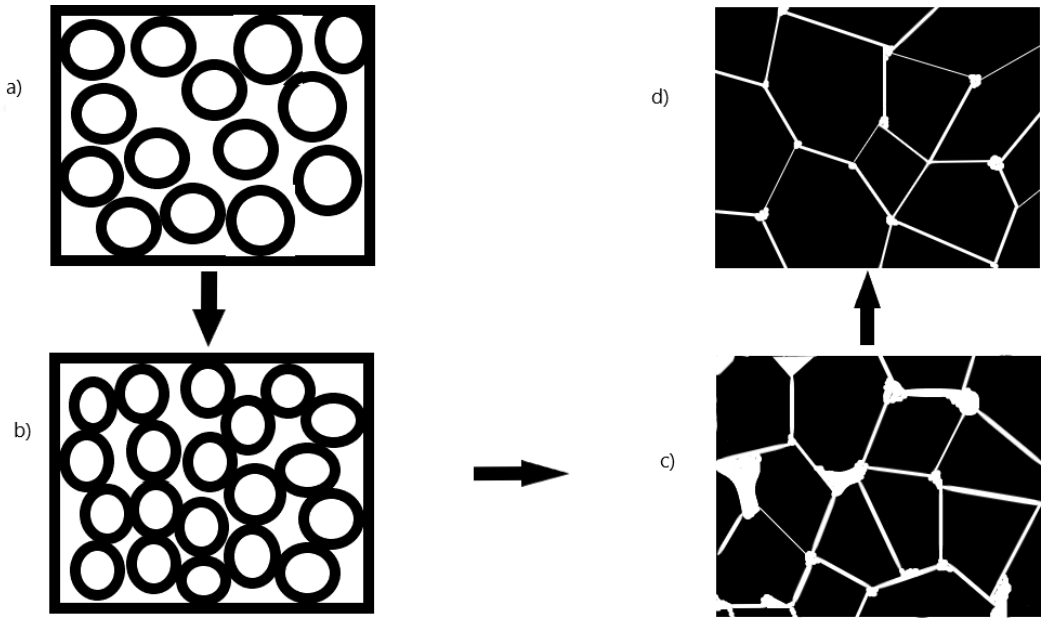

Figure 1.5. *Sintering steps: a) powder compact, b) initial step, c) intermediate step, d) final step*

Ceramic parts that are produced at room temperature have a porous structure. A sintering step is needed to decrease or eliminate voids between particles in a ceramic structure. A schematic diagram for illustrating changes during sintering is shown in Figure 1.5. At first, there is only powder and powder-powder contacts. While temperature increases, neck formations occur between particles. Diffusion to this neck region from grain boundaries (white arrows show this phenomenon) (Figure 1.6) decreases void sizes and enhance densification. Black arrows show the diffusion from particle surface to neck regions which contribute to coarsening but not to densification. A non-porous structure can be achieved when densification surpasses coarsening (Rahaman, 2017). Further increase in temperature enhances higher diffusion rate and voids between particles

shrinks and particles evolve to grains. At the final stage voids between grains shrink further and become grain boundaries (Francis, 2016).

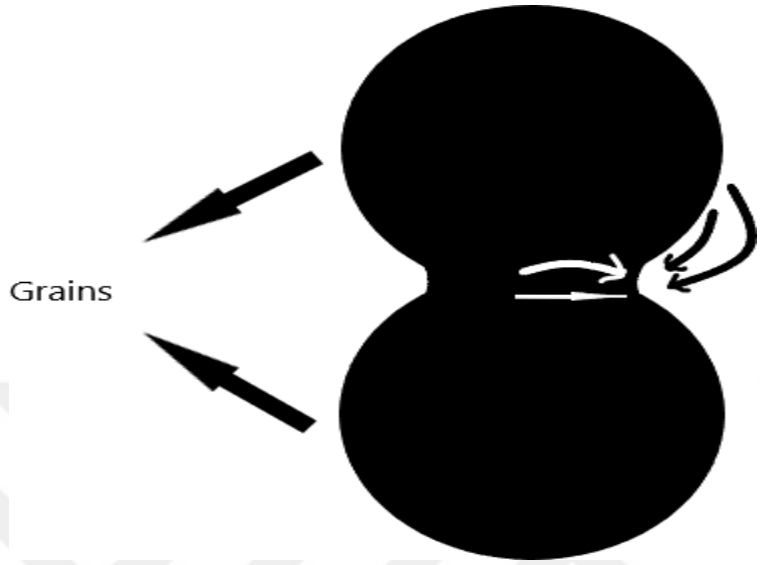

Figure 1.6. *The chemical formula of paracetamol*

Liquid phase and solid-state sintering are classified as two main types of sintering. In the solid-state sintering: there is not any liquid phase and by the movement of atoms from one vacant site to the next, in the lattice, a massive change in dimensions and microstructure occur. Solid-vapour interfaces are eliminated by diffusion (Figure 1.5 a-b) and grain boundaries are formed (Figure 1.5 c-d) (Francis, 2016).

Sintering is a process in which discrete particles in contact with pores evolve to a microstructure that contains grains, grain boundaries, and residual pores (if full densification is not achieved). This evaluation cause shrinkage of the sample in three dimensions. Because of the reasons mentioned above, densification can be tracked either by observing microstructure via microscopy techniques or monitoring part dimensions (density changes).

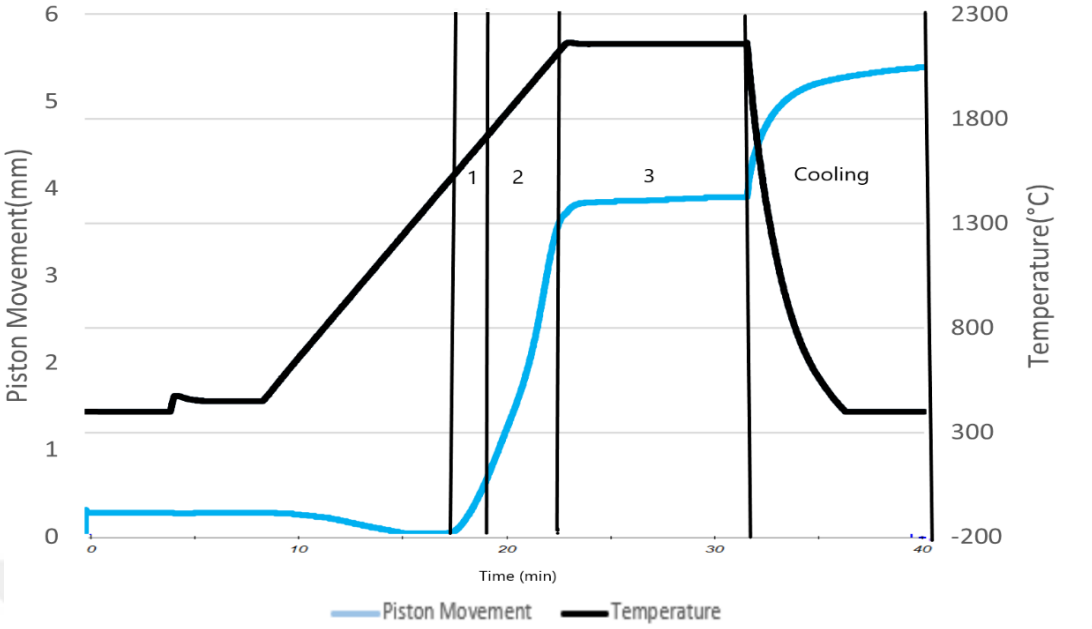

Figure 1.7. *Spark Plasma Sintering graph of B_4C-ZrB_2 composite.*

Figure 1.7 shows an example of densification of the B_4C-ZrB_2 sample by spark plasma sintering (SPS). Densification is separated into three regions (Initial, intermediate and final steps) due to the movement of the piston over time. In the first region, there is relatively low densification this region can be defined by evaluation of Figure 1.5-a to Figure 1.5-b. An increase in temperature results in a higher densification rate which is the result of enhancing driving force to particles. At the end of the second step, pore percentage and size are decreased and pores become isolated from each other. Besides densification, grain growth occurs in this step.

In the final stage, pores are enclosed by grains and a small amount of densification (as seen in the third step of Figure 1.7) is observed. Longer holding time can serve to grain growth rather than densification.

Formation of liquid phase on sintering of a powder enhances to have both higher densification with the same sintering regime and similar densification rates at lower peak temperatures (Francis, 2016b). The key point is the well wetting of powder particles by liquid phase and dissolution of powders in the liquid phase is preferable. There are several roles of the liquid phase during sintering. To begin with, if the liquid phase forms before significant solid-state diffusion then it will improve particle rearrangement to a denser state. Secondly, in the low diffusion pathway that the liquid phase provides to solid particles, powder dissolves and reprecipitates in other surfaces to serve densification. The

effect of the liquid phase on densification is limited with a range of densification that is why further densification is again obtained by solid-state sintering (German et al., 2009).

There are two downsides of liquid phase sintering. The first one is the effect on pore coarsening and the second one is the degradation of the properties of the product.

Reactive sintering, also referred to as reaction sintering, is a particular sintering method in which the reaction of starting powders yields another phase that is not involved in starting powders, and sintering is both achieved in single heat treatment.

This system can be divided into two sub-groups which are single-phase or composite systems (Rahaman, 2017). While boron carbide production from starting powders of boron trioxide and carbon (Reaction 2.13) is an example of single-phase reactive sintering, reaction 2.14 is an example of the production of B_4C/ZrB_2 composite production by starting powders of B_4C, ZrO_2, and C. Beside two sub-groups mentioned above, reactive sintering can be varied by liquid phase or solid-state sintering. Some powders have a eutectic temperature (e.g. $ZrSiO_4$) which is below the formation temperature of the final phase (e.g. ZrB_2) because of that a liquid phase sintering should be considered. Reaction 2.15 is an example of this issue. While the sintering temperature of ZrB_2 is over 2000 °C, the eutectic point of $ZrSiO_4$ is at 1677 °C (Kaiser et al., 2008), (Chamberlain et al., 2006). While reactive sintering of ZrB_2 at temperatures above 2000 °C, SiO_2 enhances liquid phase sintering.

$$2B_2O_3 + 7C \rightarrow B_4C + 6CO \quad (2.13)$$

$$2ZrO_2 + 2B_4C + 4C \rightarrow 2ZrB_2 + B_4C + 4CO \quad (2.14)$$

$$3ZrSiO_4 + 2B_4C + C \rightarrow 3ZrB_2(s) + B_2O_3(l) + 3SiO_2(l) + 3CO(g) \quad (2.15)$$

Reactive sintering provides a new strategy for densification of ceramics which includes producing expected phases and sintering in a process. The reaction takes place, during reactive sintering, promoting densification by releasing heat and promoting the diffusion of interfacial particles. Another advantage is interfacial products improve interfacial binding energy by changing bonding from physical to metallurgical (Wu et al., 2020).

Reactive sintering can be performed by a variety of sintering methods: SPS, Hot Isostatic Pressing (HIP), Hot Pressing (HP), Pressureless Sintering (PS) and Self-

propagating High-Temperature Synthesis (SHS) are some of them. These techniques will be mentioned in the next section with the basics of reactive sintering to understand the effects of reactive sintering on each system.

There are several reactive systems for production either monolithic B_4C or B_4C composite. Reaction 2.13 can be an example of monolithic B_4C production via reactive sintering.

Cobalt (Co) addition is another system for producing B_4C-Co composite in which CoB and Co_2B phases are produced during sintering (Ortiz et al., 2017). TiO_2 is another additive for reactive sintering and production of B_4C-TiB_2 composite (Saeedi Heydari et al., 2015). Si infiltration is another system in which Si reacts with C, SiC phase is produced by reactive sintering and B_4C-SiC composite is produced (Song et al., 2016). Also, three phases can be produced in some systems: reaction between B_4C and $TiSi_2$ is a method to produce B_4C-TiB_2-SiC composite (Wang et al., 2020).

There are many different sintering techniques and different application areas for each of them. To compare the composite material produced in this thesis via SPS with other works that used different sintering techniques, the basics of five different sintering techniques are going to be mentioned. These techniques are Pressureless sintering, Hot pressing, Hot Isostatic Pressing, Spark plasma Sintering, and Microwave Sintering. To understand the effect of each technique on densification, source of heat, and the way of conducting it, pressure directions should be considered carefully.

Pressureless sintering has taken the attention of industry due to lower cost and enhancing complexity to samples. Pressure-assisted sintering techniques have the advantage of better densification yet limits sample size and shape. The disadvantage of pressureless sintering is the need for a relatively higher temperature compared to pressure-assisted techniques. Researchers working on this drawback mostly use sintering aids to promote densification. There are many sintering aids but carbon shows the highest effectiveness compared to others (W. Zhang et al., 2019).

Pressureless sintering involves graphite heaters which are the source of heat generated during sintering (Figure 1.8-a). Generated heat warms the chamber and the sample inside the graphite die up. Many set-ups for this sintering type can be done and

some parts may differ. Even spark plasma sintering is used for creating a pressureless sintering system (Cai et al., 2021).

Three issues need to be considered while pressureless reactive sintering has been chosen. Firstly, sintering additives cause second phases in a matrix material which deteriorates some properties of the product. Second, despite the positive effect on densification, a higher sintering aid content is needed for higher relative densities which promote a negative effect in the first case above. The last case is the homogeneous distribution of the second phase in the microstructure which is especially hard for carbon (W. Zhang et al., 2019).

While pressureless reactive sintering shows a value for producing complex shapes at lower temperatures than non-reactive PS, there are many disadvantages when compared with pressure-assisted sintering techniques. Higher sintering temperature, longer sintering time, grain growth, and relatively low mechanical properties are some of the drawbacks of PS.

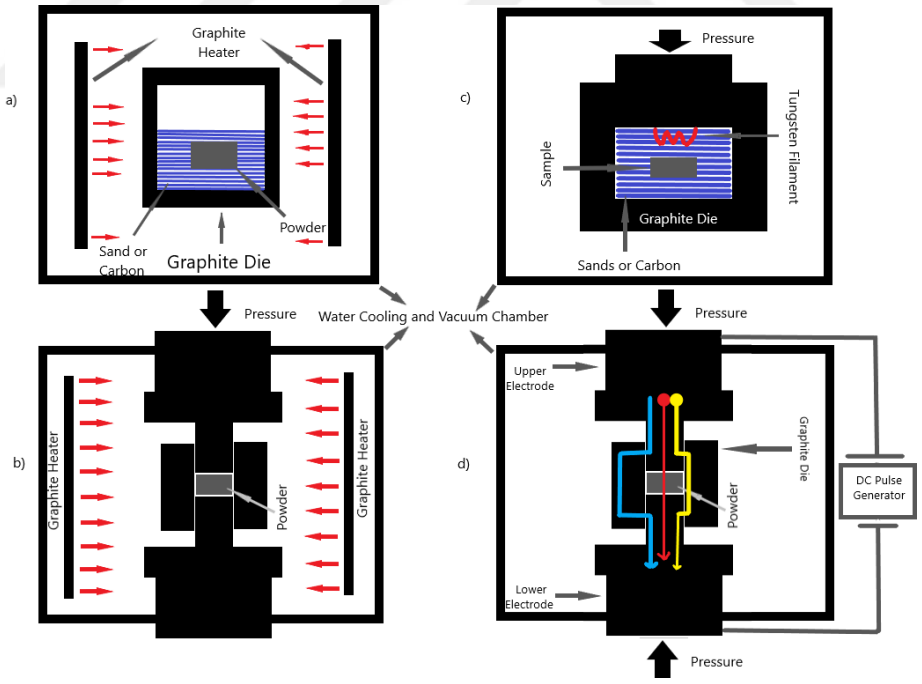

Figure 1.8. Simplified views of; a) Pressureless Sintering, b) Hot Pressure Sintering, c) Self-propagating High-Temperature Sintering, d) Spark Plasma Sintering.

Pressure-assisted sintering methods are used especially for materials with high melting temperature, decreasing sintering temperature, and/or sintering time. For pressureless sintering without additives, the driving force for sintering is the temperature.

When reactive sintering is involved, reactions enhance the driving force for densification. Besides these two driving forces, pressure is another parameter that eases sintering.

Due to pressure application, driving force increases in highly stressed regions where particles contact more. The driving force for sintering can be increased by more than 20% via pressure assistance(Kuang et al., 1997). Mainly four effects of pressure assistance on the production are:

1) Reduction in sintering time.

2) Reduction in sintering temperature. Less grain growth compared to PS.

3) Minimization of the percentage of the residual porosity.

4) Better mechanical properties because of the effects mentioned in the second and third effects of pressure on production.

The setup of HP is very similar to PS as seen in Figure 1.8-b. The only difference is the application of pressure from the upper side. Like PS, the heat source is the graphite heaters at the sides of the chamber. Heat is conducted to powder through graphite die and punches.

Pressure-assisted techniques are not used on an industrial scale due to higher costs yet they enhance a great time saving for research areas.

SHS also mentioned as combustion synthesis is a recent technology for material science that emerged in the twentieth century. The system setup is shown in Figure 1.8-c may differ from machine to machine, it involves a tungsten filament that produces heat for sintering. Sample stands in an area filled with carbon or sand. Pressure is applied by a mobile upper punch. Besides producing a dense ceramic body this method is widely used to produce starting powders for other sintering techniques (e.g., SPS) (Orrù & Cao, 2013) or porous structures (Wu et al., 2020).

The mechanism of reactive-SHS can be divided into three parts. In the first part, the exothermic reaction of raw materials is started via external energy which is produced by tungsten filament for the system in Figure 1.8-c. Second, the combustion wave produced by reactions covers the whole system and enhances the continuity of started reactions. In the end, the heat released by reaction in the system provides the driving force for sintering and the sample is densified by that(Wu et al., 2020).

The main advantage of this method is, no external energy need once raw materials are ignited. The cost of sintering can be reduced dramatically by this method. Other advantages of the method are high heating and cooling rates, improved purity of the product, and simplicity of equipment (Group & Metallurgical, 1992).

As an example, boric acid (H_3BO_3) and Al powders are used to produce B_4C/Al_2O_3 composite via reactive-SHS process (Ebrahimi & Torabi, 2012). Reactions 2.16 and 2.17 show the changes during the sintering process. The reaction between Al and B_2O_3 releases heat to complete sintering.

$$2H_3BO_3(s) \rightarrow B_2O_3(s) + 3H_2O(g) \quad (2.16)$$

$$4Al(s) + 2B_2O_3(s) + C(s) \rightarrow 2Al_2O_3(s) + B_4C(s) \quad (2.17)$$

Hot isostatic pressing is a technique that takes advantage of gas pressure at the high temperatures to produce dense materials. Setup of the system is like PS, yet the atmosphere of the HIP enhances to create high pressure (50-300 MPa) (Atkinson & Davies, 2000).

The system is heated via heating coils from two sides of the specimen and the gas pumping system ensures desired pressure (Figure 1.9). The process starts with filling the tank, closing, and venting it. After heating and increasing the pressure, the sample is soaked under constant pressure then cooling is the final step of the process (Dobrzanski et al., 2017).

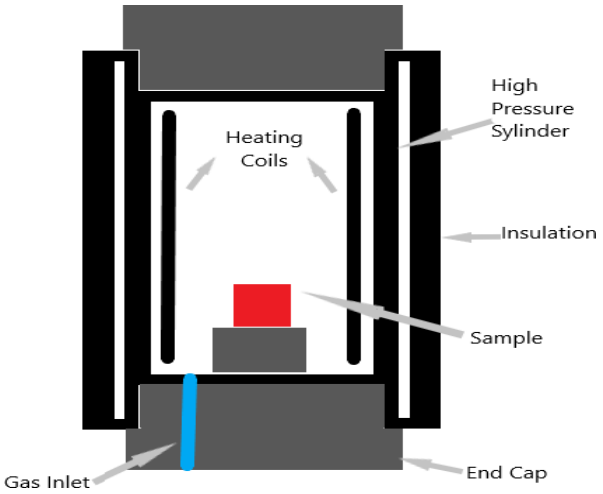

Figure 1.9. *Schematic representation of HIP.*

Spark plasma sintering also called (Field Assisted Sintering Technology) is one of the most broadly used sintering techniques recently. Figure 1.10 shows yearly publications involving SPS which illustrates the improving importance of the technique in the world. When the effect of the pandemic is considered in 2020 and 2021, it can be said that publications about SPS increased every year. The first patent that involved sintering via electric current was in 1913 in the US patent and the spark plasma sintering technique was first developed in 1930. Due to the lack of scientific development, the technique could not be used efficiently up to the 1980s. Via new developments variety of laboratories have begun to use the technique. After the 1990s, the patent of Inoue's expired, several companies started to produce the device, and usage in research increased dramatically (Cavaliere, 2019).

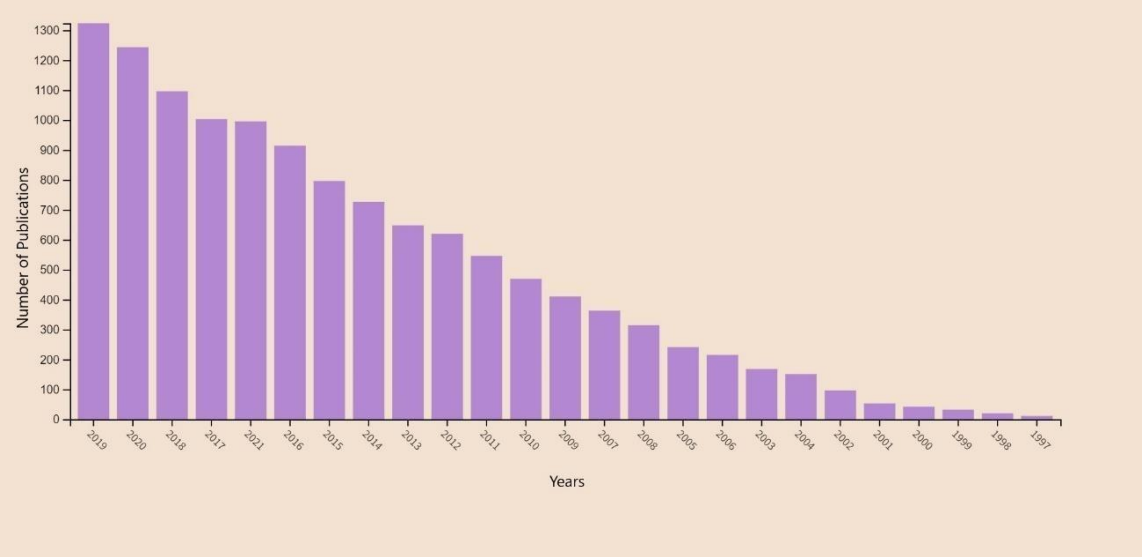

Figure 1.10. Yearly analysis of publications have (Spark Plasma Sintering) in their title (adapted from www.webofscience.com)

Spark Plasma Sintering is most widely used in material science, as seen in Figure 1.11, when compared to other fields it almost has half of the publications. Besides ceramic materials, SPS can be used for metals, alloys, and composites. During sintering, a DC Pulse generator (Figure 1.8-d) creates a current that goes through material and carbon die. Pressure and electric field that are produced by applied voltage produce the driving force for sintering(Cavaliere, 2019). The difference of SPS compared to HP, HIP or PS is the heating sources. While for those pressure-assisted techniques, mentioned above, an external heat source is used and the chamber is heated by them. SPS heats both chamber and material at the same time. The mechanisms lie upon a different heating system of

SPS is connected to a created electric field, via pulsed direct current, that passes through conductive die and sample (Kessel et al, 2006).

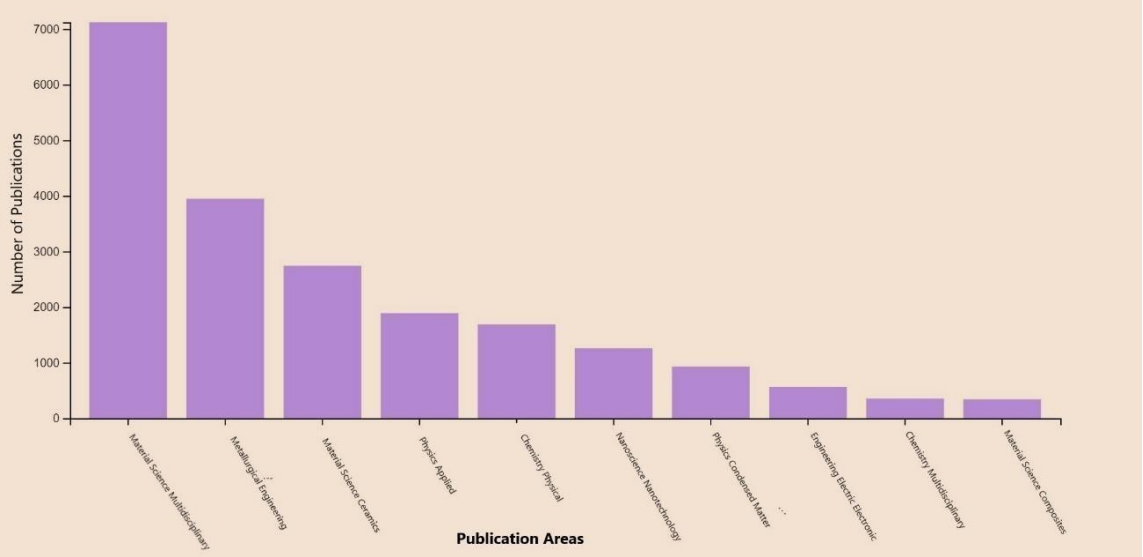

Figure 1.11. Fields of publications that have SPS in their title. (adapted from www.webofscience.com)

Device parameters can be both controlled from the device interface or a computer connected to the device. Controlling the sintering regime carefully is the key to getting a product with desired properties.

The pressing chamber is the place where the sintering of material is performed. This part should be capable of withstanding $1x10^{-4}$ mbar vacuum condition and 2200 °C temperature. The size of the chamber depends on the mold set that is planned to use(Cavaliere, 2019). Parts of the chamber are:

- Stainless steel chamber
- Water-cooled, double-walled vacuum chamber
- Front-loading type
- Ports of loading and weaving pyrometer
- Two additional blind flanges to install additional devices and gauges
- Inert gas inlet and air admittance
- An additional glass window for positioning lamp outside the chamber

The power supply to the furnace should be proportionate for reaching peak temperature (2200 °C) in three-atmosphere conditions (vacuum, nitrogen, or argon atmosphere). Another limit of the device 0000000is the heating rate (800 °C/min) and the power supply should be sufficient for it. The current needed to reach to set temperature

varies due to the size of the die and sometimes it may differ with dies from different suppliers due to the properties of the die. Even heating rate can be increased to peak value, it is not recommended to prevent heterogeneities especially for dies with higher volumes(Tib & Nbo, 2010).

The vacuum pumping system is the part of the device that control atmospheric condition inside the chamber. The vacuum of the chamber should be between $5x10^{-2}$ - $1x10^{-4}$mbar.

The temperature of the device is controlled by two systems: an infrared (IR) pyrometer and a thermocouple. IR pyrometer is expected to measure temperatures between 700-2200°C. Accuracy of the temperature measurement is one of the important parameters to become sure about the application of the planned sintering regime. The accuracy of the system depends on the distance (between spot and device) to spot area (Lowe & Owen, 2007).

When SPS is compared to other sintering techniques (e.g., HIP, HP, PS), the most important difference is the source of the heat. While many techniques use an external heat source to create a driving force for sintering, SPS creates heat both inside the sample and in the chamber by an electric field that moves through the die and sample (Figure 1.8-d). In conventional techniques, the heat of the sample and chamber shows differences due to distance to a heat source. Compared to those techniques, the sintering temperature maybe a few hundred degrees lower in SPS (Cavaliere, 2019). There is a temperature gradient in the system containing chamber, dies, and sample. Measured temperature via IR pyrometer from the die is less than the temperature of the sample. Heterogeneity of the temperature gradient depends on properties of the sample, heating rate, thermal and electrical conductivity of the die (Tib & Nbo, 2010). As an example, the conductivity of the sample completely changes the generation of heat. While conductive powders are heated by Joule Effect, non-conductive powders are heated via their resistance (Groza & Zavaliangos, 2000). Also, the difference between real and pyrometer measured temperature can vary by the properties of the sample. The difference in temperature for non-conductive powders varies 10-15% when compared to conductive powders (Mcwilliams et al., 2006).

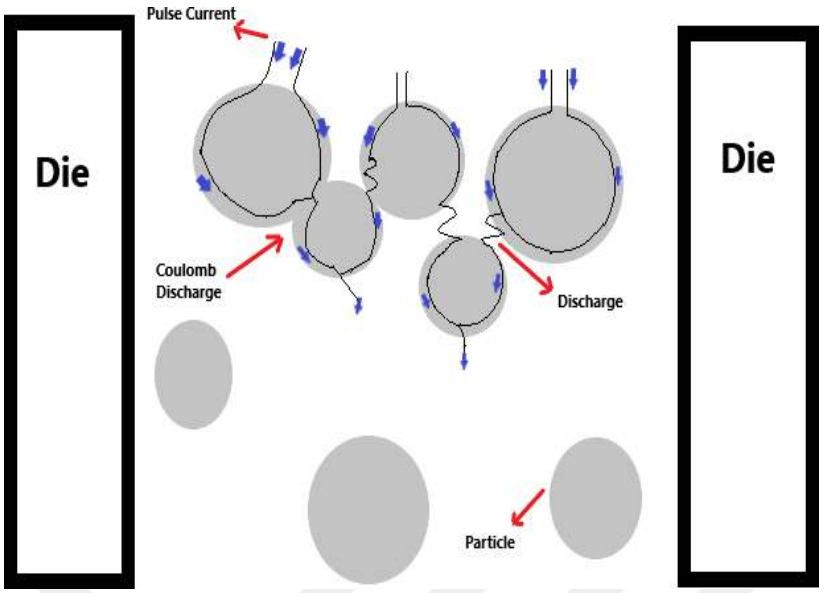

Figure 1.12. *Movement of pulsed current between powder particles.*

In addition to the three stages of sintering mentioned before, cooling can be considered as another stage for SPS. The initial stage of SPS starts with discharge production by ON-OFF pulse generation. Within the dies, pulsed current moves along the surfaces of the particles, and discharge is produced in the void between them (Figure 1.12). Electric discharge produced by DC current and pressure assistance are the main sources of driving

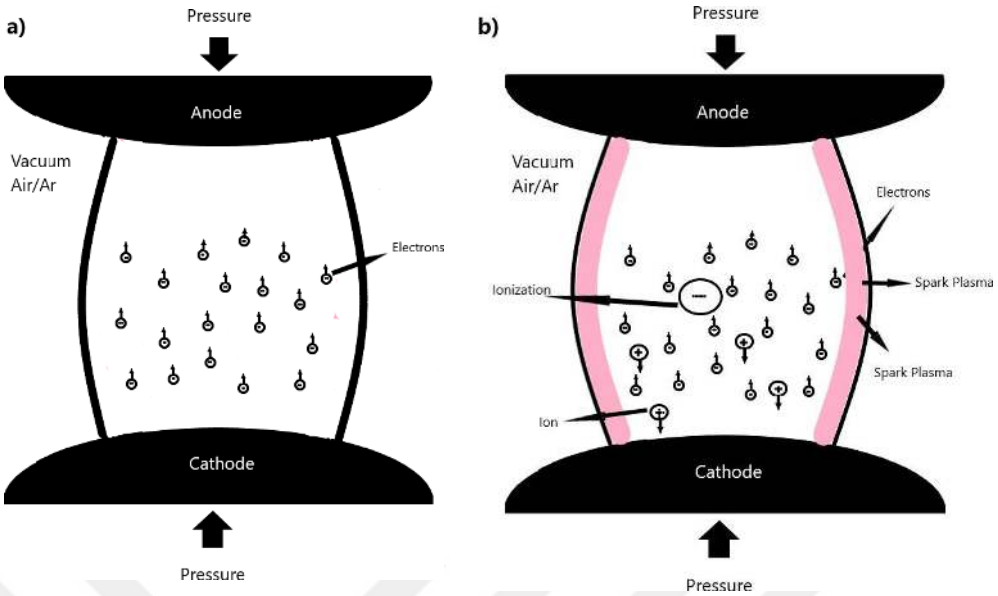

Figure 1.13. *The first and second stages of SPS, a) Initial step (spark discharging), b) generation of spark and ionization*

force during sintering. Spark is generated during discharge, on the contact points of powder particles or space. Spark generation increases temperature locally, first ionization starts and electron-ion flow between cathode and anode starts (Figure 1.13-b).

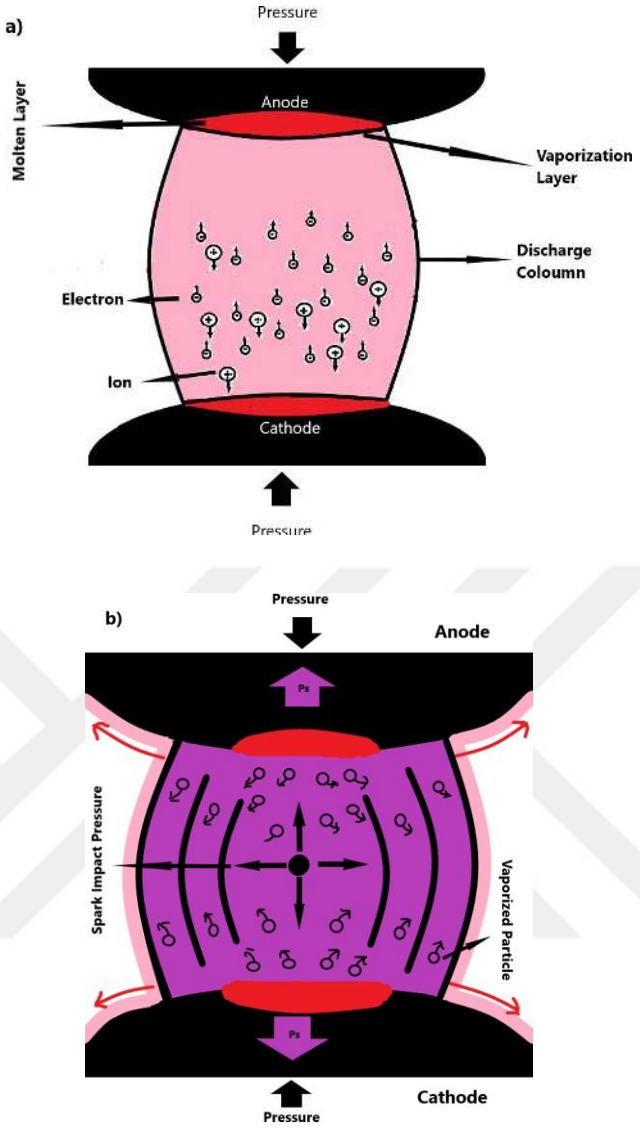

Figure 1.14. *Third and Fourth stages of SPS, a) Surface of particles start to melt and vaporize, b) Sputtering of vaporized-melted particles via generated spark impact pressure*

In the third step, the temperature generated by the spark melts the surfaces of powder particles (Figure 1.14-a). The movement of vaporized particles from the molten region to the outer region can be considered as preparing for neck formation. The intense movement of vaporized particles is further supported by Spark Impact Pressure and particles push toward outer regions (Fig 1.14-b). Finally neck forms between particles (Figure 1.15).

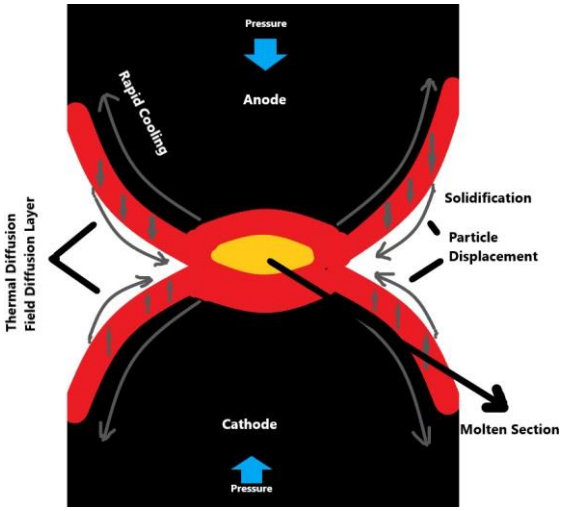

Figure 1.15. *V. stage of SPS (Neck formation).*

In addition to the effect of sparks on densification, another important point is pressure assistance. Especially at the start of the process, pressure application increases the contacts between particles and enhances better packing of powder. Besides increasing contact points and area, possible agglomerates may break via pressure. All these effects of pressure improve the densification of material and help to eliminate pores at lower steps of sintering. Densification at lower temperatures creates a greater value than at higher temperatures due to low contribution to grain coarsening (Ya, 2006).

While positive effects of pressure on the densification in the initial stages are obvious, it may create a problem in the evacuation of gaseous products during reactive sintering (Huang et al., 2014). Densification on reactive sintering has a relatively different mechanism. Firstly, expected phases should be formed then densification of the ceramic material needs to be achieved. Reaction 1.14 shows that the formation of ZrB_2 from B_4C and ZrO_2 starting powders also generates a gaseous product (CO). On one hand, high pressure and rapid increase in temperature enhance densification at lower steps which is a desirable case as mentioned before. On the other hand, this early densification may cause entrapment of the voids filled with gaseous products, which is called bloating(Fang, 2010). The elimination of bloating is more difficult due to pressure created by gas which increases with the shrinkage of the void which entraps it.

The first advantage of SPS is the ability to sinter at lower temperatures compared to conventional methods. Furthermore, the process is rapid and enhances control of the microstructure (Kessel et al., 2006).

Another advantage is to maintain high relative densities by, spark impact pressure, applied pressure(Cavaliere, 2019).

SPS is an efficient technique to produce composites by dissimilar materials. Rapid heating and microstructure control enhance nanomaterial production as well as functionally graded materials (FGM)(Gok, 2021).

High production rate, high heating rate, and low sintering time make SPS a cost-effective method. Comparison of the costs shows that SPS is 50-80% cheaper than traditional techniques(Cavaliere, 2019).

All advantages mentioned above made SPS a widespread method, especially for laboratories, to produce dense materials via sintering. Figure 1.10 can be considered as evidence of the increasing value of the method.

2. SCOPE OF THE THESIS

Boron Carbide is a widespread material, in various applications (Lightweight armor, neutron absorber, etc.), due to its excellent mechanical properties (Solodkyi et al., 2019). Boron Carbide has excellent hardness (the highest after diamond and cubic boron nitride), low density, high melting point, good wear resistance, and chemical inertness (Li et al., 2020). Strong covalent bonds between the boron and carbon atoms obstruct the densification of the boron carbide. To overcome this obstacle, sintering aids are used for the densification of the boron carbide. There are numerous additives used to densify the boron carbide. Some of the sintering additives are Carbon, Aluminum, Silicon, Titanium Dioxide, and Zirconium Dioxide (Zhang et al., 2019).

In this thesis, Zirconium Dioxide and Zirconium Silicate are chosen as sintering additives to produce Boron Carbide-Zirconium Diboride composite. To reduce the price (by using ZrO_2 and $ZrSiO_4$ instead of ZrB_2) and increase densification, by using reactive sintering, oxide additives are used. The main differences between ZrO_2 and $ZrSiO_4$ are the presence of Si in the Zirconium Silicate and the price. Both Zirconium sources are used to produce the ZrB_2 phase in the Boron Carbide matrix.

Zirconium silicate is a natural mineral that is used, as a zirconium source, to compare with zirconia. The effects of both additives on the densification and properties are examined. The problem with the usage of $ZrSiO_4$ is to evacuate the Si from the samples. Due to the presence of Oxygen Silicon forms SiO_2 which is a phase that deteriorates the properties of the composite. By changing the parameters (e.g., dwelling time pressure) of the sintering process, the SiO_2 phase is forced to move towards the side of the samples. In this way, B_4C-ZrB_2 composite without SiO_2 is produced in the interior part. By using a machining process B_4C-$ZrSiO_4$ can be a path to be used to produce B_4C-ZrB_2 composite instead of the B_4C-ZrO_2 route. In this way, the price of raw materials is decreased.

3. EXPERIMENTS

Four different commercial powders (ZrB_2, $ZrSiO_4$, ZrO_2, C) are used to produce B_4C/ZrB_2 composite by reactive sintering. To compare reactive sintering and non-reactive sintering methods first, B_4C and ZrB_2 powders are sintered.

The First route, as reactive sintering, is to use ZrO_2 as an additive without carbon to produce B_4C/ZrB_2 composite and the second route is to use $ZrSiO_4$ and carbon powders. The effects of both reactive and non-reactive sintering routes on the densification of samples are going to be analyzed in section 10.

Five different kinds of powders are used in experiments. The first one is B_4C which is the matrix phase of samples (d50 = 1.2±0.3μm). The other four additives are used for improving the sintering of B_4C. The percentages of each sintering additive are listed in Table 3.1. Percentages of second phases are chosen as thirty weight percent of total powder mixture to enhance better comparison. While the final amount of the ZrB_2 phase is changing by the kind of additive (ZrB_2, ZrO_2, and $ZrSiO_4$), the difference of the effect of this second phase on densification is going to be expressed in section 10a. ZrO_2 powder has relatively high particle size (d50 = 5μm) which results in lower densification of parts that involve ZrO_2. The particle size difference during three hours of ball milling is in Figure 3.1. The ball milling time of the powder mixtures involving $ZrSiO_4$ is three hours. After three hours of milling d50 of the powder becomes 0.679 μm. The surface area of the carbon black is 42 ± 6 parent). Surface area of carbon black improves its chemical reactivity.

Table 3.1. *Weight percentages of four different powder mixtures.*

Powder Mixture Name	**Powder-1 (wt%)**	**Powder-2 (wt%)**	**Powder-3 (wt%)**	**Powder-4 (wt%)**	**Powder-5 (wt%)**
	B_4C	**ZrO_2**	**$ZrSiO_4$**	**C**	**ZrB_2**
B-Zr	70	-	-	-	30
B-O	70	30	-	-	-
B-Si	70	-	30	-	-
B-Si-C	68	-	30	2	-

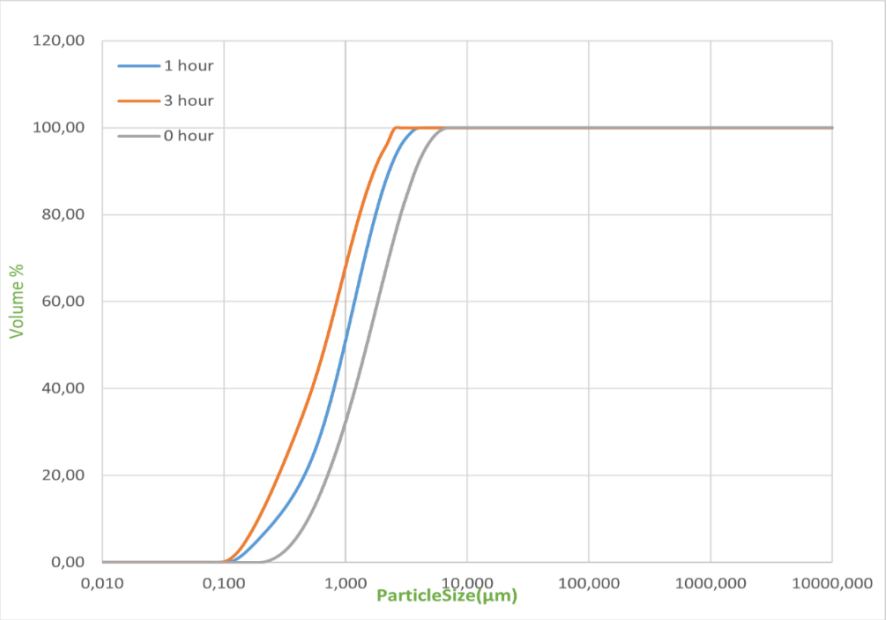

Figure 3.1. *Particle size distribution of $ZrSiO_4$ powder during three hours of ball milling.*

The production procedure starts with mixing powders to create a homogeneous mixture before sintering. B_4C/ZrO_2 and B_4C/ZrB_2 powder mixtures are the first balls milled for 60 minutes in absolute 2-propanol media at a rotational speed of 300 rpm. To improve chemical reactions, $ZrSiO_4$ powder is the first ball milled for 1 hour to decrease average particle size. Then B_4C powder is added to $ZrSiO_4$ and milling is performed one more hour. Carbon addition to $B_4C/ZrSiO_4$ mixture is done after two hours of milling and to create a homogeneous slurry milling is performed one hour too. Details of the mixing process are listed in table 3.2.

Table 3.2. *Parameters of the mixing process of powders.*

Name of Powder Mixture	Rotational Speed (rpm)	Time (hour)	Number of sections
B_4C/ZrB_2	300	1	1
B_4C/ZrO_2	300	1	1
$B_4C/ZrSiO_4$	300	2	2
$B_4C/ZrSiO_4/C$	300	3	3

The slurries are dried by a rotary evaporator for 1 hour and waited on a stove at 90°C for one day. Dried powder ball milled for 15 minutes and then sieved under 250 µm to break agglomerates.

Sintering of B_4C/ZrB_2 composites carried out under vacuum in an SPS furnace. Powder mixture covered with carbon foil (Image 3.1) (20 mm to roll powder and 4 spheres, 2 for top and 2 for bottom) to inhibit die-powder reactions and put into a graphite die.

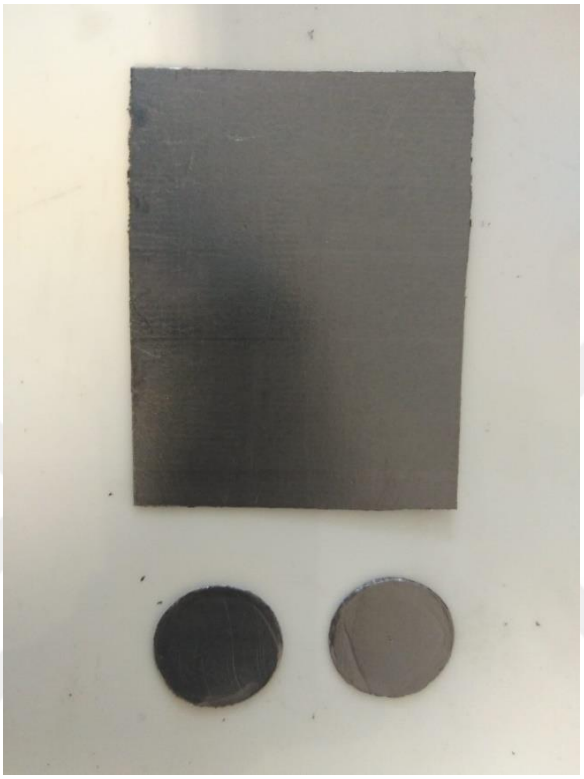

Image 3.1. *Carbon foils are used to cover powder samples inside carbon dies.*

Before observing the effect of pressure on the densification, sintering of samples is done with minimum pressure that the device allows (5 kN = 15.7 MPa). After examining the XRD, SEM, and relative density results, pressure is doubled (31.4 MPa) to observe the effect of pressure on the densification. The pressure increase is not applied at the beginning of the process. The reason for this application is not to prevent gas evacuation produced by the reactions. Bloating is observed in the SEM image of the B_4C-ZrO_2 powder mixture. To eliminate bloating defects, the pressure increase is applied at peak temperature for B_4C-ZrO_2 mixtures. During sintering at peak temperature, the gas pressure of the vessel is observed, and minor points are enhanced after five minutes at sintering temperature. Because of these reasons, pressure increased five minutes later than reaching 2000 °C.

The sintering regime of the B_4C-$ZrSiO_4$ powder has some differences from the B_4C-ZrO_2 powder mixture. The first difference is the dwelling temperature whose reasons are

explained in detail in section 10.1. Another difference is the point where pressure is applied. Unlike the B_4C-ZrO_2 powder mixture, the problem is not to evacuate gaseous products but to eliminate a secondary phase. Because of this reason pressure is applied at the beginning of the dwelling temperature (1500 °C).

Samples are cut into three pieces and these pieces are used to measure weights for Archimedes Method, XRD, and SEM analysis.

After cutting carbon foil is removed from the surface of the sample then milled to create a powder of samples. Reason for preparing powders after sintering is to prohibit miss-analysis of the phases in different regions of samples. Another important property for this thesis is achieved higher relative density at the produced materials.

Theoretical density is calculated by the rule of mixtures. Archimedes Method is used to calculate the relative density of the samples.

The last part of the characterization is the microstructure analysis. Before the analysis sample preparation is needed. Sample preparation has two steps: the first one is mounting which enhances grinding and polishing of the sample automatically. After polishing, samples are characterized by SEM.

4. RESULTS OF EXPERIMENTS

Results of the experiments are evaluated in four subtitles which are needed to be examined separately. After this evaluation, results are going to be discussed as a whole, and suggestions for future works are going to be made.

4.1. Analysis Of X-ray Diffraction Results

XRD analysis of the composites, produced via reactive sintering method, has significant importance. After applying this method, it can be understood whether the complete formation of desired phases is done or not. To evaluate the sintering regime, SPS is used to form a phase map for B_4C-ZrO_2 powder. Powder mixtures are heated to temperatures; 1000, 1100, 1200, 1300, 1400, 1500, and 1600 °C. Samples were held at those temperatures for one minute to observe the evaluation of reactions. This phase map formation is done to detect the phase changes to evaluate the sintering regime. Consumption of ZrO_2 phase in B_4C-ZrO_2 powder mixture is nearly completed at 1600 °C. Although the formation of ZrB_2 is started at 1200 °C, the complete formation of the phase is retarded due to a high particle size of ZrO_2 powder (5 μm). Any residual ZrO_2 phase is observed in the XRD analysis of the sintered sample (Figure 4.1). While the complete formation of ZrB_2 is achieved, the residual carbon phase is observed as the result of reaction 5.1. Besides residual carbon, there are unnamed peaks at 44.7 ° which is contamination caused by the grinding process. The purpose of the grinding process is to prevent possible misleading data of bulk samples because of non-homogeneous samples. The B_2O_3 phase formed during ZrB_2 formation leaves the system as a gaseous side product.

To restrict boron loss and remove residual carbon (e.g., Reaction 5.2), two steps sintering route is applied after the first sample. Even though a complete formation of ZrB_2 is not achieved at 1600 °C, considering the positive effect of longer dwelling time (5,10,15 minutes for sintered samples) at 1600 °C on ZrB_2 formation, this temperature is agreed as an acceptable point for two-step sintering.

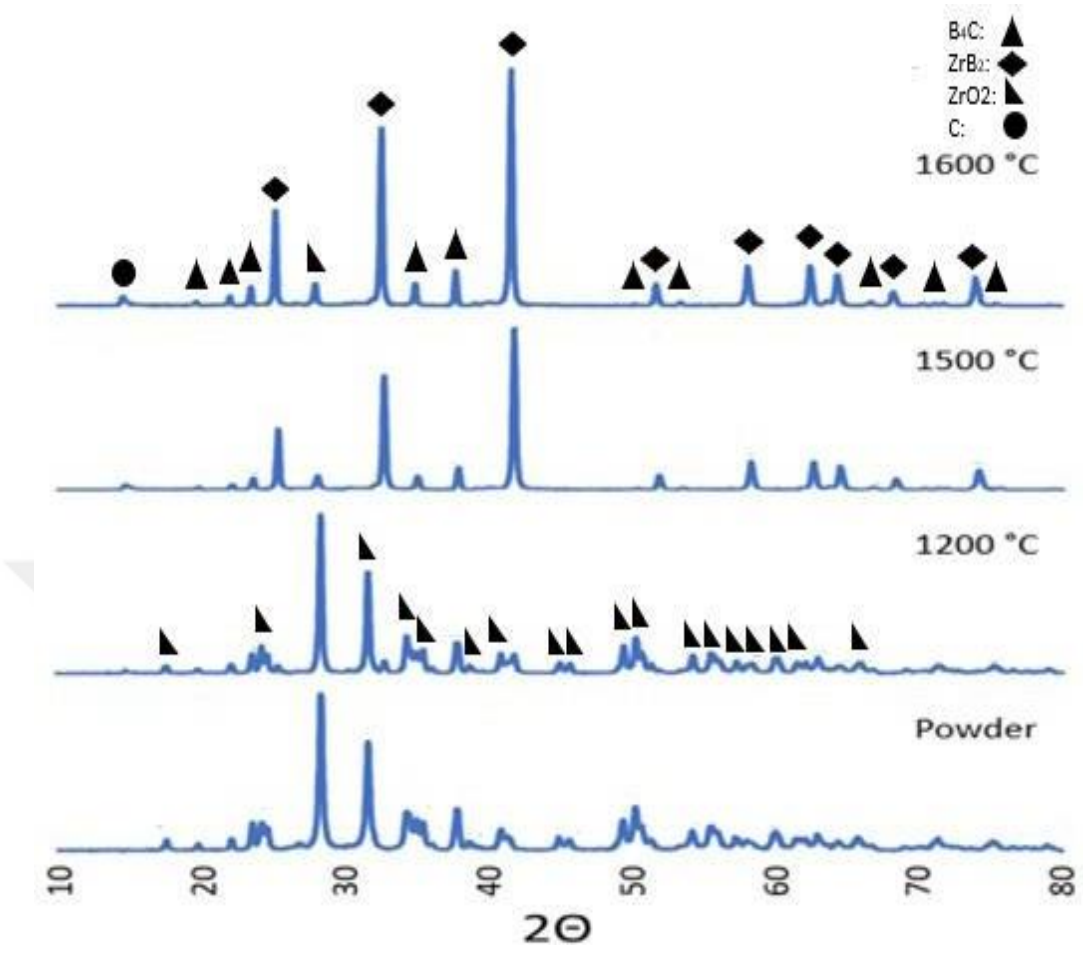

Figure 4.1. *XRD analysis of B-O: composites heated to 1200,1500 1600 °C and raw powder*

As a result of two-step sintering residual carbon phase is not observed in XRD analyses (e.g., Figure 4.2-d). Besides the elimination of carbon peaks, contamination during grinding is prevented by decreasing the grinding time.

The second route to produce B_4C-ZrB_2 composite by reactive sintering is to use $ZrSiO_4$ powder as a Zr source. While the price of this raw material is much cheaper than ZrO_2, silicon existence stands as a problem. Before preparing a sintering regime for this production route, the B_4C-$ZrSiO_4$ powder mixture is heated to 1000, 1100, 1200, 1300, 1400, 1500, and 1600 °C. Powders are held for a minute at peak temperatures.

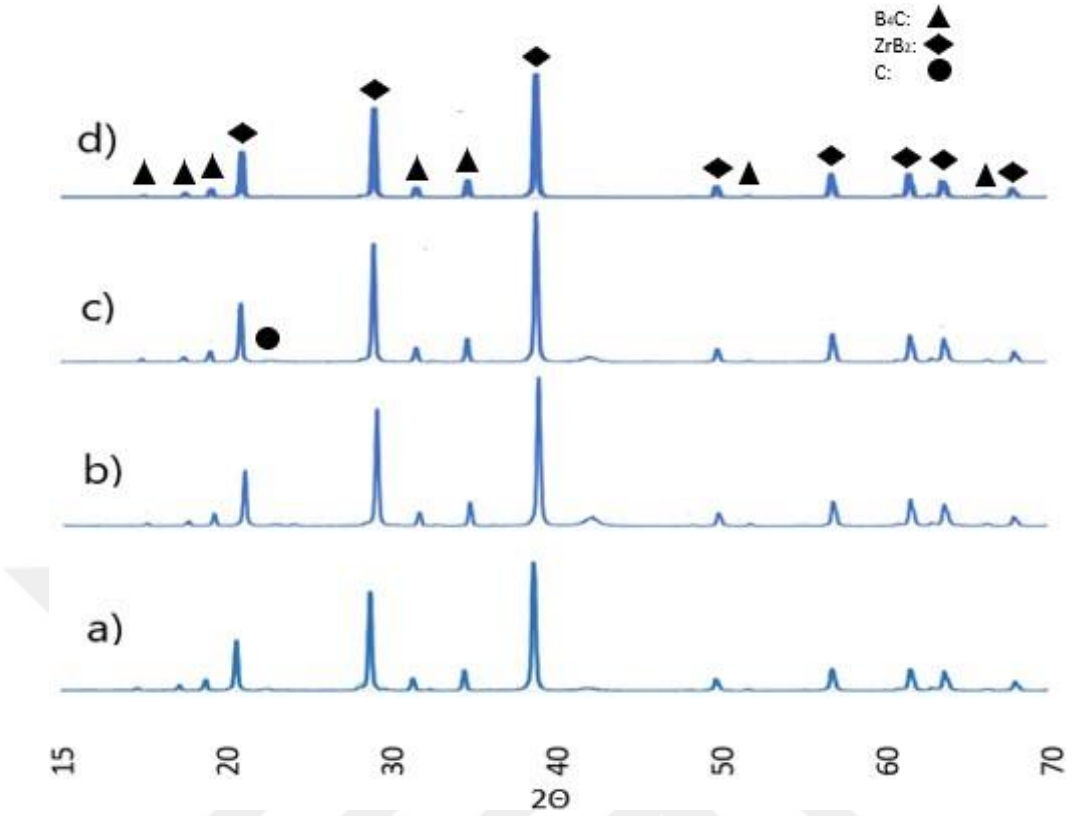

Figure 4.2. XRD analysis of B-O samples: a) one step sintered sample at 2090 °C (15.7 MPa), b) Two-step sintered sample at 2090 °C (15.7 MPa), c) Two-step sintered sample at 2000 °C (15.7 MPa), d) Two-step sintered sample at 2000 °C (31.4 MPa).

$$5B_4C(s) + 6ZrO_2(s) \rightarrow 6ZrB_2(s) + 4B_2O_3(s) + 5C(s) \quad (5.1)$$

$$2B_2O_3(s) + 7C(s) \rightarrow B_4C(s) + 6CO(g) \quad (5.2)$$

Figure 4.3 shows critical phase changes at temperatures mentioned above. While ZrB_2 formation is observed at 1200 °C like B_4C-ZrO_2 powder mixture, SiO_2 or C phases are not seen. When the amount of SiO_2 and C phases are increased, by the dissolution of $ZrSiO_4$ phase and ZrB_2 formation, they are seen at 1400 °C.

When the temperature increased to 1500 °C complete dissolution of $ZrSiO_4$ and formation of ZrB_2 is achieved. While there is Carbon in the system any SiC phase is observed at 1500 °C. The aim of this thesis for the B_4C-$ZrSiO_4$-C powder mixture is to evacuate SiO_2 to the surface of the sample and produce a B_4C-ZrB_2 ceramic composite in the core. SiO_2 flow is observed in SEM images and going to be analyzed in detail in the next sections.

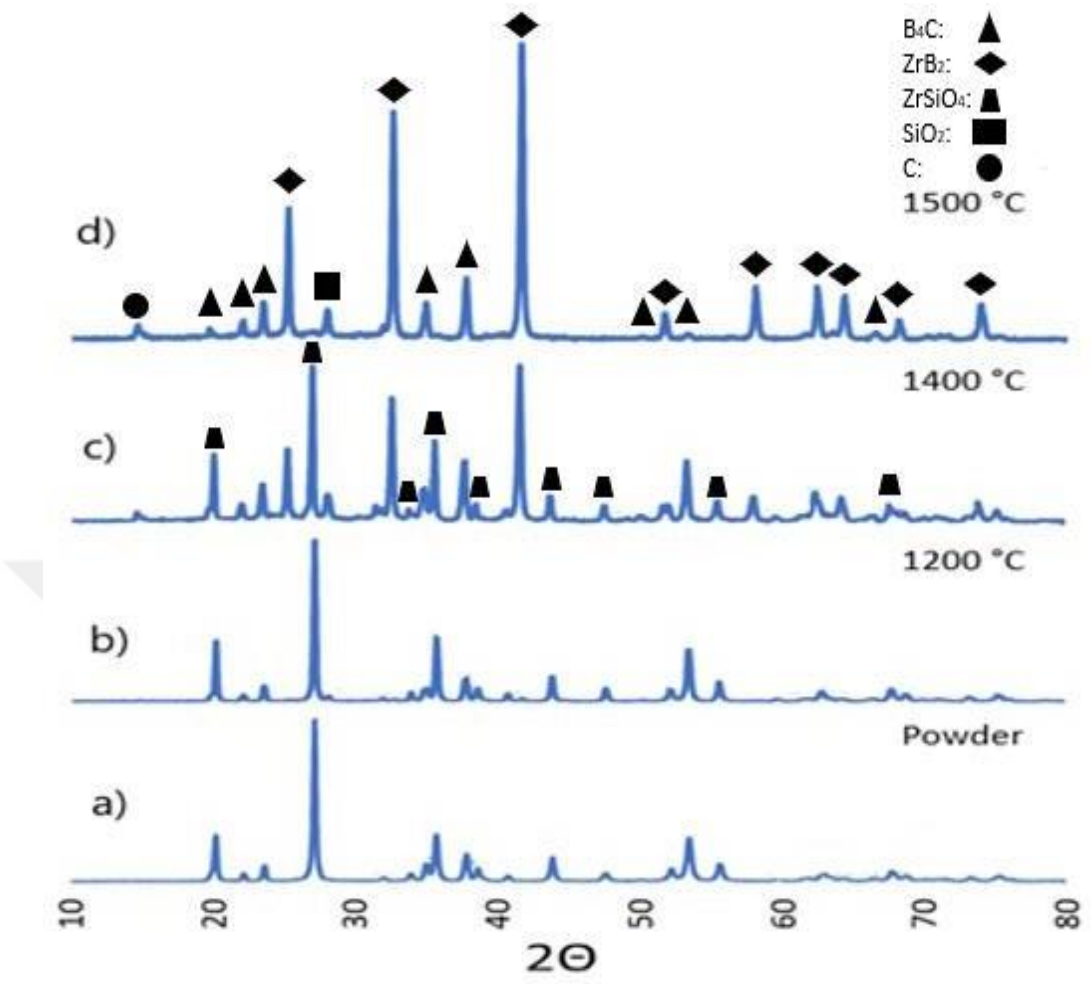

Figure 4.3. *XRD analysis of B-Si-C: composites heated to 1200,1500 1600 °C and raw powder*

The first sample is sintered at 2093 °C for 15 minutes and XRD analysis (Figure 4.4-a) shows the complete formation of ZrB_2. Besides the SiO_2 phase, there is a significant amount of C in the system. SiO_2 phase forms SiC at temperatures above 1500 °C yet an uncomplete formation of SiC with residual carbon is the result of heterogeneous distribution of SiO_2 (Biernacki & Wotzak, 1989).

The reason for the heterogeneous distribution of SiO_2 is the flow towards the surface of the sample. Due to the overflow of SiO_2 through the surface carbon die becomes unusable. To overcome this situation sintering temperature is lowered to 2010 °C. There is no significant change in the XRD analysis of the second experiment, yet SiO_2 overflow leads to a decrease in sintering temperature. At 1930 °C SiO_2 phase is vanished and SiC formation is relatively low which is the result of SiO_2 flow towards the surface and staying

in a small region. During removal of carbon paper from the surface of the sample, most of the SiO_2 phase is removed and XRD analysis did not show a SiO_2 peak.

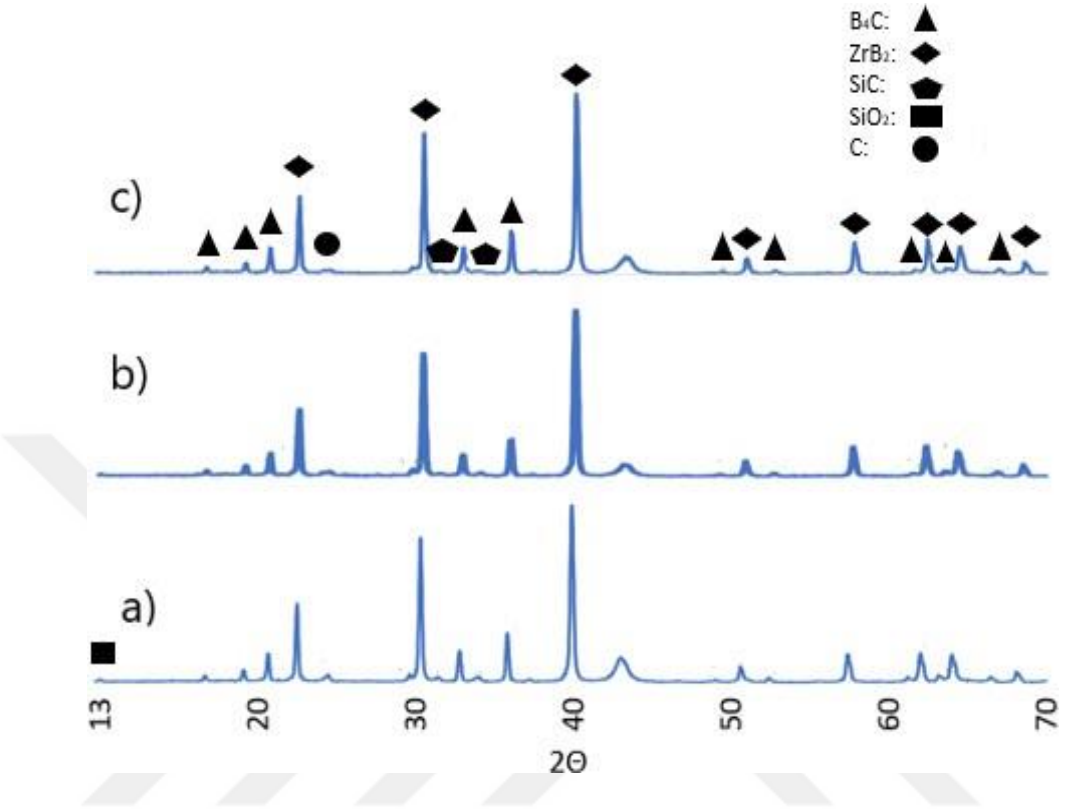

Figure 4.4. *XRD analysis of one-step sintered B-Si-C samples at a) 2093 °C, b) 2012 °C, c) 1930 °C*

To inhibit SiC formation, two-step sintering is performed after three experiments. The second step aims to enhance the flow of the SiO_2 phase before the formation of SiC. To achieve this purpose second step is chosen as 1500 °C. The reason for choosing 1500 °C is, complete dissolution of $ZrSiO_4$ and this temperature is below the formation temperature of SiC.

Results of different dwelling time at 1500 °C is shown in Figure 4.5. There is a slight increase in the peaks of SiC with higher dwelling time which shows that the SiC phase forms at 1500 °C. Similar to one-step sintering there is not any SiO_2 peak in the XRD analysis of sample dwelled 5 minutes at 1500 °C. After dwelling time increased to 10-15 minutes, the SiO_2 phase is observed.

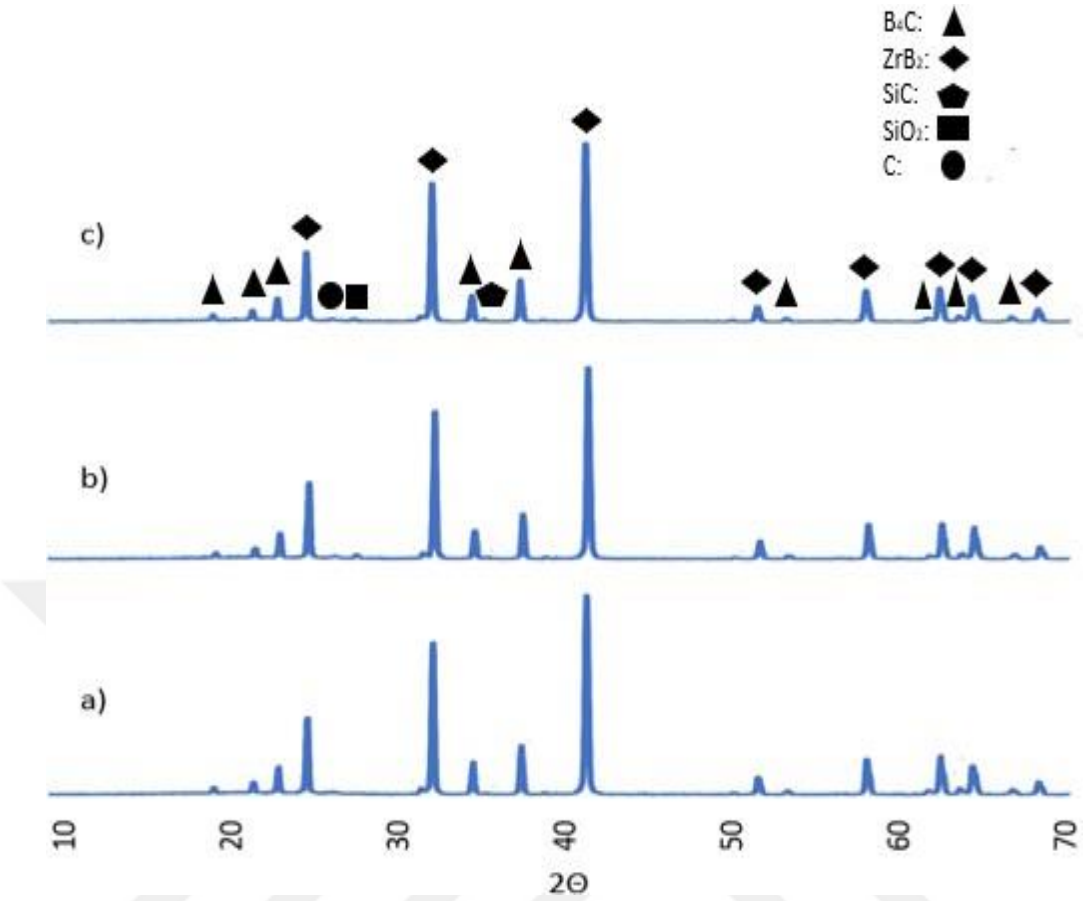

Figure 4.5. *B-Si-C powder mixture sintered at 1930 °C and dwelled at 1500 °C for; a) 5 minutes, b) 10 minutes, c) 15 minute*

After cutting of samples and removal of carbon paper from the surface to prepare for characterization, an oxide layer is formed on the surface. Image 4.1 shows the oxide layer formed on the surface of samples waited for one day after cutting. During cutting, samples are exposed to water which improves oxide formation. After the oxide layer is removed from the surface, there is slight oxidation is observed which is related to water existence.

Image 4.1. Oxide layers on the surface of the B-Si-C samples.

Figure 4.6 shows the XRD analysis of the oxidized layer which is characterized as the SiO_2 phase. The formation of SiO_2 is related to the formation of Si or SiO phases which create an oxide layer on the surface at room temperature. Reactions 5.3 and 5.4 show the formation of Si and SiO phases (Biernacki & Wotzak, 1989).

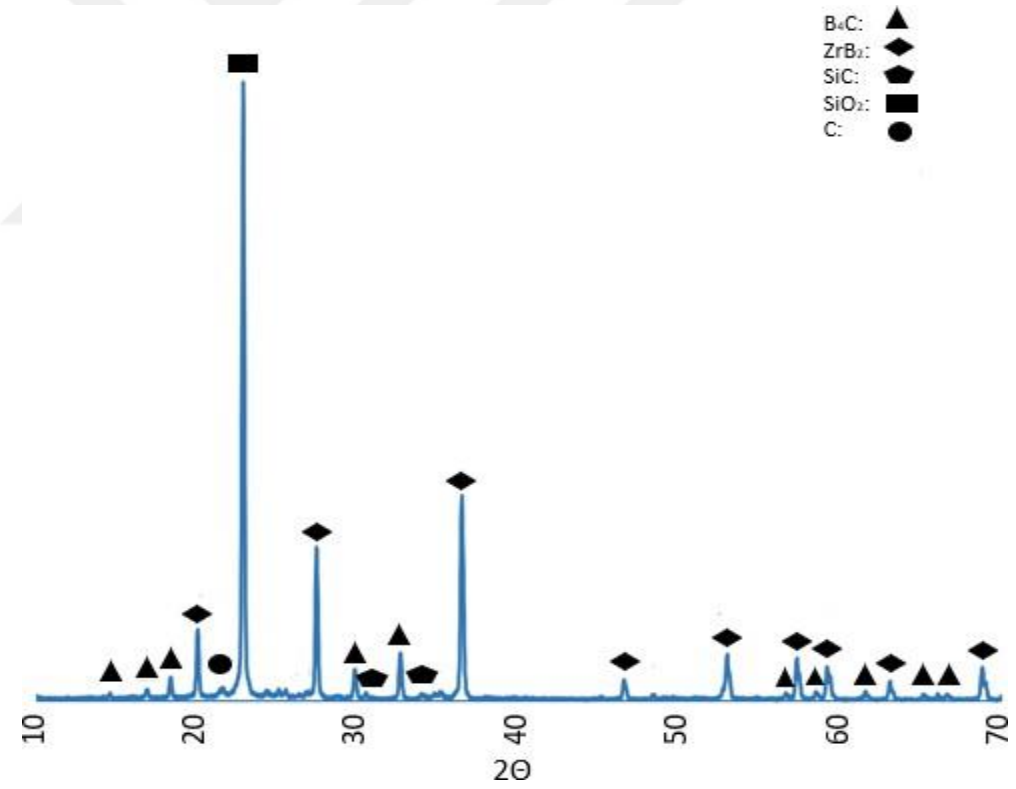

Figure 4.6. XRD analysis of the oxidized layer of B_4C-$ZrSiO_4$ sample

$$SiC + 2SiO_2 \rightarrow 3SiO + CO \quad (5.3)$$

$$2SiC + SiO_2 \rightarrow 3Si + 2CO \quad (5.4)$$

4.2. Analysis of Spark Plasma Sintering Results

Graphs of Spark Plasma Sintering devices provide many parameters (e.g., Temperature, Piston Displacement, Force, etc.). Graphs of these parameters can be used to understand the changes during experiments, relate them with properties of a material, and compare these changes between experiments.

Pressure and heating rate effects on the sintering of B-O samples are illustrated in Figure 5.8. After the heating rate is lowered to 50 °C/min from 100 °C/min, the displacement between 1600-2000 °C is increased by around 14.7%. The purpose of this parameter change at those temperatures is to enhance easier gaseous side-product evacuation before achieving higher densification rates. This parameter is both related to higher time at elevated temperatures where intense densification is happening and promotes the elimination of pores that do not keep gaseous side-product inside them. Achieving higher densification rates before elimination of gaseous products results in bloating which is going to be examined with SEM images in the next sections.

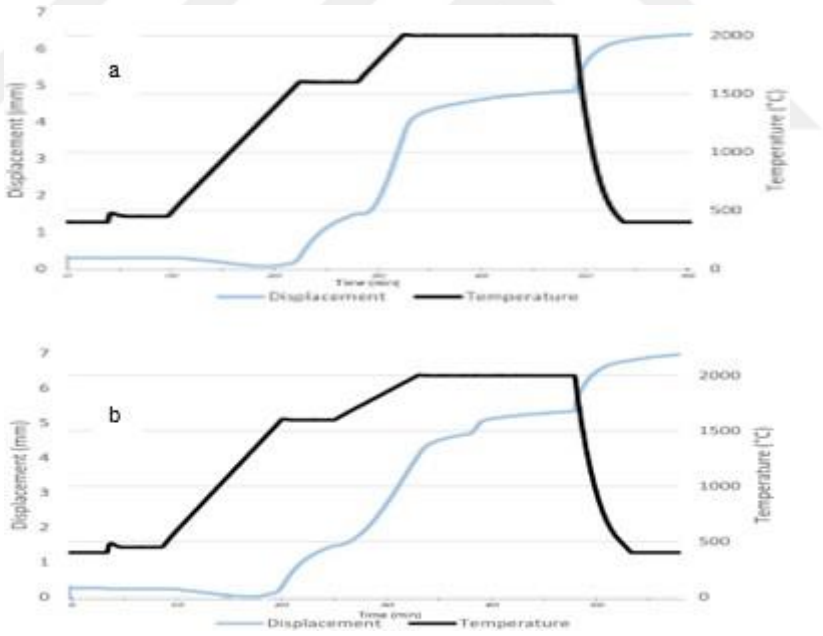

Figure 4.7. *SPS graph of B-O samples; a) Heating rate constant (100 °/min), pressure constant (15.7 MPa), b) Heating rate is lowered to 50 °/min between 1600-2000 °C and 31.4 MPa pressure is applied after 39th minute to the end of the process.*

While there is a relatively similar displacement speed between the temperatures of 0-1600 °C after dwelling displacement speed is higher on a sample that has a high heating

rate (Figure 5.8). When reactive sintering is considered, lower displacement speed before peak temperature is an advantage for the elimination of gaseous side-products. Having a relatively porous structure before this elimination prevents bloating formation. As mentioned above displacement is increased by 14.7%, this displacement is achieved while dwelling time is doubled. The effect of this lower displacement speed is positive yet it also has the potential to promote grain growth which affects properties of material diversely.

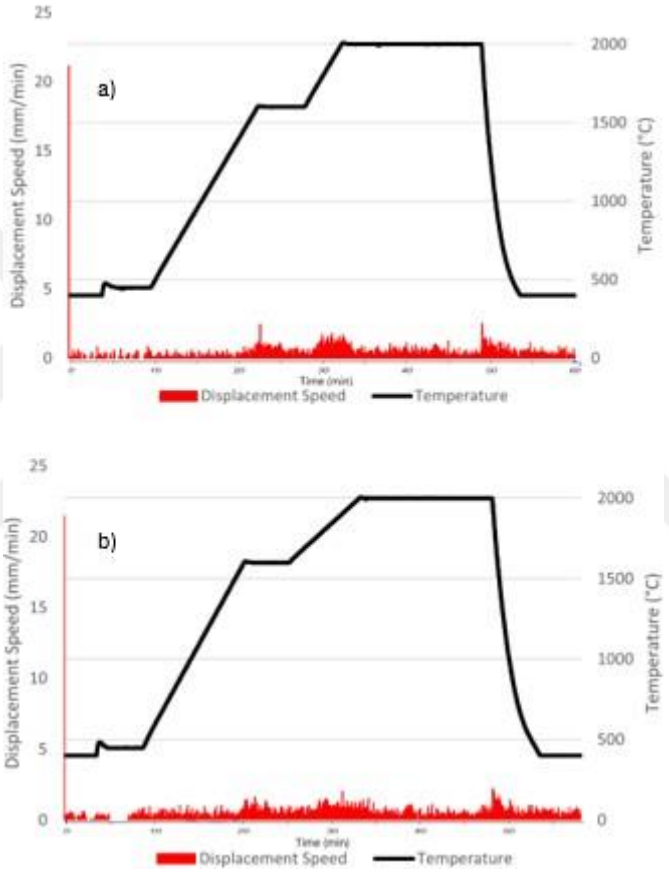

Figure 4.8. *SPS graph of B-O samples: a) Heating rate constant (100 °C/min), pressure constant (15.7 MPa), b) Heating rate is lowered to 50 °C/min between 1600-2000 °C, 31.4 MPa pressure is applied after 39th minute to the end of the process.*

Another parameter that affects the displacement is pressure. As seen in Figure 5.9-b, there is an abrupt change in the 39th minute where pressure is increased. Despite lowering the heating rate, pressure provides rapid displacement which means higher displacement speed in a smaller ti. As mentioned before lower displacement speed at lower temperatures is desired for reactive sintering which is adversely affected by pressure. As a result, a lower pressure (15.7 MPa) is preferred at lower temperatures to

evacuate gaseous side-products, yet it should be noted that increasing pressure is very effective on densification. The final displacement of the B-O sample (Figure 5.8) is improved by 12.1% by increasing pressure and decreasing the heating rate. Details of displacement of these two samples are shown in Table 5.1.

Table 4.1. *Displacement data of the B-O samples: a) with the constant Heating rate (100 °C/min), pressure constant (15.7 MPa), b) Heating rate is lowered to 50 °C/min between 1600-2000 °C, pressure increased to 31.4 MPa at 39th minute.*

Sample Name	Piston Position at (0 °C)	Piston Position at (1600 °C)	Piston Position at (1600 °C)	Piston Position at (2000 °C)	Piston Position at (2000 °C)
A	0.31	0.30	1.5	3.57	4.85
B	0.26	0.27	1.48	4.02	5.35

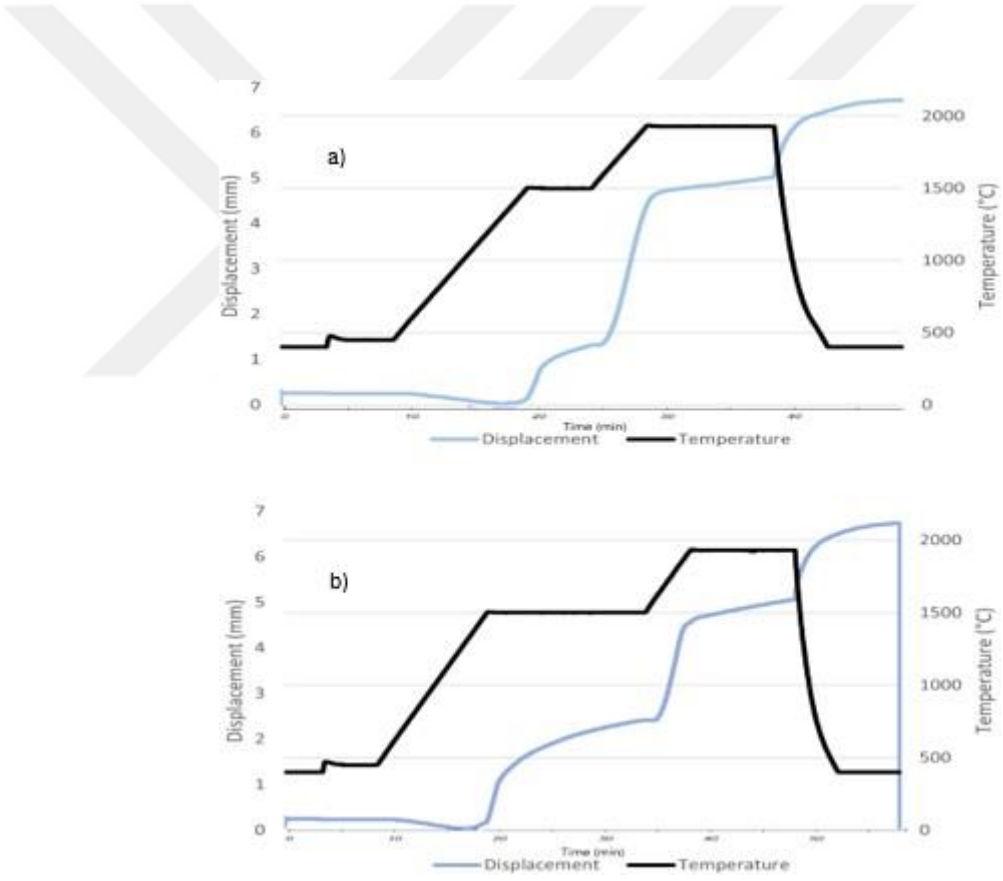

Figure 4.9. *SPS graphics of B-Si-C samples; a) 5 minutes held at 1500 °C, b) 15 minutes held at 1500 °C*

The effect of dwelling time on the densification of the B-Si-C samples is illustrated in Figure 5.10. The pressure of both samples is increased from 15.7 MPa to 31.4 MPa at the beginning of the dwelling at 1500°. By increasing the pressure at dwelling temperature, both evacuation of gaseous side-products and removing SiO_2 phase is aimed. Figure 5.10 shows that there is 87% higher displacement when dwelling time increased

from 5 minutes to 15 minutes. The effect of dwelling time on the final displacement is relatively low when compared with displacement on the dwelling.

Table 4.2. *Header styles*

Sample Name	Piston Position at 0 °C	Piston Position at 1500 °C	Piston Position at 1500 °C	Piston Position at 1930 °C	Piston Position at 1930 °C
A	0.26	0.12	1.31	4.37	5.02
b	0.23	0.19	2.42	4.68	5.06

As mentioned before dwelling time is in the second stage of sintering which explains the reason for a small effect on final displacement.

An important point that should be considered in Figure 5.10 is there is only a 1.47% change on the final displacement yet, the distribution of the displacement varies. While dwelling time is increased from 5 minutes to 15 minutes, displacement is increased 87% of sample a (Table 5.2). Another critical data is the decrease in displacement during heating after dwelling. There is a 26% decrease in displacement between 1500 °C and 2000 °C, which is both related to densification and evacuation of gaseous side-product in the longer dwelling section instead of the heating section. The most important part of the densification of the sample is performed at peak temperature which decreased 41.5% with higher dwelling time. As a result, two different mechanisms contribute to displacement which is the removal of gas and densification. Achieving the removal of gas at lower temperatures contribute to the elimination of pores and improves densification.

4.3. Analysis of Secondary Electron Microscope Analysis

Scanning electron microscope images provide plenty of data (e.g., grain size, distribution of phases, pore size and distribution, etc.) about the microstructure of samples. To make accurate comments on the images, the device user should know the exact location of the images on the sample. To explain the locations of the SEM images, Figure 5.11 is used to separate the sample into regions. After SPS production, samples are cut into three pieces to use for characterization (Figure 5.11-a). The first part is used for Archimedes Method to calculate relative density. The second and third parts, which have equal sizes, are used for SEM and XRD analysis. There is not any difference between the second and third parts. SEM samples are divided into four regions to

distinguish the differences related to their position. Surface-1 and Surface-2 are separated to understand the effect of the pressure applied direction. The side of the sample and surfaces are covered by carbon foil which affects these regions by carbon diffusion. 'Centre' is the only region that does not have a connection with carbon foil.

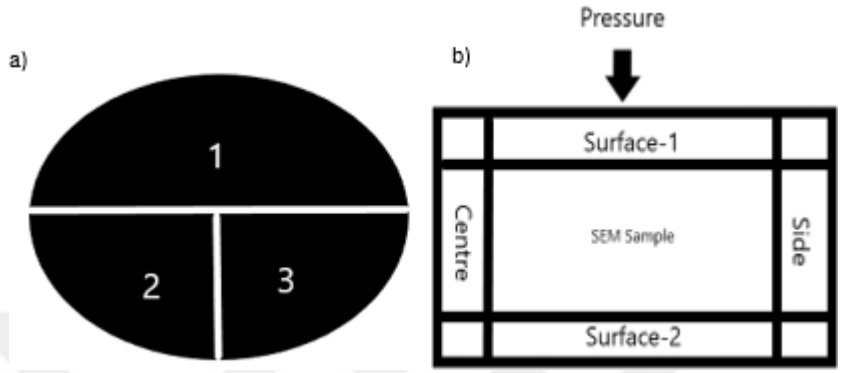

Figure 4.10. *SPS samples: a) Sections created by cutting, b) Sections named to identify the locations of SEM images*

SEM analyses are used to observe the microstructures of the samples. Figure 5.12 shows the difference in the microstructures of the B-Zr sample and B-O samples with three different sintering regimes. Reactive sintering has a positive effect on producing samples with low grain sizes. While the sizes of the ZrB_2 grains exceed 20 µm, ZrB_2 grains in B-O samples mostly have a size of a few µm. The positive effect of two-step sintering on densification can be seen in Figure 5.12 (b-c). Despite the positive effect on densification, two-step sintering increased the ZrB_2 grain sizes. When peak temperature is lowered from 2140 to 2000, there is not a visible effect on either densification or grain sizes. The effect of these parameters on densification is going to be analyzed in the next sections in detail.

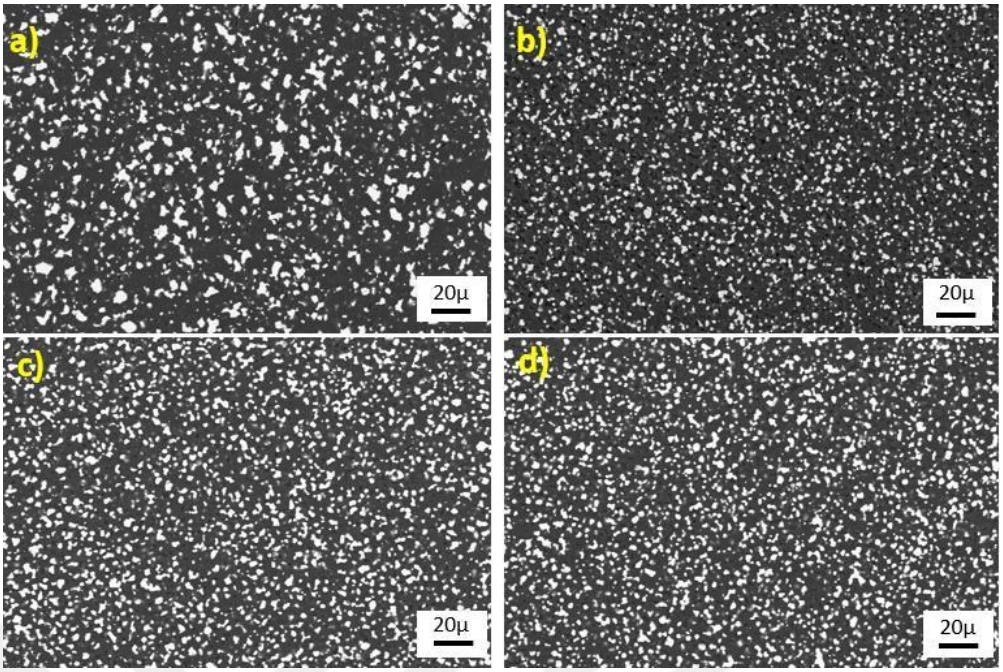

Figure 4.11. *SEM images of the center of samples: a) B-Zr sample sintered at 2150 °C, b) B-O sample one step sintered at 2139 °C, c) Two-step sintered B-O sample at 2140 °C and dwelled at 1600 °C, d) B-O sample two-step sintered at 2000 °C and dwelled at 1600 °C*

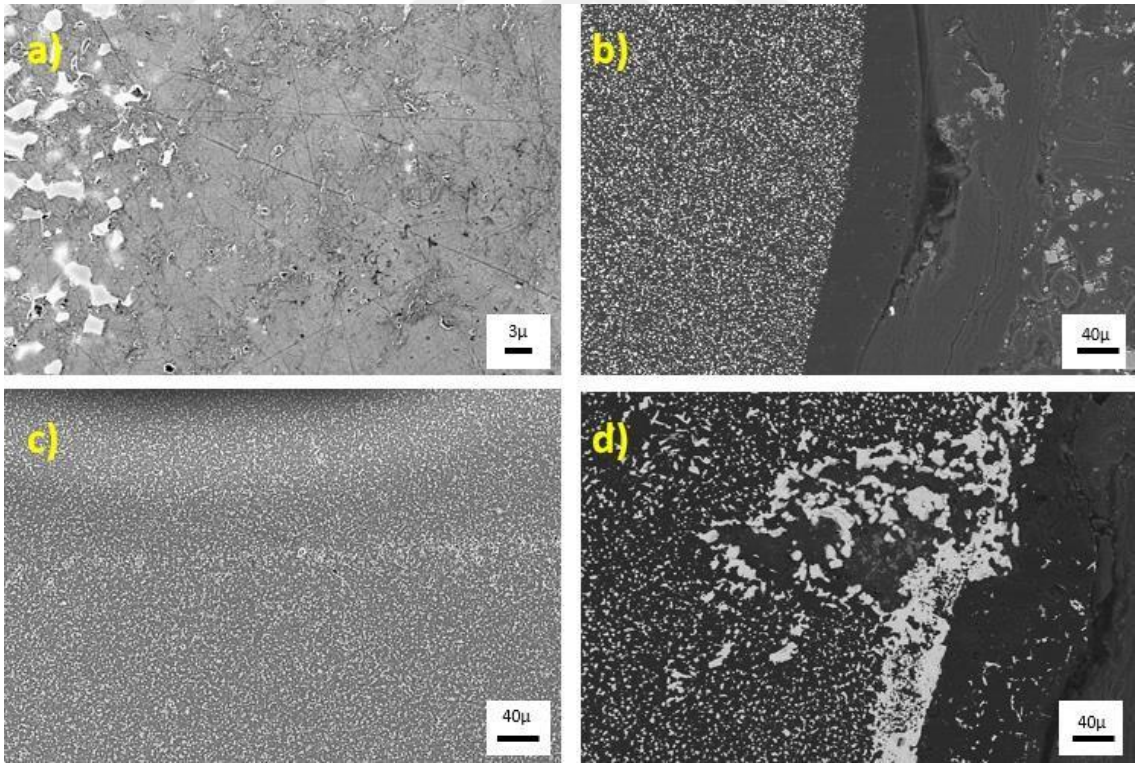

Figure 4.12. *SEM images of B-O samples: a, b, and d images taken from sides of samples, c is taken from Surface-2*

SEM images of B-O samples show two different defects which are illustrated in Figure 5.13. B_4C particles evaporate and condensate and move from region to region during SPS production yet, they are moving towards the sides of the sample which is the first defect. Figure 5.13-b shows that there is a black line between the mold and material which is B_4C particles moved from the inner sides of the specimen. Another issue is, as a result of B_4C particle flow, ZrB_2 cluster formation (Figure 5.13-d). Both clusters of ZrB_2 and B_4C particle flow are deteriorating the homogeneous microstructure of B-O samples. Besides the negative effects of B_4C flow, there is relatively higher densification in the region that B_4C flowed (Figure 5.13-a). The second defect is bloating which is the result of early densification around the pores before the evacuation of gaseous side-products. Gaseous side-products are trapped in pores which obstruct the elimination of this kind of pores (bloating).

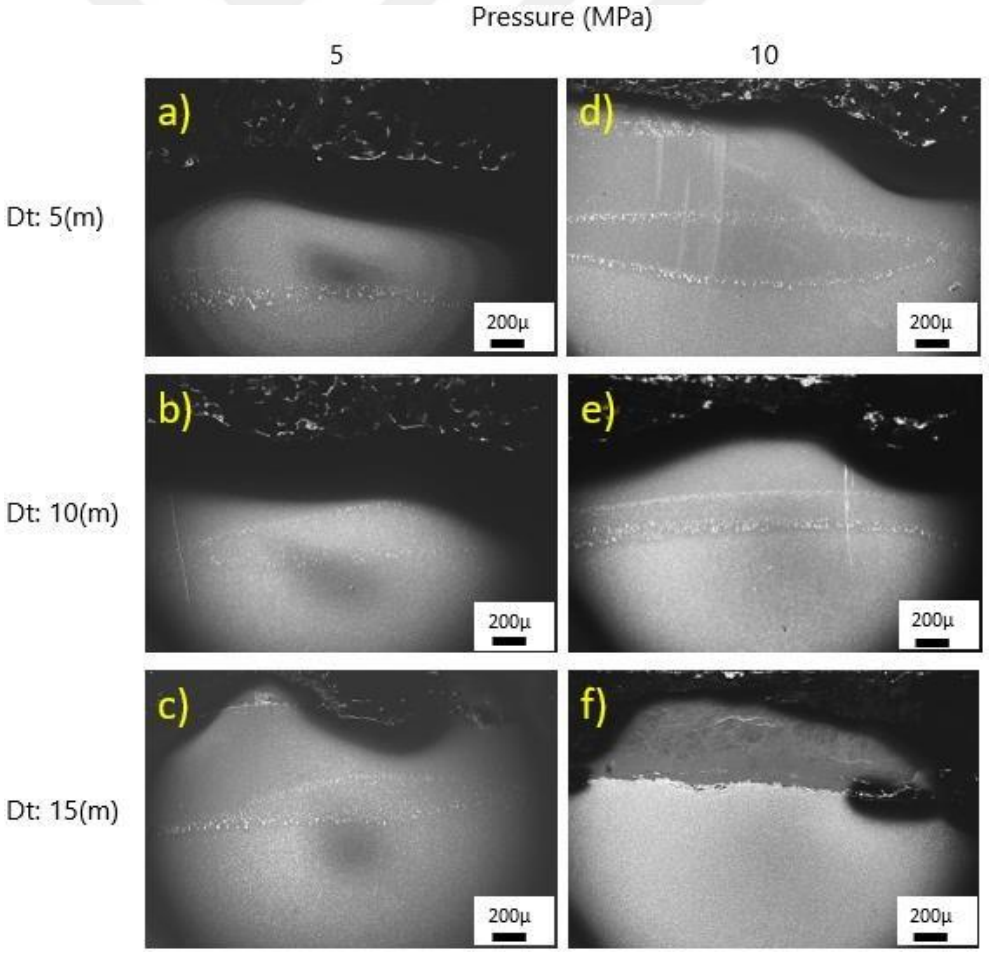

Figure 4.13. *SEM images of B-O samples with 5,10,15 minutes of dwelling time and 15.7-31.4 MPa pressures*

To solve the bloating defect of the B-O samples and improve densification, the dwelling step is introduced. To observe the positive or negative effects, different dwelling times have been performed. While the dwelling time increases bloating line is first divided into two lines then approached the surface Figure (5.14-a, b, c). Even 15 minutes of pressure was not efficient enough to remove bloating, longer time is needed with the same conditions. Short sintering time is one of the most important advantages of SPS which can be deteriorated with longer dwelling time. Because of this reason, instead of increasing dwelling time, the same dwelling times performed with a higher-pressure rate. Similar to the lower pressure case, the first bloating line approached the surface and by 15 minutes of dwelling, bloating is removed from the system.

The amount of ZrB_2 phases in the images of the B-Si-C sample is lower compared to B-Zr and B-O samples which are connected to starting powder $ZrSiO_4$ that contains less Zr. Starting powders of B-Si-C samples contain a higher amount of Oxygen compared to B-O samples. While 34.7% of the weight of $ZrSiO_4$ is Oxygen, 26% of the weight of the B-O sample is Oxygen.

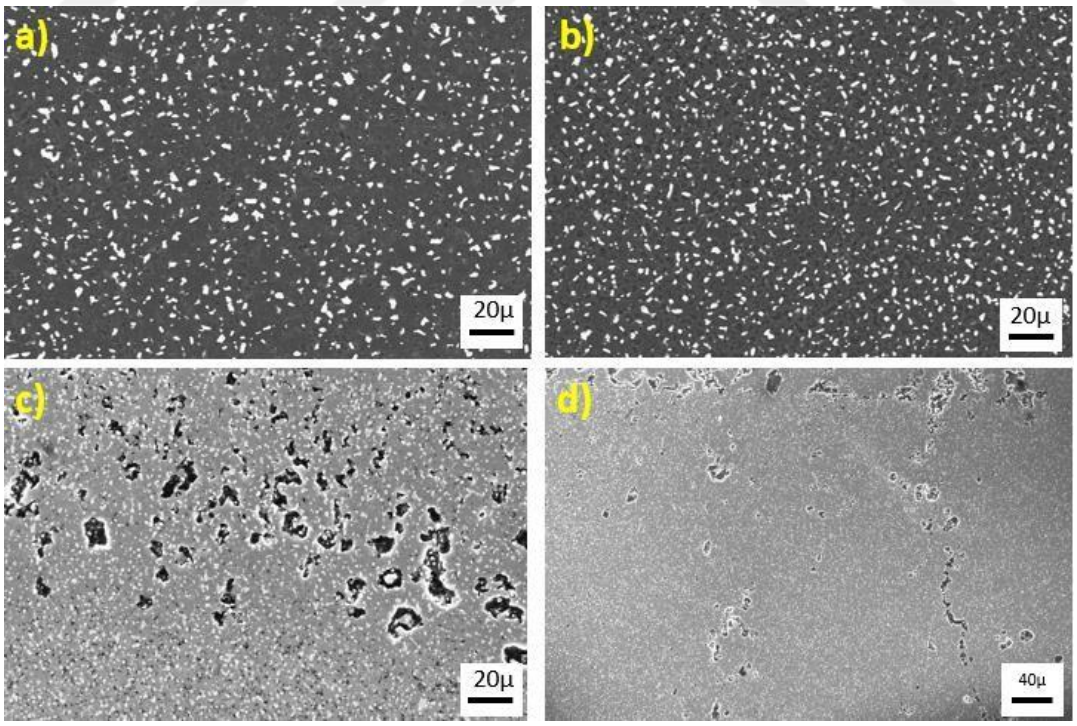

Figure 4.14. *SEM images of Z-Si-C samples: a) Surface-1, b) Surface-2, c) Surface-2, d) Surface-2*

This difference results in a higher amount of gaseous side-product during sintering which deteriorates the densification. As mentioned before pressure direction of the SPS lead the liquid and gas phases in the opposite direction. The result of this property of the device is illustrated in Figure 5.15 a-b. While the densification of Surface-1 has a higher densification image, Surface-2 has a more porous structure. Not only the pressure but also temperature gradient and gas-liquid phase flow direction affect this densification difference. Besides the non-homogeneous densification, bloating is an issue for B-Si-C samples like B-O specimens. As mentioned before Oxygen content of the B-Si-C samples is higher which causes a severe bloating effect (Figure 5.15 c-d). In addition to a more severe bloating effect, there is not a line of pores near Surface-2. Pores can be seen inner parts of the specimen which led this work to two-step sintering.

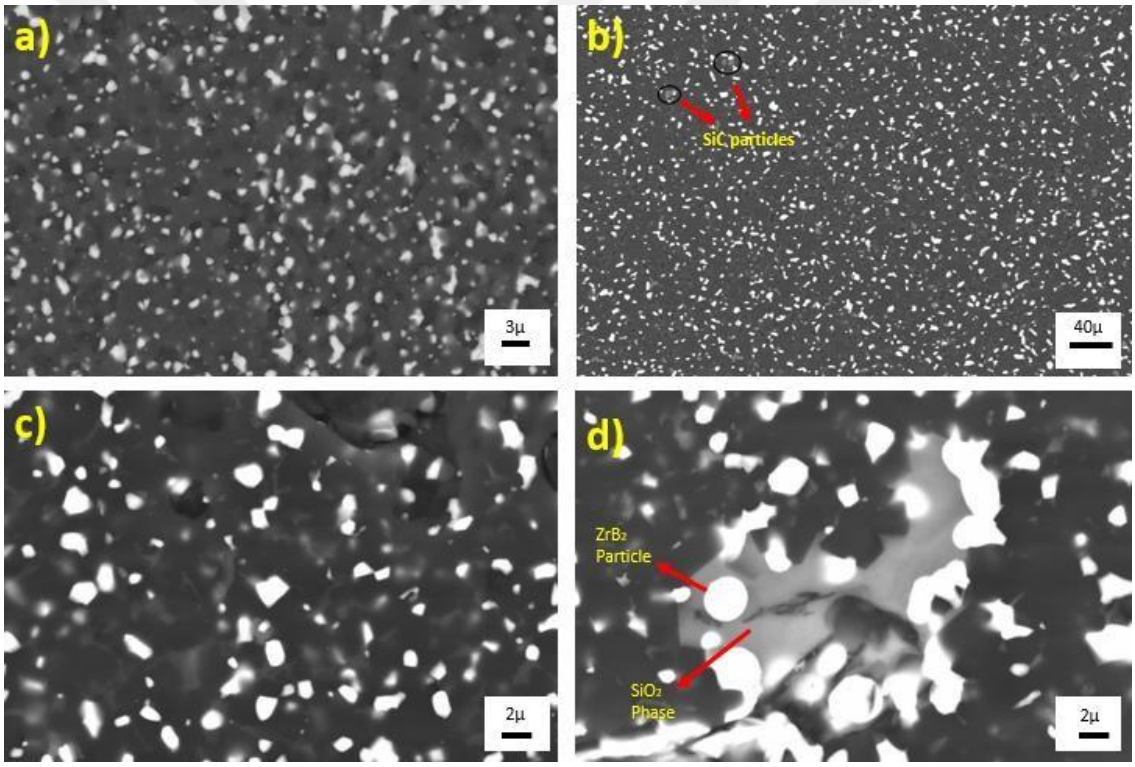

Figure 4.15. *SEM images of B-Si-C samples: a) Centre of the sample, b) Inner part of the Side region, c) Middle part of Side region, d) Middle part of Side region*

As mentioned before, for $ZrSiO_4$ containing powder mixture, this work aims to eliminate the SiO_2 phase and produce B_4C-ZrB_2 composite with a cheaper Zr source. But SiO_2 phase stands as a problem for the usage of $ZrSiO_4$. Figure 5.16 shows the result of the flowing SiO_2 phase toward the sides of the specimen.

Besides the flow of SiO_2 toward the sides, it also flows from inner regions to Surface-2. While SiO_2 flows from center to side, it leaves pores behind and worsens densification (Figure 5.16-a). On the other hand, the sides of the sample have better densification due to the flow of SiO_2. There are two reasons for better densification at the sides and Surface-2: the first one is the SiO_2 phase fills the pores and provides liquid-phase sintering (Figure 5.16 c-d), the second one is the formation of SiC from SiO_2 enhances driving force for densification. While there is not any sign of SiC on the inner parts of the sample, the SiC population increases near to sides (Figure 5.16-b, black spheres point to SiC grains). There are two reasons for higher SiC population on the sides: first, the flow of SiO_2 starts before the formation of SiC (which is deliberately created the effect by a dwelling), the second one is there is a carbon diffusion on the surfaces and sides of the powder which provides carbon source for SiC formation.

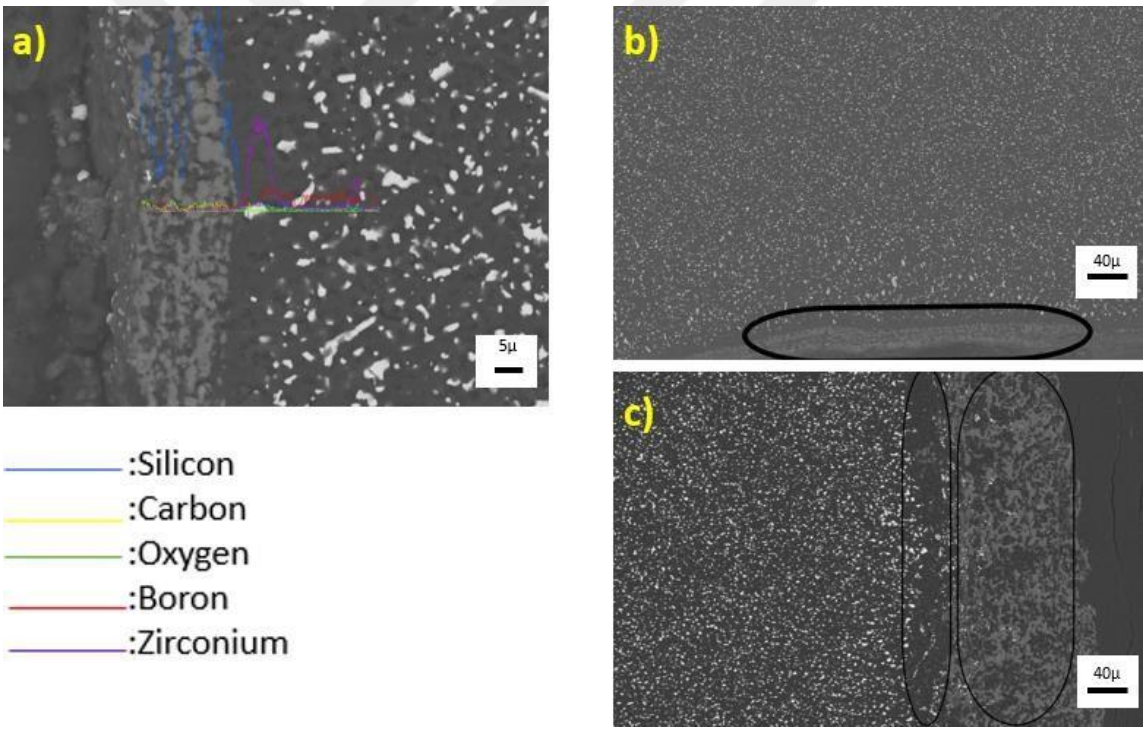

Figure 4.16. *SEM images of B-Si-C samples: a) Side region (dwelling time 5 minute), b) Surface-2 of the sample (dwelling time 5 minute), c) Side region (dwelling time 15 minute*

To observe the SiC formation that is detected in XRD analysis, SEM images of the samples are investigated and the majority of the SiC grains are found in the Side and Surface-2 regions. EDS analysis is done to identify these lines and line analysis shows the distribution of elements in that region (Figure 5.17-a). Pressure leads the liquid phase to move from center to side yet it does not affect the Carbon phase. Transformation of the

SiO_2 phase to SiC is strongly dependent on the diffusion of carbon from carbon foil. Observation of a thinner SiC lane on the Surface-2, compared to Surface-1, can be analyzed as the result of the temperature gradient of SPS Figure 5.17-b). There is a decrease in temperature from top to bottom which can affect the diffusion of carbon. Dwelling time increases the flow of the SiO_2 phase toward sides and impacts the densification of liquid phase sintering becomes effective in a smaller region.

The effect of the dwelling on the B-Si-C samples is shown in Figure 5.17 (a-d). When dwelling temperature is increased from 5 minutes to 10 minutes, the thickness of the region of SiC is increased which means that less SiO_2 phase is left inside the sample. The lower effect of higher temperatures on the densification of B-Si-C samples is affected by this phenomenon. While the SiO_2 phase amount reducing, the liquid-phase sintered region is reduced too. Both change on densification mechanism (liquid-phase to solid-state) and the pores that SiO_2 phase left behind decrease the amount of densification.

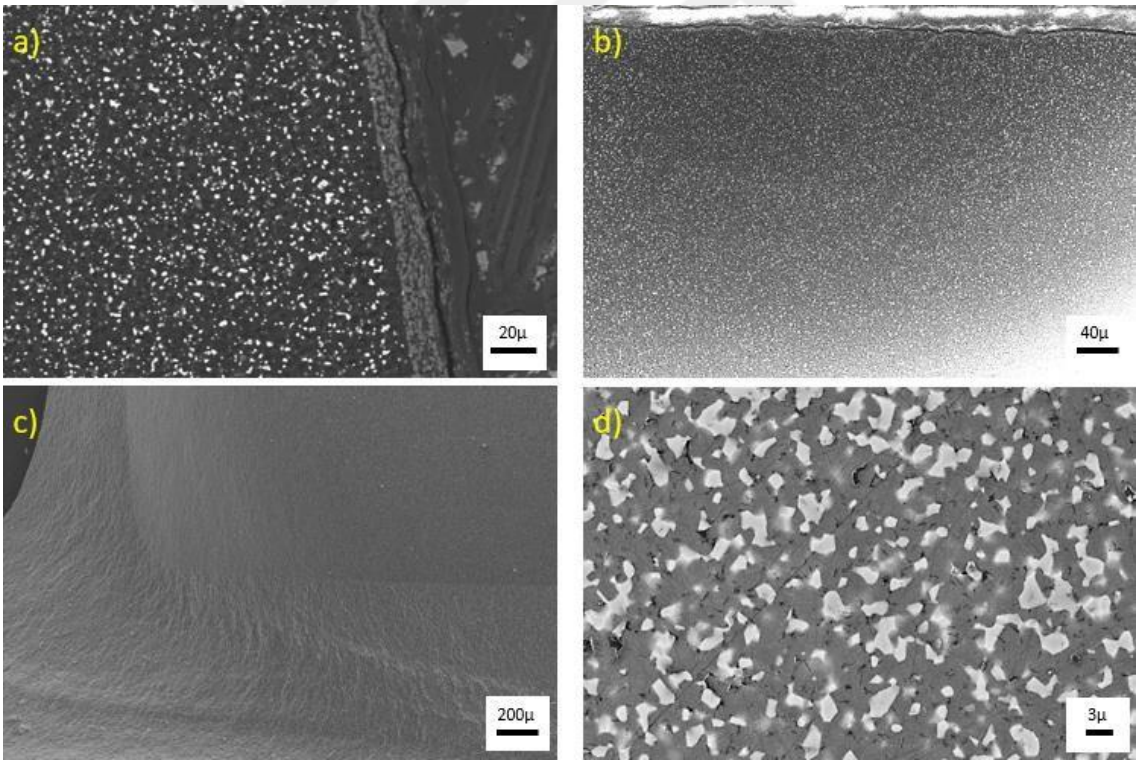

Figure 4.17. *SEM images of B-Si-C sample sintered at 2107 °C, by 15.7 MPa pressure, with 10 minutes of dwelling at 1500 °C: a) Side of the sample, b) Surface-2 of the sample, c) Smashed piece of the sample (Surface-2), d) Centre of the sample*

Figure 5.18 shows the SEM images of the sample have 96.1% relative density. While the sintering temperature of the sample is increased from 1930 °C to 2107 °C, there is only a 3.0% increase in the relative density which is related to both pores created by

severe SiO_2 movement to the surface and absence of liquid phase sintering enhanced by SiO_2. Even the center of the sample shows a small amount of pore compared to samples sintered at a lower temperature (Figure 5.18-d). There is a more homogeneous densification distribution when almost the whole of the SiO_2 phase is moved to the surface. Besides the temperature, elimination of the bloating has a positive effect on densification (Figure 5.18-b). To see the morphology of the sample before cutting and polishing, a sample is smashed and pieces are observed by SEM Images.

There is a certain difference in the texture and properties of the materials as seen in Figure 5.18-c. While the surface of the material shows a metal-like texture, inner parts are more related to a ceramic figure. As mentioned before oxidation of these samples after sintering can be connected to either Si or SiO phases.

The presence of metallic Si may cause a change between the inner part and the surface of the sample. Although the presence of the Si or SiO phases is not observed in the XRD analysis, the existence of these phases in the smaller regions may prevent observation on the XRD due to the low weight percentage.

4.4. Analysis of Relative Density Results

Densification is the main purpose of this thesis which affects all properties of materials. Several parameters that affect densification: sintering temperature, pressure assistance, raw powder properties (e.g., particle size, particle size distribution, impurities, pre-operations like pressure, etc.) are some of them. To make an accurate comparison, many parameters should be considered. Especially for systems like SPS, even changing the die used for sintering can change the result while everything else is the same. It is always better to compare systems with as least a possible change in a single step. In this thesis, many different dies had to be used because reactive sintering caused die loss many times. Some of the data may be misleading because of this case.

Using different additives to densify B_4C has been a widespread solution to difficulties in the compaction of monolithic B_4C. Table 2.1 represents many examples that are used for this purpose.

There are not many works on the B_4C/ZrB_2 composite in the literature, which is one of the reasons for this thesis. Mostly ZrO_2 with or without carbon addition is used to produce B_4C/ZrB_2 composite(Murthy et al., 2018) (Xiong et al., 2018), yet there are

different routes used (e.g., using B, C, and Zr as raw powders) (Shcherbakov et al., 2017). Although the final composites consist of the same phases, percentages of these phases and methods create a difference in the final properties of the samples. Table 5.3 illustrates different samples for B_4C/ZrB_2 composites as well as monolithic B_4C (example 5). While monolithic B_4C(Goldstein et al., 2001) have only 87% of relative density, the addition of 30 wt% ZrO_2 in this thesis (Table 5.3, example 1) resulted in more than 10% improvement. In addition to the similarities, it should be noted that the particle size of the monolithic B_4C is bigger which worsens final density. Besides particle size applied pressures show a big difference which is also decisive on relative density.

Table 4.3. Comparison of B_4C sintering with and without additives.

Numbers of Examples	**Powder Types**		**Sintering Parameters**					
	B_4C (wt%)	**ZrO_2 (wt%)**	**Time (min)**	**Dwelling Time and Temperature**	**Temperature (°C)**	**Pressure (MPa)**	**Pre-Pressure (MPa)**	**Relative Density (%)**
1	70 (1.2µm)	30 (5µm)	15	1600 (°C) 5 (min)	2000	15.7	15	97.2
2	70 (1.2µm)	30 (30-70 nm)	60	1500 (°C) 30 (min)	2160	-	250	97.5
3	70 (1 µm)	15 (0.5 µm)	60	-	2100	-	180	96.7
4	100 (3.68 µm)	-	10	1800(°C) 10(min)	2000	40	15.9	87

Another comparison can be done with the second example(Lin et al., 2017) in which 15 wt% phenolic resin is used besides ZrO_2 additive. Carbon source differs from the route of reactive sintering, without carbon addition boron loss by B_2O_3 evaporation happens.

With a suitable sintering regime, some part of B_2O_3 can be transformed to B_4C by the reaction with in-situ formed C during ZrB_2 formation. One of the purposes of two-step sintering used in this work was to decrease B_2O_3 evaporation. While the second example is sintered without pressure assistance there is a 160 °C temperature change compared to this work. While B_4C powders have the same particle size, particle sizes of ZrO_2 powders show an enormous difference which affects both densification and reactions.

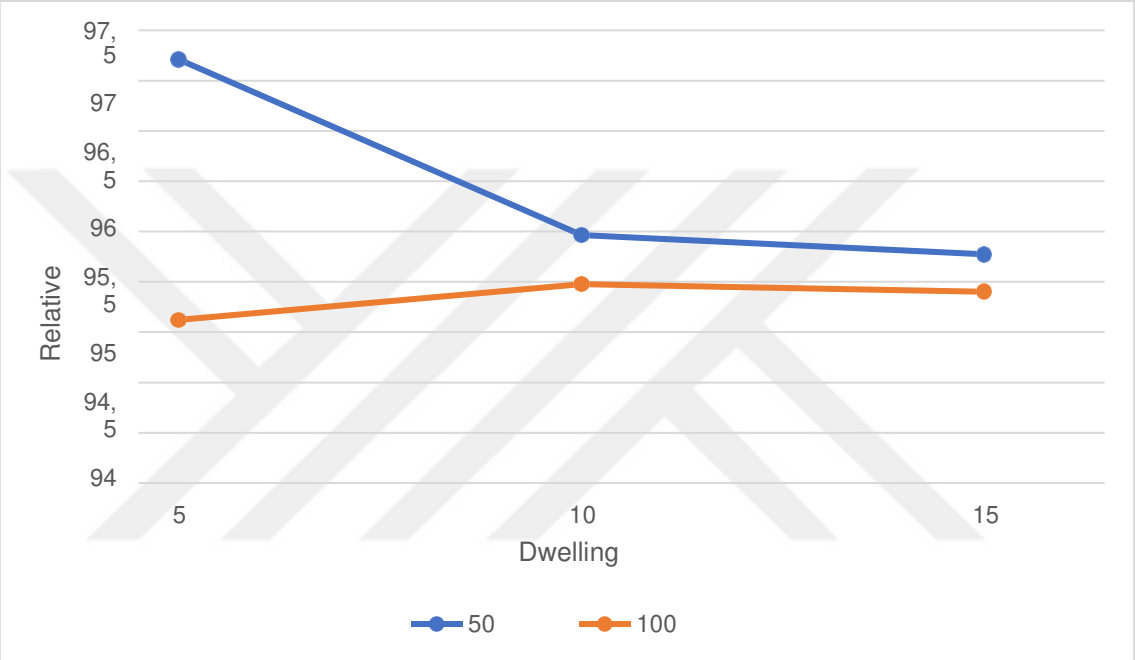

Figure 4.18. *Effect of dwelling time and heating rate on the relative density of B-O samples*

By producing many samples, the effects of different sintering parameters are observed. The dwelling step is one of the parameters added after observing bloating defects in a single step. sintered samples. The Effect of different dwelling times on the relative density is shown in Figure 5.19. Besides dwelling time effect of the heating rate is also evaluated in the figure. All samples shown in Figure .19 are heated by 100 °C/min up to 1600 °C. 50 °C/min heating rate is applied between 1600-200 °C to improve evacuation of gaseous side products and improve densification. For the samples that have a heating rate of 100 °C/min for the whole process, there is a positive effect of increasing dwelling time from 5 to 10 minutes and a slight decrease on densification when dwelling time is increased to 15 minutes. When the heating rate is decreased to 50 °C/min after 1600 °C, there is an improvement in the relative densities. For the dwelling times 10 and 15 minutes, the evolvement of relative density is similar. The highest relative density

(97.211) among B-O samples is achieved by applying 15.7 MPa pressure, with 5 minutes of dwelling, decreasing heating rate to 50 °C/min (between 1600-2000 °C) and sintering at 2000 °C for 15 minutes.

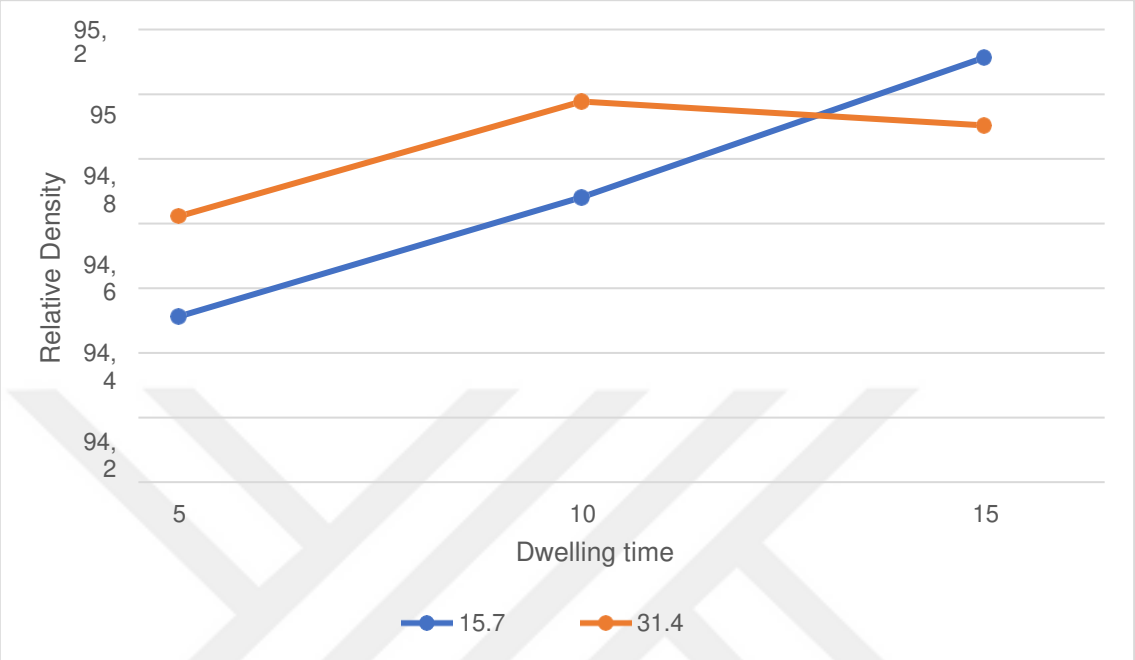

Figure 4.19. *Effect of dwelling time and pressure on the relative density of B-O samples*

After applying two steps of sintering, another parameter changed to improve densification is pressure. The pressure of samples increased from 15.7 to 31.4 MPa and an increase in pressure is applied 5 minutes after reaching 2000 °C. The purpose of the increase of pressure at 2000 °C is not to prevent gas evacuation and waiting 5 minutes before increase has the same purpose. For both pressures, relative density showed an increase from 5 to 10 minutes. Although the relative density of the sample kept increasing after raising the dwelling time to 15 minutes for sample sintered by 15.7 MPa, there is a drop in the relative density for the sample sintered by 31.4 MPa with 15 minutes of dwelling (Figure 5.20).

The effect of sintering time on the relative density is shown in Figure 5.21. The sintering parameters of samples in Figure 5.21 are 31.4 MPa pressure, dwelling for 15 minutes, decreasing the heating rate to 50°C/dk after 1600 °C, and sintering 15 minutes at 2000 °C. While one minute of sintering has a relatively low relative density (91.0%), increasing sintering time to 5 minutes resulted in a change of more than 2 percentage. The highest relative density is achieved with 15 minutes of sintering (95.3%).

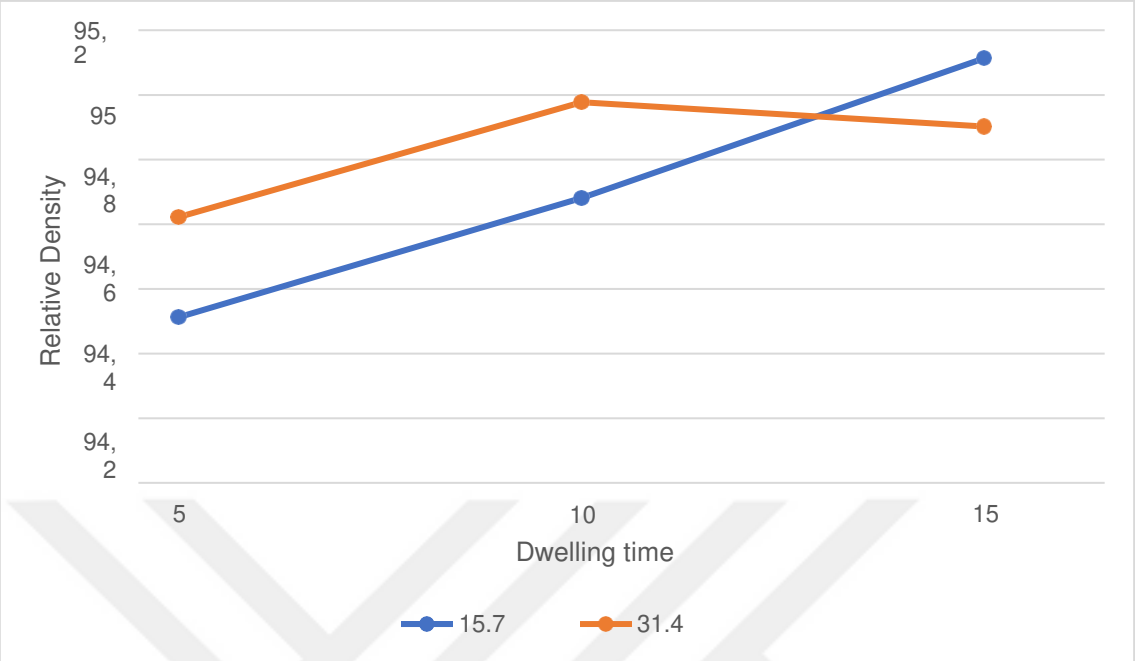

Figure 4.20. *Effect of dwelling time and pressure on the relative density of B-O samples*

Analysis of the B-O samples produced by SPS shows that reactive sintering of these samples requires a second step to solve bloating defects. Besides removing the bloating defect, dwelling improves the densification of the samples. Another issue is the flow of the B_4C toward surfaces which is remained in all samples that are sintered with different parameters. Improvement on the densification that lower heating rate ensured

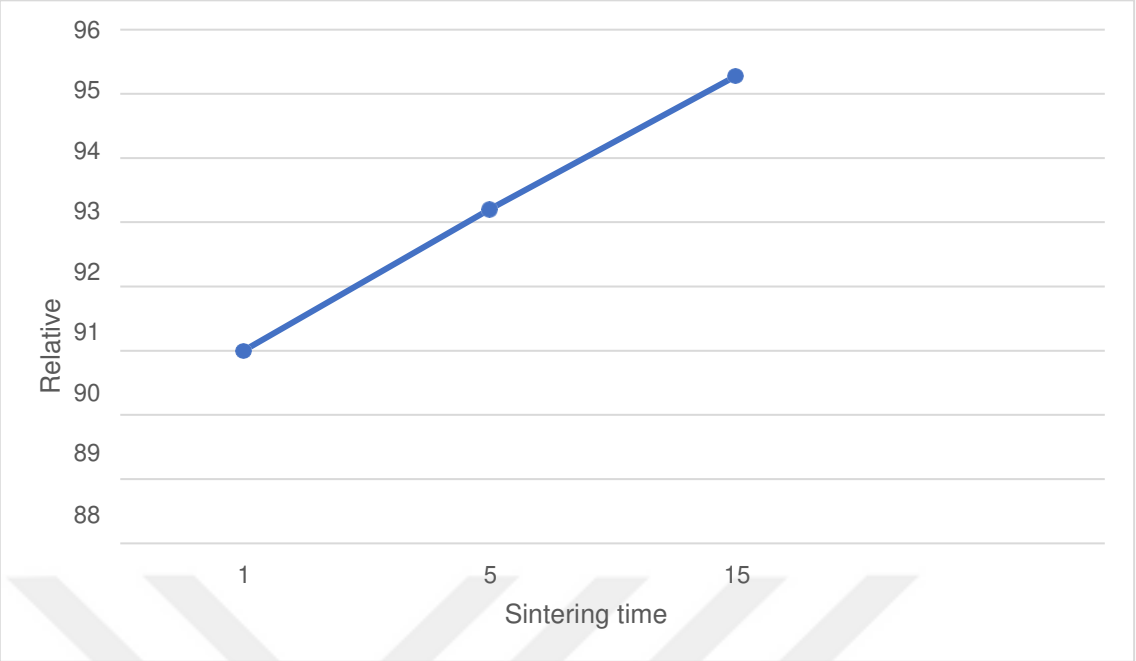

Figure 4.21. Effect of Sintering Time on the relative density of B-O samples

can be used as an alternative to the dwelling. Lower heating rates over 1200 °C where reactions start can enhance the time to eliminate gasses and prevent bloating.

As B-O samples, different parameters of sintering are changed to improve the densification of the B-Si-C samples. Figure 5.13 shows the important phase changes while heating the specimen from 1000°C to 1500 °C. Dissolution of $ZrSiO_4$ is finished at 1500 °C that is why this temperature is chosen as dwelling temperature. The dwelling step has the advantage to complete the reaction in lower temperatures and give time to gaseous side-products to leave the system. In addition to these advantages, another reason for adding a dwelling step for the B-Si-C sample is to transport to SiO_2 phase to the surface. Using $ZrSiO_4$ as a Zr source is a reasonable solution to decrease the expenses of the project. There is not an example of usage $ZrSiO_4$ as an additive for reactive sintering of B_4C/ZrB_2 that is why data of this thesis carries great importance for other possible works on this area.

The Dwelling section has great importance for reactive sintering which enhances to control of phase changes and gas evacuation. With this control on the specimen, defects (bloating) can be prevented and densification can be promoted. To understand the role of the dwelling on the densification of B-Si-C samples, different dwelling times (5, 10, 15 minutes) are applied with different pressures (15.7 and 31.4 MPa).

Another difference in the sintering regime of B-Si-C samples compared to B-O specimens is the point where pressure is increased. As mentioned before the increase in the pressures is not applied at the beginning of the SPS. For the B-Si-C specimens, the starting point of the dwelling temperature (1500 C°) is chosen. The reason for increasing the pressure at the starting point of the dwelling is to promote SiO_2 movement toward surfaces. The important point here is not to form SiC from the SiO_2 phase before leading SiO_2 to the surface. As mentioned before the aim of this thesis is to produce a B_4C/ZrB_2 composite.

While reaction 5.6 transforms the SiO_2 phases that came from $ZrSiO_4$ into SiC, Reactions 5.5 and 5.7 are more favorable for this work. While reaction 5.5 produces more B_2O_3 phase which is a loss for a B_4C matrix composite, Reaction 5.7 is desired for producing ZrB_2 and removing SiO_2 by the movement to surfaces and removing Oxygen as CO instead of B_2O_3.

$$5B_4C(s) + 7ZrSiO_4(s) \rightarrow 7ZrB_2(s) + 3B_2O_3(g) + 5CO(g) + 7SiO_2(l) \quad (5.5)$$

$$2ZrSiO_4(s) + B_4C(s) + 9C(s) \rightarrow 2ZrB_2(s) + 2SiC(s) + 8CO(g) \quad (5.6)$$

$$3ZrSiO_4(s) + 2B_4C(s) + C(s) \rightarrow 3ZrB_2(s) + 3SiO_2(l) + B_2O_3(g) + 3CO(g) \quad (5.7)$$

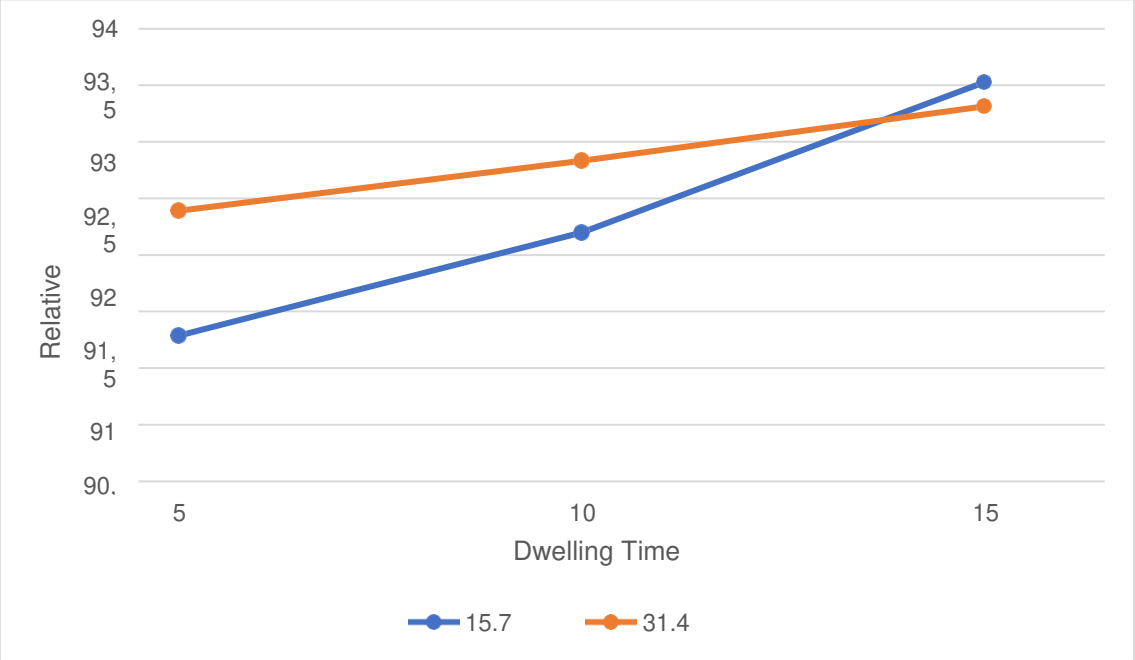

Figure 4.22. Effect of pressure and dwelling time on relative densities of B-Si-C samples

As Figure 5.22 shows, increasing dwelling time has a positive effect on the densification of B-Si-C samples, yet there is a higher contribution of dwelling time for lower pressure when it is 15 minutes. Sintering of the samples in Figure 5.22 is carried at 1930 °C which is not high enough for densification above 95%.

It is shown that to improve the relative density of B-Si-C samples over 95%, increasing the temperature is crucial. While B_4C-$ZrSiO_4$ powder mixtures cause loss of dies in one experiment, even 2 wt% of carbon addition made a more stable system. The importance of the dies for this thesis is not only related to cost but also a comparison of different specimens is affected by changing the die.

To achieve further improvement on relative density, the effect of temperature is observed with 10 minutes of dwelling time and without pressure increasing. The effect of the dwelling time on the formation of SiC is illustrated in Figure 4.5 because an increase in SiC content of 10 minutes of dwelling is chosen for further experiments. Effect of dwelling time on the formation of SiC also observed in SEM images (Figure 5.17). While there is a sharp increase in the relative density from 1930 °C to 1988 °C, there is a smaller change after increasing temperature to 2107 °C. The relative density of the B-Si-C sample is reached 96.1% which is the highest relative density for this specimen (Figure 5.23).

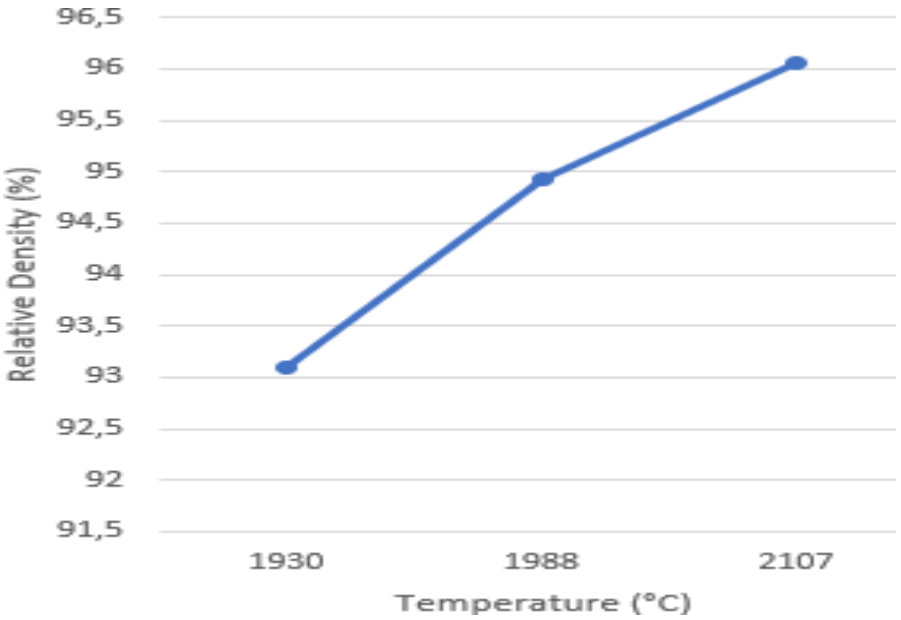

Figure 4.23. Effect of Temperature on the relative densities of B-Si-C samples, an applied pressure is 15.7 MPa, dwelling time is 10 minutes

In addition to increasing the temperature, the effect of pressure at higher temperatures is shown in Figure 5.24. While the higher relative density is achieved at 2080 °C compared to 1930 °C, there is a slight decrease in the densification when the temperature increased to 2120 °C. To understand the role of the pressure in the densification of B-Si-C samples better, further experiments are needed which can be a future work of this thesis.

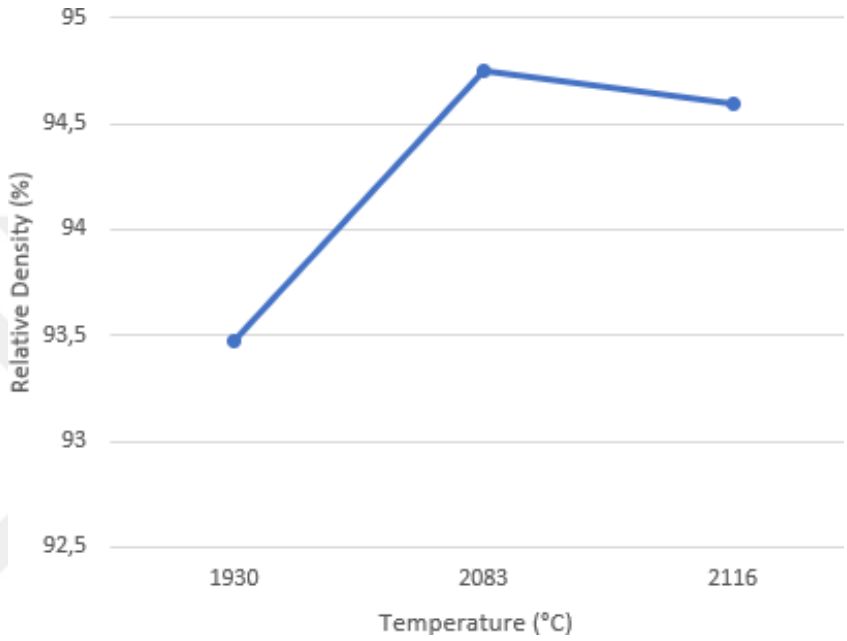

Figure 4.24. Effect of temperature on relative densities of B-Si-C specimens, an applied pressure is 31.4 MPa, and dwelling time is 10 minutes.

4.5. Analysis of Electrical and Mechanical Properties of Boron Carbide Zirconium Diboride Composite

Evaluation of properties of materials is crucial to compare the performances. As produced Boron Carbide-Zirconium Diboride samples are prepared for hardness and electrical conductivity tests.

Vickers Indentation test is used to measure the hardness of materials. 10 kg force is applied with 10 seconds of dwell time. To measure an overall and accurate hardness value, five indentations were taken. As well as the number of the indentation, the spots are chosen for measurement carries great importance. As mentioned before there are density differences between different parts of the samples shown by SEM images (Figure 5.15 a-b).

Figure 5.25 shows the change in the hardness value of B-O samples as the relative density of the samples change. While the relative density increases from 95.3% to 97.2%, hardness rises from 21.1 GPa to 21.8 GPa. There is a considerable decrease in the hardness while the relative density of the sample increases from 95.3% to 95.4%. This reverse change is connected to the inhomogeneity of the microstructure of the samples.

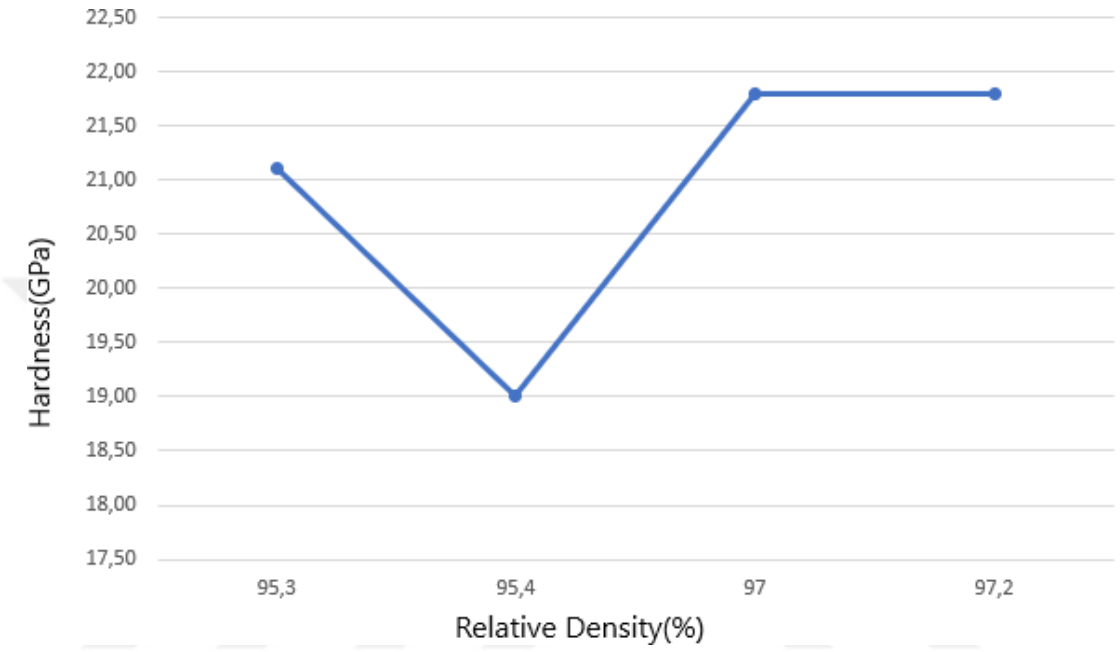

Figure 4.25. Effect of relative density on the Hardness of B-O samples.

The overall hardness calculated from five indentations is 21.8 GPa for the sample have a relative density of 97.2%. On the other hand, there is a 7 GPa change between the smallest and the highest indentation value of the sample. This change is directly connected to the density gradient between the surfaces of the sample.

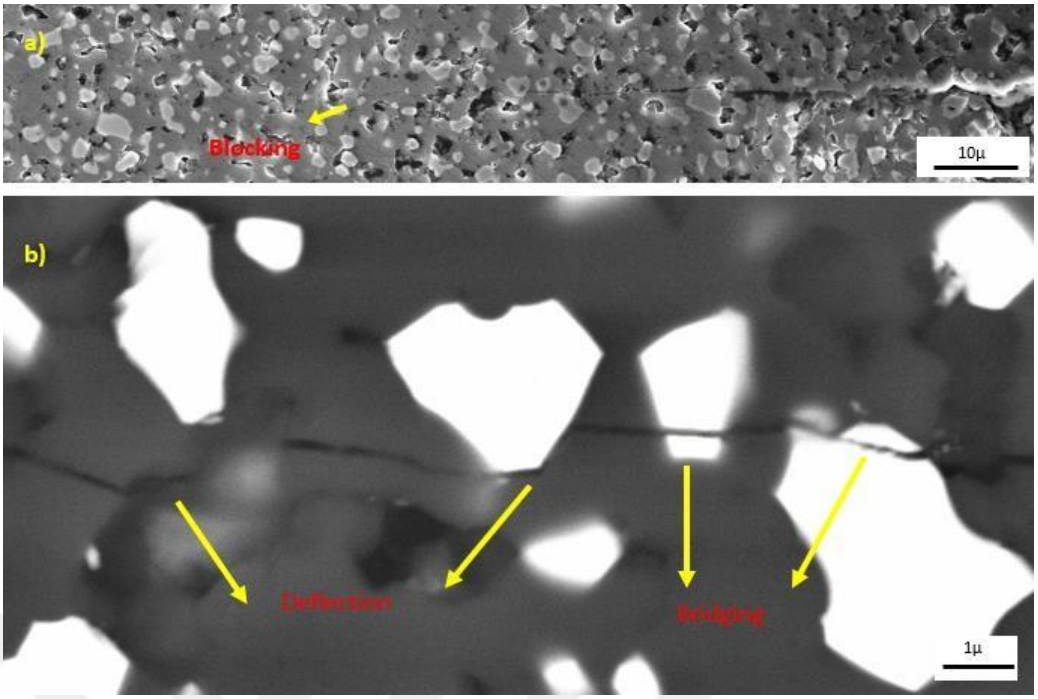

Figure 4.26. *Crack propagation of B-O sample (97.2% relative density, 21.8 ±3.5 GPa Hardness) a) Propagation and blocking of crack, b) Toughening mechanisms*

Figure 5.26-a shows the propagation of the crack during the indentation test. During the propagation, the energy of the crack is reduced by both deflection and bridging mechanism enhanced by in situ formed ZrB_2 grains (Figure 5.26-b). These mechanisms reduced the energy of the crack, thinned it, and the crack is blocked by a ZrB_2 grain.

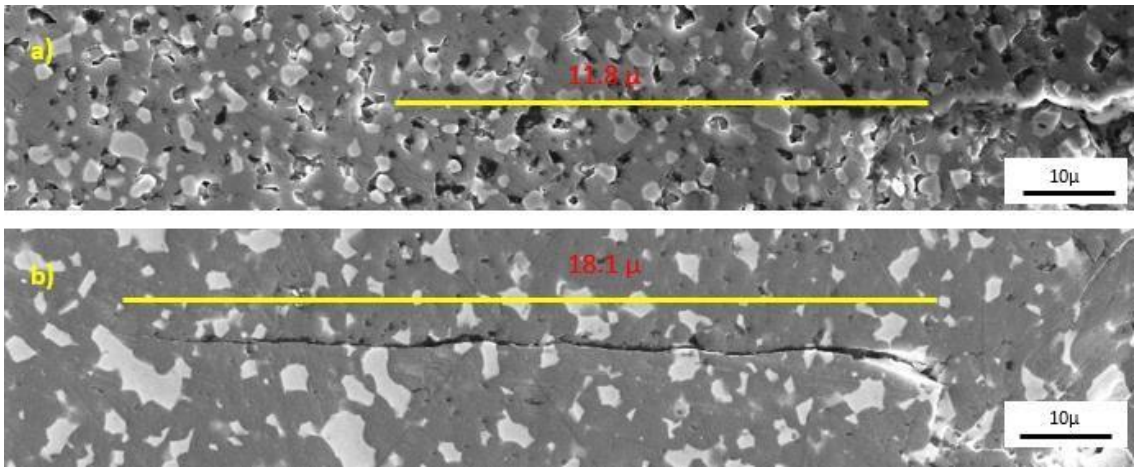

Figure 4.27. Crack propagation of a) B-O sample with 97.2% relative density, b) B-Zr sample with 99.5% relative density

Figure 5.27 shows the positive effect of reactive sintering on fracture propagation. Even with lower relative density (97.2%), the B-O sample has a lower crack length (11.8µ) compared to the crack length of the B-Zr sample (18.1µ). Prohibiting the growth

of B_4C grains is the first reason for better performance during cracking. Besides the B_4C grains, ZrB_2 grains are smaller when a reactive sintering route is preferred. Pores in the structure, which decrease the energy of the crack, are another reason for shorter crack length.

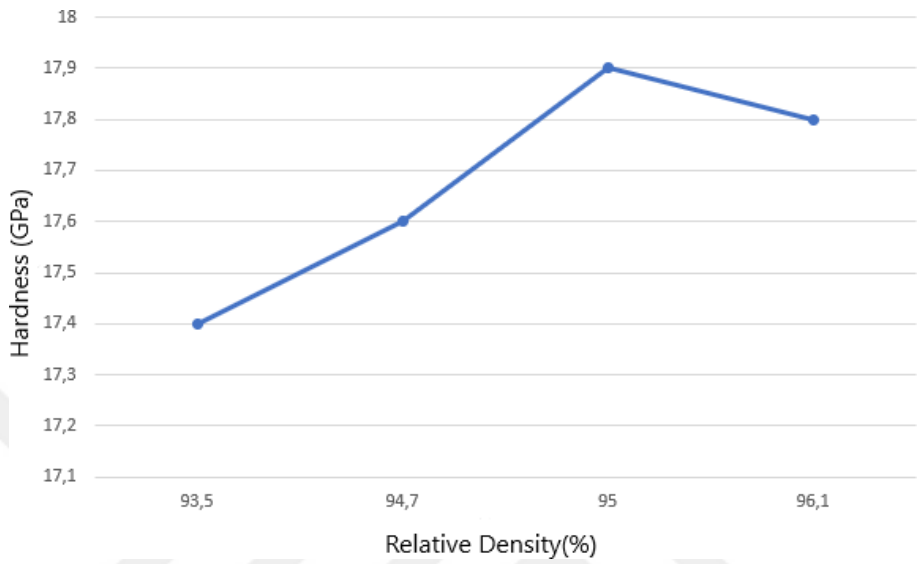

Figure 4.28. Effect of relative density on the Hardness of B-Si-C samples.

The effect of relative density on the hardness of the B-Si-C samples is shown in Figure 5.28. Although there is a decrease in the hardness while the relative density increases from 95% to 96.1%, the highest indentation results are observed in the sample with a relative density of 96.1%. Like B-O samples, there is a gradient of density on the B-Si-C samples too. Besides this densification difference, there are phase gradients in B-Si-C samples as shown in Figure 5.17. The B-Si-C sample with 96,1% relative density has a hardness of 17.8 ±2.5 GPa which showed better performance in the denser regions compared to the B-Si-C sample with 95% relative density that has a hardness of 17.9 ±2.0 GPame interval.

Table 4.4. *Comparison of the effect of ZrO_2 and $ZrSiO_4$ additives on the mechanical properties of B_4C.*

Sample Number	Composition (wt%)				Relative Density(%)	Hardness (GPa)	Fracture Toughness ($MPam^{1/2}$)
	B_4C	ZrO_2	$ZrSiO_4$	C			
This Study	70	30	-	-	97.2	21.8 ±3.5	-
This Study	68	-	30	2	96.1	17.8 ±2.5	
1	95	5	-	-	95.4	33 ±2	3.6 ±0.5
2	90	10	-	added	98.8	33 ±1.3	4.1 ±0.2

Table 5.4 shows the effect of the $ZrSiO_4$ and ZrO_2 additions on the mechanical properties of Boron Carbide. ZrB_2 addition has a negative effect on the hardness of the Boron Carbide due to the low hardness of Zirconium Diboride. Sample one (Murthy et al., 2018) shows that 5 wt% addition of ZrO_2 resulted in a hardness value of 33 ±2 GPa which is the highest value compared to other works in the table. Sample two (Guo et al., 2015) shows a similar hardness compared to sample one yet the addition of a higher amount of ZrO_2 increases fracture toughness as a second phase in the matrix of Boron Carbide. The addition of 30 wt% ZrO_2 to the Boron Carbide decreased the hardness to 21.8 ±3.5. The effect of a variety of different indentation is caused by the non-homogeneous densification of the samples. When B-O samples are considered, indentations of sites show better densification are over 25 GPa. On the other hand, B-Si-C samples showed relatively lower hardness values. Because the relative density of B-Si-C samples is lower than B-O samples, hardness values showed a worse performance. Besides the relative density, another effect on lower hardness value is the existence of the SiO_2 glassy phase. While the more densified parts of B-O samples showed considerably good performance, this phenomenon could not be observed on the B-Si-C sample due to the existence of the SiO_2 phase.

Porous structures of samples hindered the calculation of fracture toughness. Because the better-densified parts are close to the edge of the samples, applying an indentation test on those parts very close to the edge is not safe for the indenter.

Improved electrical conductivity makes ceramics a candidate for high-temperature electrothermal elements in oxidizing environments, cathodes in high-

temperature fuel cells, and electrodes for magnetohydrodynamic power generation (Jingzhe et al., 2020). Besides these usage areas higher electrical conductivity is needed for the machining (especially the electrical discharge method) process too (Pramanick et al., 2020).

There are 47 valence electrons and 24 valance bands in the Boron Carbide. The vacant sites at the valence band make Boron Carbide a metallic conductor (Pramanick et al., 2020). To understand the effect of the ZrB_2 phase on the conductivity of Boron Carbide, the resistance of the samples is measured, and conductivity is calculated from the equation below.

$$\sigma = \frac{L}{RA}$$

The conductivity of the material is calculated by the equation where L (m) in thickness, R (Ω) is resistance and, A (m^2) is the surface area of the specimens.

The electrical conductivity of monolithic B_4C is measured as 47.78 $S\ m^{-1}$ (Pramanick et al., 2020). The second phase can alter the properties of the matrix phase dramatically. Adding or in-situ formation of the TiB_2 phase improves the electrical conductivity of the material by about 100% (Jingzhe et al., 2020).

An improvement in the resistivity of the B_4C-ZrB_2 composite is expected due to relatively higher resistivity value of ZrB_2 (0.09 $\mu\Omega\ m^{-1}$) (Muchlinsky et al., 1932). Table 5.5 shows the effect of relative density and in-situ formed phases on the electrical conductivity of the B_4C/ZrB_2 composite. ZrB_2 phase decreases the conductivity of the Boron Carbide by more than 9.8%. Besides the ZrB_2, C has a positive effect on the conductivity for B-O samples as shown in Table 5.5. When the C phase is observed in the XRD analysis of the sample, conductivity is about two times higher compared to the sample without C (C was not observed in the XRD analysis).

Table 4.5. Effect of relative density and in-situ formed phases on the electrical conductivity of B_4C/ZrB_2 composite.

Sample Name	Relative Density (%)	In-situ Formed Phases (except ZrB_2)	Conductivity $mS\ m^{-1}$
B-O	96.9	C	1.1
B-O	95.4	C	0.64
B-O	97.2	-	0.34

B-Si-C	96.1	SiO_2, SiC, C	0.51
B-Si-C	93.5	SiO_2, SiC, C	0.5
B-Si-C	94.7	SiO_2, SiC, C	0.34

Besides the ZrB_2 phase, another phase that decreases the conductivity is SiO_2 for the B-Si-C samples. For some of the samples, resistivity could not be measured by the device because of the insulating nature of SiO_2. Like hardness, resistivity calculations are affected by the sample prepared for measurement (different regions have different densification and phase composition). As mentioned before SiO_2 phase flows towards the sides of the specimen. When the resistivity calculation is done at the sides of the sample, resistivity could not be measured. Despite the B-O samples, there is not much difference between electrical conductivity values of B-Si-C samples. It should be noted that any value in table 5.5 is from the sides (which consists of the biggest portion of the SiO_2 phase). The electrical conductivity of the B-Si-C samples was expected much lower than B-O samples due to the existence of the SiO_2 phase. There are two reasons for the comparable electrical conductivity of B-Si-C samples. The first one is the flow of SiO_2 results in a very low SiO_2 phase in the interior parts of the sample. The second reason is the higher peak of the C phase which increases electrical conductivity.

5. CONCLUSION AND FUTURE WORK

Four different powder mixtures produce B_4C/ZrB_2 ceramic matrix composite. Table 3.2 shows these four different powder mixtures. To observe the effect of reactive sintering on the densification of B_4C/ZrB_2 composite, at first non-reactive path is followed. Achieving a relative density over 99% at 2150 °C showed the need for improvement on the process to decrease the sintering temperature. Next, reactive sintering paths are followed to monitor the densification behavior of the samples. While the B_4C-ZrO_2 powder mixture showed a relatively better performance than powder mixtures containing $ZrSiO_4$, relative densities near the non-reactive path could not be achieved. The first reason for relatively lower densities of reactive sintering paths is problems with the evacuation of side products of reactions (e.g., SiO_2, CO).

To overcome these problems, two steps sintering is preferred. First, the effect of the dwelling is monitored by three different characterization methods (SEM, XRD, SPS). With the help of data provided by those techniques, the effect of dwelling is interpreted on relative densities of samples. Results show that dwelling is a crucial step for reactive sintering, which is powder production for non-reactive sintering methods.

Dwelling B_4C-ZrO_2 powders at 1600 °C for 15 minutes is observed as a good segment for eliminating bloating defects. The effect of dwelling on the bloating of B_4C-$ZrSiO_4$ and B_4C-$ZrSiO_4$-C samples is commented as an unclear phenomenon. While bloating is observed on samples with higher dwelling time, it is not observed which have lower dwelling time on some samples. This part of the thesis is considered as future work.

Besides bloating, another problem of the samples containing $ZrSiO_4$ is eliminating the SiO_2 phase and preventing SiC formation. The purpose of using $ZrSiO_4$ is to find a much cheaper raw material for producing B_4C/ZrB_2 composite. SiC is a phase that can contribute to many properties of the material, yet it is not a part of the scope of this thesis. Producing B_4C/ZrB_2/SiC ceramic matrix composite using a reactive sintering route via $ZrSiO_4$ powder can be excellent future work. The $B4C/ZrB_2$/SiC composite can be considered an alternative to the B_4C/TiB_2/SiC composite.

Even though it does not have many examples in the literature, the B_4C-ZrO_2 powder route showed a relatively good performance on the densification. Hardness values of

these samples are within the examples in the literature (when the relative densities are considered). Electrical resistivities of the samples are increased by the ZrB_2 phase, which restricts the application of B_4C/ZrB_2 composite.

$ZrSiO_4$ powder is not used as an additive for B_4C. That is why this work can be an example for others who intended to use $ZrSiO_4$ as an additive. For example, this additive's hardness and electrical conductivity are examined. The hardness of B-Si-C samples is lower than B-O samples due to the SiO_2 phase and lower relative density. Due to the poor densification of inner parts of B-Si-C samples, performance comparison with B-O samples can be misleading.

Overcoming the non-homogeneous densification and examining the mechanical properties of the samples can be future work.

REFERENCES

Yürekli, A. (2019). Lisansüstü Eğitim Enstitüsü Tez Yazım Kılavuzu. *Eskişehir Teknik Üniversitesi Lisansüstü Eğitim Enstitüsü*, 1-12.

Aizat, M., Mohd, H., Mustapha, M., & Kurnia, J. C. (2017). *Silicon carbide- from synthesis to application : a review*. *04003*, 1–6. https://doi.org/10.1051/matecconf/201713104003

Amit Bandyopadhyay, S. B. (2016). *Additive manufacturing*.

Atkinson, H. V., & Davies, S. (2000). Fundamental aspects of hot isostatic pressing: An overview. *Metallurgical and Materials Transactions A: Physical Metallurgy and Materials Science*, *31*(12), 2981–3000. https://doi.org/10.1007/s11661-000-0078-2

Balak, Z., Shahedi Asl, M., Azizieh, M., Kafashan, H., & Hayati, R. (2017). Effect of different additives and open porosity on fracture toughness of ZrB_2–SiC-based composites prepared by SPS. *Ceramics International*, *43*(2), 2209–2220. https://doi.org/10.1016/j.ceramint.2016.11.005

Biernacki, J. J., & Wotzak, G. P. (1989). Thermogravimetric study of the C + SiO_2 reaction. *Journal of Thermal Analysis*, *35*(5), 1651–1667. https://doi.org/10.1007/BF01912940

B.J., K., & Lange F.F., B. J. G. P. (1990). *Advanced Ceramic Processing and Technology*. *Advanced Processing Concepts for Increased Ceramic Reliability*, 1–37.

Blackburn, S., & Wilson, D. I. (2008). *Shaping ceramics by plastic processing*. *28*, 1341–1351. https://doi.org/10.1016/j.jeurceramsoc.2007.12.013

Cai, P., Guo, L., Liu, L., Zhang, Q., Li, J., & Lue, Q. (2021). Rapid manufacturing of silica glass parts with complex structures through stereolithography and pressureless spark plasma sintering. *Ceramics International*, *June*. https://doi.org/10.1016/j.ceramint.2021.08.345

Cavaliere, P. (2019). Spark plasma sintering of materials: Advances in processing and applications. In *Spark Plasma Sintering of Materials: Advances in Processing and Applications*. https://doi.org/10.1007/978-3-030-05327-7

Chamberlain, A. L., Fahrenholtz, W. G., & Hilmas, G. E. (2006). Pressureless sintering of zirconium diboride. *Journal of the American Ceramic Society*, *89*(2), 450–456. https://doi.org/10.1111/j.1551-2916.2005.00739.x

Dobrzanski, L. A., Hajduczek, E., & Matula, G. (2017). *Fabrication Technologies of the Sintered Materials Including Materials for Medical and Dental Application World ' s largest Science , Technology & Medicine Open Access book publisher*. *March*. https://doi.org/10.5772/65376

Ebrahimi-kahrizsangi, R., & Torabi, O. (2012). Combination of mechanochemical activation and self-propagating behavior for the synthesis of nanocomposite Al_2O_3/B_4C powder. *Journal of Alloys and Compounds*, *514*, 54–59. https://doi.org/10.1016/j.jallcom.2011.10.075

Fang, Z. Z. (2010). *Sintering of advanced materials*. Woodhead Publishing Limited.

Francis, L. F. (2016). *Ceramics and Polymers*.

G. Heinrich, J., & M. Gomes, C. (1977). Introduction to Ceramics Processing. *Journal of The Electrochemical Society*, *124*(3), 152C.

German, R. M., Suri, Æ. P., & Jin, Æ. S. (2009). *Review : liquid phase sintering*. 1–39. https://doi.org/10.1007/s10853-008-3008-0

Gok, M. G. (2021). *Spark Plasma Sintering of Nano Silicon Carbide Reinforced Alumina Ceramic Composites*. *5*, 64–70.

Goldstein, A., Geffen, Y., & Goldenberg, A. (2001). Boron Carbide-Zirconium Boride in Situ Composites by the Reactive Pressureless Sintering of Boron Carbide-Zirconia Mixtures. *Journal of the American Ceramic Society*, *84*(3), 642–644. https://doi.org/10.1111/j.1151-2916.2001.tb00714.x

Group, C. S., & Metallurgical, D. (1992). *Review Self-propagating high-temperature synthesis*. *27*, 6249–6273.

Groza, J. R., & Zavaliangos, A. (2000). *Sintering activation by external electrical field*. *287*, 171–177.

Guo, W., Wu, L., You, Y., Lin, H., & Zhang, G. (2015). Three-step reactive hotpressing of B_4C–ZrB_2 ceramics. *Journal of the European Ceramic Society*, 3–9. https://doi.org/10.1016/j.jeurceramsoc.2015.11.022

Huang, S. G., Vanmeensel, K., & Vleugels, J. (2014). Powder synthesis and densification of ultrafine B_4C-ZrB_2 composite by pulsed electrical current sintering. *Journal of the European Ceramic Society*, *34*(8), 1923–1933. https://doi.org/10.1016/j.jeurceramsoc.2014.01.022

Iethschmidt, K. L. L., Gmbh, E. K., & Grefrath, W. (1974). *Silicon Carbide*. https://doi.org/10.1002/14356007.a23

Iii, J. P., Subhash, G., Zheng, J., Halls, V., & Jannotti, P. (2015). The rate-dependent fracture toughness of silicon carbide- and boron carbide-based ceramics. *Journal of the European Ceramic Society*. https://doi.org/10.1016/j.jeurceramsoc.2015.08.027

Imran, Z. M., Tanaka, S., & Uematsu, K. (2009). Effect of polyacrylic acid (PAA) binder system on particle orientation during. *Powder Technology*, *196*(2), 133–138. https://doi.org/10.1016/j.powtec.2009.07.003

Jingzhe, F., Weixia, S., Zhuangfei, Z., & Chao, F. (2020). Preparation and properties of B_4C-TiB_2 ceramics prepared by spark plasma sintering. *Journal of Advanced Ceramics*, 4–6.

Kaiser, A., Lobert, M., & Telle, R. (2008). Thermal stability of zircon ($ZrSiO_4$). *Journal of the European Ceramic Society*, *28*(11), 2199–2211. https://doi.org/10.1016/j.jeurceramsoc.2007.12.040

Kessel, H. U., Hennicke, J., Schmidt, J., Weißgärber, T., Kieback, B. F., Herrmann, M., & Räthel, J. *" FAST " field assisted sintering technology- a new process for the production of metallic and ceramic sintering materials*.

Kuang, X., Carotenuto, G., & Nicolais, L. (1997). *A Review of Ceramic Sintering and Suggestions on Reducing Sintering Temperatures*. *274*, 257–274.

Lafayette, W. (1991). *No Title*. *57*, 59–88. https://doi.org/10.4028/www.scientific.net/KEM.56-57.59

Lin, X., Ai, S., Feng, Y., Gao, D., Guo, X., Liu, Y., Xie, B., Gong, H., & Zhang, Y. (2017). Fabrication and properties of in-situ pressureless-sintered ZrB_2/B_4C composites. *Ceramics International*, *43*(17), 15593–15596. https://doi.org/10.1016/j.ceramint.2017.08.115

Lowe, D., & Owen, H. C. M. M. (2007). *A Mid-IR Pyrometer Calibrated with High-Temperature Fixed Points for Improved Scale Realization to 2 , 500 ◦ C*. 2059–2066. https://doi.org/10.1007/s10765-007-0284-x

Mcwilliams, B., Zavaliangos, A., Cho, K. C., & Dowding, R. J. (2006). *The Modeling of Electric-Current- Assisted Sintering to Produce Bulk Nanocrystalline Tungsten*.

Monteverde, F., Bellosi, A., & Guicciardi, S. (2002). Processing and properties of zirconium diboride-based composites. *Journal of the European Ceramic Society*, *22*(3), 279–288. https://doi.org/10.1016/S0955-2219(01)00284-9

Muchlinsky, W., Rother, E., Jander, G., Pfundt, O., Göte, E., Schramek, W., Janssen, L. W., Teegan, J. A. C., Schleicher, A., Lüdicke, W., Denina, E., Preston, J. M., Rae, N., Rummel, J. K., Schierjott, K., Kolthoff, J. M., Kameda, T., Blumen, L., Pucherna, J., … Pauling, H. (1932). Leitfähigkeit. In *Fresenius' Zeitschrift für analytische Chemie* (Vol. 89, Issues 3–4, pp. 128–135). https://doi.org/10.1007/bf01350902

Murthy, T. S. R. C., Ankata, S., Sonber, J. K., Sairam, K., Singh, K., Nagaraj, A., Sengupta, P., Bedse, R. D., Majumdar, S., & Kain, V. (2018). Microstructure, thermo-physical, mechanical and wear properties of in-situ formed boron carbide -Zirconium diboride composite. *Ceramics - Silikaty*, *62*(1), 15–30. https://doi.org/10.13168/cs.2017.0041

Oleg O. Vasylkiv, Hanna Borodianska, Yoshio Sakka, P. B. (n.d.). High temperature flexural strength in monolithic boron carbide ceramic obtained from two different raw powders by spark plasma sintering High temperature flexural strength in monolithic boron carbide ceramic obtained from two different raw powders. *Ceramic Society Japan*, *May*. https://doi.org/10.2109/jcersj2.15289

Orrù, R., & Cao, G. (2013). Comparison of reactive and non-reactive spark plasma sintering routes for the fabrication of monolithic and composite Ultra High Temperature Ceramics (UHTC) materials. *Materials*, *6*(5), 1566–1583. https://doi.org/10.3390/ma6051566

Ortiz, A. L., Candelario, V. M., Moreno, R., & Guiberteau, F. (2017). Near-net shape manufacture of B4C–Co and ZrC–Co composites by slip casting and pressureless sintering. *Journal of the European Ceramic Society*, *37*(15), 4577–4584. https://doi.org/10.1016/j.jeurceramsoc.2017.07.024

Pramanick, A., Dey, P. P., & Das, P. K. (2020). Microstructure, phase and electrical conductivity analyses of spark plasma sintered boron carbide machined with WEDM. *Ceramics International*, *46*(3), 2887–2894. https://doi.org/10.1016/j.ceramint.2019.09.282

Processing and Properties of Advanced Ceramics and Composites IV Processing and Properties of Advanced Ceramics and Composites IV Ceramic Transactions , Volume 234. (n.d.).

Rahaman, M. N. (2017). Ceramic processing and sintering, second edition. *Ceramic Processing and Sintering, Second Edition*, 1–875. https://doi.org/10.1201/9781315274126

Raju, B., Mukhopadhyay, A., & Basu, B. (2020). Progress in Materials Science Review on ultra-high temperature boride ceramics. *Progress in Materials Science*, *111*(July 2019), 100651. https://doi.org/10.1016/j.pmatsci.2020.100651

R.Rice, B. J. G. P. (1999). *Advanced Ceramic Processing and Technology*. *1*(Processing of ceramic composites using colloidal method), 123–213.

Saeedi Heydari, M., Baharvandi, H. R., & Dolatkhah, K. (2015). Effect of TiO2 nanoparticles on the pressureless sintering of B_4C-TiB_2 nanocomposites. *International Journal of Refractory Metals and Hard Materials*, *51*, 6–13. https://doi.org/10.1016/j.ijrmhm.2015.01.014

Shcherbakov, V. A., Gryadunov, A. N., & Alymov, M. I. (2017). *Synthesis and characteristics of the B_4C–ZrB_2 composites*. *7*(4), 398–401. https://doi.org/10.22226/2410-3535-2017-4-398-401

Sonber, J. K., & Suri, A. K. (2011). Synthesis and consolidation of Zirconium diboride: Review. *Advances in Applied Ceramics*, *110*(6), 321–334. https://doi.org/10.1179/1743676111Y.0000000008

Song, S., Bao, C., & Wang, B. (2016). Effect of the addition of carbon fibres on the microstructure and mechanical properties of reaction bonded B_4C/SiC composites. *Journal of the European Ceramic Society*, *36*(8), 1905–1913. https://doi.org/10.1016/j.jeurceramsoc.2016.02.048

Suri, A. K., Subramanian, C., Sonber, J. K., & Murthy, T. S. R. C. (2010). *Synthesis and consolidation of boron carbide: a review* (Vol. 55, Issue 1). https://doi.org/10.1179/095066009X12506721665211

Telle, R., Sigl, L. S., & Takagi, K. (2000). *7 Boride-Based Hard Materials*.

Thévenot, F. (1990). Boron carbide-A comprehensive review. *Journal of the European Ceramic Society*, *6*(4), 205–225. https://doi.org/10.1016/0955-2219(90)90048-K

Tib, T., & Nbo, N. K. (2010). *Spark Plasma Sintering Enhancing Grain Sliding , Deformation and Grain Size Control Doctoral Thesis 2010*.

Wang, S., Li, L., Yan, S., Deng, Y., Gao, S., & Xing, P. (2020). Preparing B4C-SiC-TiB2 composites via reactive pressureless sintering with B4C and TiSi2 as raw materials. *Journal of Materials Research and Technology*, *9*(4), 8685–8696. https://doi.org/10.1016/j.jmrt.2020.05.124

William D. Callister, Jr. (2007). *Materials Science and Engineering; An Introduction 7th Edition*. https://doi.org/10.1007/BF01184995

Wu, C., Li, Y. K., & Wan, C. L. (2020). Reactive-sintering B4C matrix composite for armor applications. *Rare Metals*, *39*(5), 529–544. https://doi.org/10.1007/s12598-020-01404-6

Xiong, Y., Du, X., Xiang, M., Wang, H., Wang, W., & Fu, Z. (2018). *Journal of the European Ceramic Society Densi fi cation mechanism during reactive hot pressing of B_4C-ZrO_2 mixtures*. *March*. https://doi.org/10.1016/j.jeurceramsoc.2018.05.016

Ya, Mohnagı (2006). *The effect of electric field and pressure on the synthesis and consolidation of materials : A review of the spark plasma sintering method*. *1*, 763–777. https://doi.org/10.1007/s10853-006-6555-2

Zhang, W., Yamashita, S., & Kita, H. (2019). Progress in pressureless sintering of boron carbide ceramics–a review. *Advances in Applied Ceramics*, *118*(4), 222–239. https://doi.org/10.1080/17436753.2019.1574285

Zipse, H. (1997). *Finite-ElemIent Simulation of the Die Pressing and Sintering of a Ceramic Component J (J-J ' + (l + a ~ :, cos # J2*. *17*.

I. Solodkyi, O. Bezdorozhev, M. Vterkovskiy, I. Bogomol, V. Bolbut, M. Krüger, P. Badica, P. Loboda. (2018). Addition of carbon fibers into B4Cinfiltrated with molten silicon

APPENDIX

CURRICULUM VITAE

Education Background:

2011-2018, Anadolu University Materials Science and Engineering

2019-Present, Eskişehir Technical University, Department of Advanced Technologies, Nanotechnology